A Genetic, Biochemical, and Biomechanical Study of Plant Cell Wall Dynamics in Pollen Tubes

---

Dissertation

zur

Erlangung der naturwissenschaftlichen Doktorwürde
(Dr. sc. nat.)

vorgelegt der

Mathematisch-naturwissenschaftlichen Fakultät

der

Universität Zürich

von

Christian Draeger

aus

Deutschland

Promotionskomitee

Prof. Dr. Beat Keller (Vorsitz)
PD Dr. Christoph Ringli (Leitung der Dissertation)
Prof. Dr. Ueli Grossniklaus

Zürich, 2012

ZUSAMMENFASSUNG

Pflanzenzellen sind von einer Zellwand umgeben, welche die physikalische Eigenschaften, das Wachstum und die Form der Zelle beeinflusst. Polysaccharide und Proteine gehören zu den Hauptbestandteilen der Zellwand. Über die mechanischen Eigenschaften der Zellwand ist nur wenig bekannt, und der Beitrag der einzelnen Zellwandkomponenten zur Zellwanddynamik ist nicht vollständig aufgeklärt. Deshalb wurde in dieser Arbeit eine neue Technologie, Cellular Force Mikroskopie (CFM), etabliert, um den Einfluss der Zellwandkomponenten auf die mechanischen Eigenschaften der Zellwand zu verstehen. Dazu wurden Pollenschläuche von *Lilium longiflorum* (Lilie) verwendet, da sie sehr schnell wachsen, relativ gross sind und nur aus einer Zelle bestehen. Experimentelle Daten wurden mit einem theoretischen Modell kombiniert, um die Grösse des Young's Modulus, der mechanische Eigenschaften beschreibt, zu bestimmen. Dabei wurde gezeigt, dass die CFM Technologie dazu geeignet ist zelluläre Prozesse zu identifizieren und die mechanische Festigkeit der Zellwand von Pollenschläuchen zu beschreiben.

In einem nächsten Schritt wurde das CFM auf den wesentlich kleineren Pollenschläuchen der Modellpflanze *Arabidopsis thaliana* (Arabidopsis) angewendet. Die Analyse verschiedener Arabidopsis Zellwandmutanten (*xxt1 xxt2*, *xeg113*) deutet auf einen synergistischen Effekt zwischen dem Zellwandpolymer Xyloglucan und den strukturellen Zellwandglykoproteinen, den Extensinen, hin. Dies lässt vermuten, dass zwischen diesen zwei Zellwandkomponenten ein kompensatorischer Mechanismus abspielen könnte. Folglich können Veränderungen der Zellwandzusammensetzung sich massiv auf das Wachstum, die Bildung und die mechanische Festigkeit pflanzlicher Zellen auswirken.

Während eines Arabidopsis Mutanten-screens wurden *ATPEX* kodierte Zellwandproteine identifiziert, die zur Familie der LRR-Extensine (LRX) gehören und die Morphologie des Pollenschlauchs beeinflussen. Eine Antikörperanalyse zeigte, dass *atpex* Mutanten eine Veränderung in der Zellwand aufweisen. Deshalb wurde mit einer weiteren biochemischen Analyse geprüft, ob die Zellwandzusammensetzung bei *lrx* Mutanten Veränderungen aufweist. Da in Pollenschläuchen nur sehr wenig Material für eine biochemische Analyse zur Verfügung steht, wurden dafür Arabidopsis Blätter als Modellsystem gewählt. Weil *ATPEX* Gene spezifisch in

Pollen expremiert sind wurden *lrx3*, *lrx4* und *lrx5* Mutanten, die eine Veränderung in der Zellstruktur von Blättern zeigen, herangezogen. Dabei wurde eine Veränderung in der Zusammensetzung der Zellwand in den drei *lrx* Mutanten gezeigt, was die Hypothese unterstützt, dass LRX Proteine an einem Prozess, der die Zellwandbildung kontrolliert, beteiligt sein könnten.

SUMMARY

All plant cells are surrounded by a cell wall which affects physical strength, plant growth, and cell shape. Polysaccharides and cell wall proteins are major components of the cell wall. But mechanical properties and contributions of the cell wall components to cell wall growth dynamics are not fully understood. Therefore, a novel technology the Cellular Force Microscope (CFM) was established to understand contributions of cell wall components to the mechanical properties of the cell wall. *Lilium longiflorum* (lily) pollen tubes (PTs) were used as a model since they grow very fast, have a relatively large cell size, and are considered to be a single cell organism. Experimental and theoretical data were combined to measure the Young's modulus, which determines mechanical properties of an elastic material. In this work it was shown that the CFM technology is an ideal tool to investigate cellular processes and mechanical properties of PTs.

In a next step CFM was used on the model plant *Arabidopsis thaliana*, which exhibits much smaller PTs. The analysis of the cell wall mutants (*xxt1 xxt2, xeg113*) revealed a possible synergistic effect between the cell wall polymer xyloglucan and structural cell wall glycoproteins called extenins. This suggests that a compensatory mechnism between these two cell wall components occurs. Therefore, a change of the cell wall composition affects cell growth, cell wall extension, and the mechanical properties of the plant cell wall.

During an Arabidopsis cell wall mutant screen *ATPEX* was identified encoding a cell wall protein, which is a member of the LRR-extensin (LRX) family and affects the PT cell wall. An antibody analysis showed cell wall modifications in *atpex* mutants. Thus, an additional biochemical analysis of the cell wall was performed to test if the cell wall composition is affected in *lrx* mutants. PTs are very small and the amount of material for a high-throuput analysis is very rare. Therefore, Arabidopsis leaves were used as a model system. *ATPEX* is specifically expressed in PTs and mutants did not show any leaf phenotype. For this reason *lrx3*, *lrx4*, and *lrx5* mutants were used since they show a pavement cell phenotype in leaves. The analysis of these three mutants revealed a difference in cell wall composition, which supports the hypothesis that LRX proteins are involved in a mechanism regulating cell wall development.

1. GENERAL INTRODUCTION

1.1 THE PLANT CELL WALL

Plant cells are encapsulated by a cell wall, a complex, dynamic, extracellular polysaccharide network. The cell wall is elastic and allows cell expansion. Simultaneously it provides mechanical strength and determines cell shape. Furthermore, the cell wall regulates the exchange of information with the surrounding tissues or the environment (Carpita and McCann, 2000). In higher plants two types of plant cell walls are found: primary walls and secondary walls. Growing cells produce relatively thin and flexible primary walls, which are constantly modified during synthesis and enlargement. In contrast, secondary walls are rigid, thick and are produced when the cell has reached its final size (Hayashi, 1989; Hematy and Höfte, 2006). Cell walls are highly dynamic structures and several hundred genes encode proteins that are involved in or functionally related to cell wall biosynthesis (Somerville et al., 2004). Generally, the cell wall consists of a variety of complex polysaccharides like cellulose, hemicellulose, pectins, and structural proteins (Fig. 1).

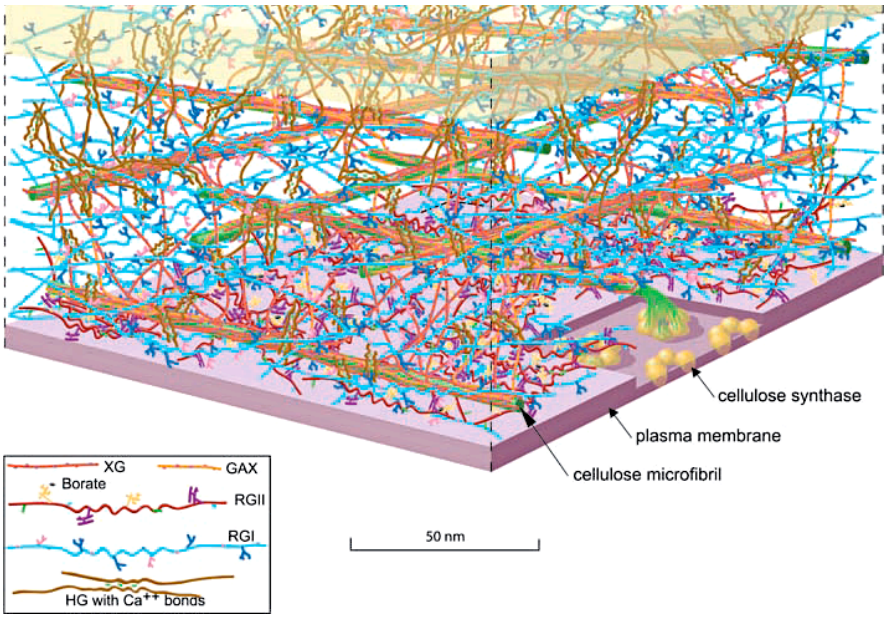

Figure 1: **Cell wall matrix model of an Arabidopsis leaf.** The cell wall is a highly conserved dynamic network of polysaccharides and this complex model underscores the challenge associated with understanding the structure, function, and synthesis of plant cell walls. Various cell wall polymers based on their approximate ratio relative to cellulose are shown. HG: Homogalcaturonan, RGI: Rhamnogalacturonan II, RGII: Rhamnogalacturonan II, XG: Xyloglucan, GAX: Glucuronoarabinoxylan (Somerville et al., 2004).

Cellulose

The molecular structure of the cell wall is relatively well described, but remarkably little is known about enzymes required for cell wall biosynthesis. Cellulose consists of glucose monomers and is present as fibrils composed of hydrogen-bonded β-(1,4)-glucose chains. Several *CELLULOSE SYNTHASE* (*CESA*) genes are known in Arabidopsis, which are essential for cellulose synthesis. Five or six CESA protein subunits form a rosette and build the main cellulose synthase complex (Fig. 2A, B; [Kimura et al., 1999]). Each CESA protein subunit synthesizes one of the β-(1,4)-glucose chains that merge to a fibril (Fig. 2C), 3-5 nm wide and up to a length of several micrometers. Cellulose synthesis occurs directly at the cell membrane (Fig. 1; [Cutler and Somerville, 1997; Somerville et al., 2004]). High resistance against enzymatic degradation and mechanical strength makes crystalline cellulose ideal as a scaffold for the cell wall matrix (Cosgrove, 2005).

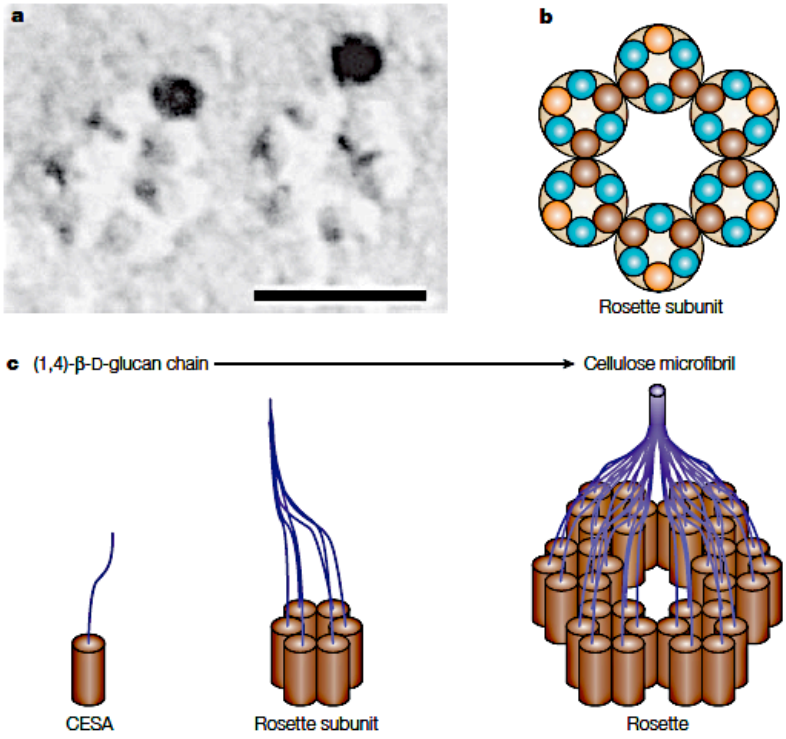

Figure 2: **Molecular structure of the cellulose synthase process.** (a) Electron microscopic picture of the cellulose synthase rosette complex (bar = 30 nm) and (b) model of the complex. (c) Cellulose synthase organization and cellulose fibril synthesis (Cosgrove, 2005).

Hemicellulose

Xyloglucan (XyG) and arabinoxylan are the most abundant hemicelluloses in the primary plant cell wall of flowering plants (Dardelle et al., 2010). Arabinoxylan consists of a β-(1,4)-xylan backbone substituted with arabinose side chains that possibly bind cellulose via ferulic acid esters (Cosgrove, 2005). The XyG β-(1,4)-glucan backbone is substituted with α-(1,6)-xylosyl residues, which are glycosylated with galactose (Gal) and fucose (Fuc) by glycosyltransferases (Fig. 3). The XyG backbone is similar to that of cellulose and interacts with cellulose fibrils (Fig. 4; [Cosgrove, 1999]). Specific galactosyl residues in XyG can be O-acetylated and may enhance the high non-covalent affinity to cellulose, but the exact biological purpose is unknown (Cavalier et al., 2008; Obel et al., 2009; Dardelle et al., 2010).

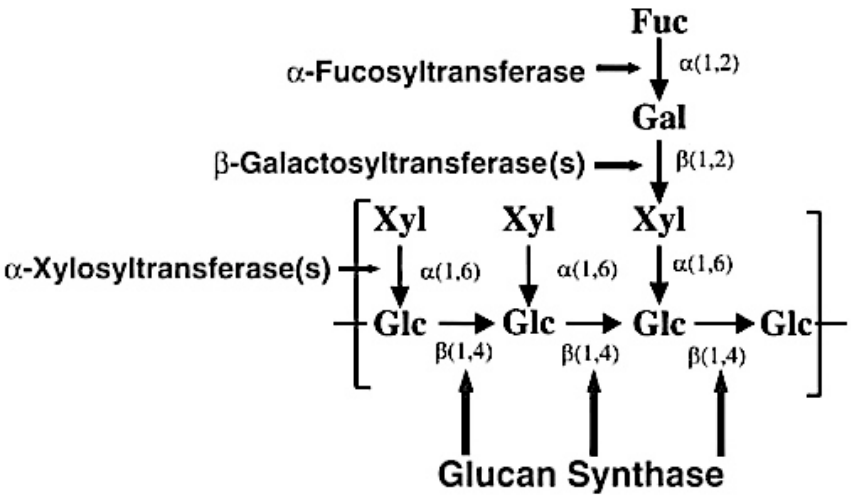

Figure 3: **XyG structure and enzymes required for XyG biosynthesis.** XyG monomer shows the typical XXFG motif (X: Xyl, G: Glc, L: Gal-Xyl, F: Fuc-Gal-Xyl; one letter code proposed by Fry et al., 1999) and XyG modifying enzymes attaching the particular monosaccharides to XXFG. Glc: glucose, Xyl: Xylose, Gal: Galactose, Fuc: Fucose (http://www.bmb.msu.edu/faculty/keegstra/cellwall.html).

Biosynthesis of XyG does not occur directly at the cell membrane. Precursors are synthesized in the Golgi, transported to the cell membrane and secreted to the extracellular matrix. Xyl of the XyG backbone derives from UDP-xylose, which is synthesized by a UDP-glucose-dehydrogenase from UDP-glucose (Strominger and Mapson, 1957). UDP-fucose and UDP-galactose are assumed to act as donors for the addition of different galactosyl and fucosyl residues. Different enzymes like the β-(1,4)-glucosyltransferase or

the α-(1,6)-xylosyltransferase, were identified and are involved in XyG assembly and modification in the cell wall (Camirand et al., 1987; Hayashi, 1989). The integration of new secreted XyG precursors into the existing wall matrix is possibly mediated by enzymes such as endotransglycosylases from the xyloglucan endotransglucosylase/hydrolase (XTH) family. The cell wall-associated XyG-*endo*transglycosylase (XET) and the endoxyloglucan-transferase (EXGT) with similar activities affect cell wall expansion and modulate or integrate new XyG subunits into the growing cell wall (Fry et al., 1992; Rose et al., 2002; Takeda et al., 2004).

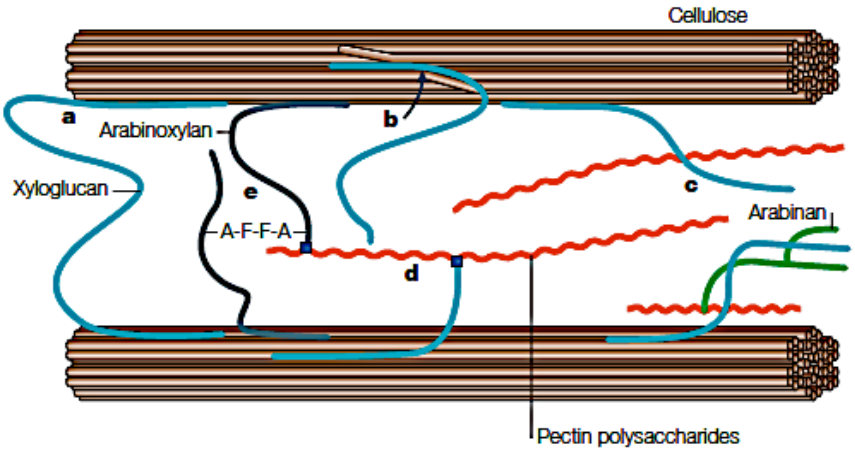

Figure 4: **Five possible models how hemicelluloses form a network with cellulose.** (a) Hemicelluloses (blue) might spontaneously bind to the surface of cellulose fibrils and connect those. (b) XyG (blue) becomes embedded during cellulose formation and anchored XyG can bind other cellulose or other matrix components (orange). (c) XyG is coating cellulose fibers and they can interact with other cell wall polymers. (d) XyG (blue) is covalent attached to pectins (orange) and the macromolecules interact with the cellulose surface. (d) Arabinoxylans (grey) build ferulic acid esters (A-F-F-A) and cross-link cellulose fibers (Cosgrove, 2005).

The cellulose-XyG network is assumed to serve as a primary load-bearing matrix of the primary cell wall during cell expansion. Modification of XyG can strongly affect cell wall properties e.g. the endohydrolysis of XyG is a possible contributor to cell wall loosening during growth (Hayashi, 1989; Willats et al., 2001; Cavalier et al., 2008). Another XyG-modifying enzyme is a XyG-specific endo-β-(1,4)-glucanase (XEG) isolated from *Aspergillus aculeatus*, which hydrolyzes structurally diverse XyGs. XEG can be a powerful tool in the structural elucidation of XyGs (Pauly et al., 1999). Hemicelluloses are relatively well described in cell walls

where they seem to be connecting cellulose microfibrils. The cellulose-XyG network is embedded in a matrix formed by pectins (Cosgrove, 1999).

Pectin

Pectins show a more diverse set of glycosidic linkages and substituted residues, and are thought to be covalently linked to each other (Williats et al., 2001). Major pectin components are homogalacturonan (HG), xylogalacturonan (XGA), rhamnogalacturonan I (RGI), and rhamnogalacturonan II (RGII) (Fig. 1). They are defined by the presence of uronic acids (Fig. 1; [Carpita and McCann, 2000]). The HG backbone is linear and consists of α-(1,4)-galacturonic acids (Fig. 5), which can bind Ca^{2+} ions (Fig. 1) or are highly methylated (Vorwerk et al., 2004). XGA contains branches of xylosyl residues, which differ in length depending on the plant species (Fig. 5). The RGI backbone is composed of alternating α-(1,2)-rhamnose-α-(1,4)-galacturonic acids decorated primarily with various β-(1,4)-arabinan and α-(1,5)-galactan sidechains (Fig. 5; [Somerville et al., 2004]). Arabinans and arabinogalactans linked to RGI are proposed to enhance wall flexibility (Jones et al., 2003). RGII is the most complex macromolecule and consists of four different side chains, with highly conserved polysaccharides across many species (Fig. 5). In plant cell wall development, RGII forms dimers through borate ester bounds (Fig. 1), which controls wall porosity and thickness (Cosgrove, 2005).

Generally, pectins are synthesized as methyl esters in the Golgi apparatus and are secreted as such. Upon demethylation, pectin can bind Ca^{2+}, which leads to a more rigid structure. The factors involved in pectin deposition are unknown (Staehlin and Moore, 1995; Somerville et al., 2004; Bosch and Hepler, 2005). Pectin is thought to be embedded in the cell wall as a gel-like substance, which can bind to the surface of cellulose (Zykwinska et al., 2005; Mohnen, 2008).

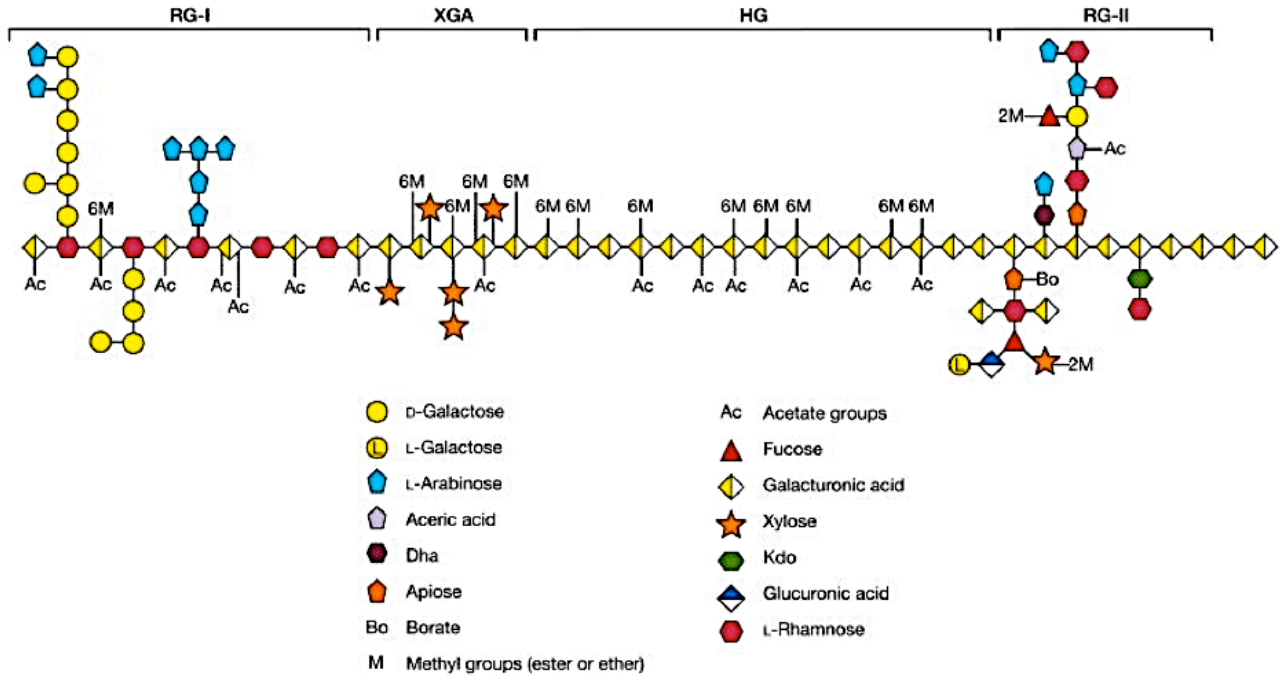

Figure 5: **Schematic pectin structure.** Pectin backbone substituted with residues for HG: Homogalacturonan, RGI: Rhamnogalacturonan II, RGII: Rhamnogalacturonan II, XGA: Xylogalacturonan. Different sugar moieties, borate, methyl and acetate modifications are shown (Mohnen, 2008).

It is still a challenge to explore how the complex pectic biosynthesis occurs and how polysaccharides are cross-vlinked. Pectin synthesis in general is partly performed by proteins and diverse sugar acceptors, which are used by the pectic transferases as precursors (Mohnen, 2008). However, pectins build networks by covalent and ionic bounds and the mechanisms of pectin cross linking are not yet determined.

Structural cell wall proteins

Cell wall-related proteins are also part of the cell wall and play an important role in expansion and development. Major cell wall glycoproteins are hydroxyprolin (Hyp)-rich glycoproteins (HRGPs) a superfamily of cell wall proteins including extensins (EXTs). EXTs are a major class of extracellular proteins, form rod-like structures, play a mechanical role, and influence physical properties of the cell wall during pathogen attack (Brisson et al., 1994). Typically, EXTs have multiple Ser-Hyp_4 motifs were Hyp is linked with arabinofuranose and Ser substituted with galactosyl residues (Showalter, 1993). Tyr residues of the EXT backbone have been

shown to be involved in protein cross-linking via the hydroxyl group of the aromatic ring, which is thought to be the chemical basis of EXT insolubilisation (Fry et al., 1982; Epstein and Lamport, 1984; Brady et al., 1998; Ringli et al., 2001; Held et al., 2004). Yet, Tyr-independent insolubilisation has also been reported (Ringli, 2010). EXTs are known to form relatively large structures and are thought to be important in bridging polysaccharides (Keegstra et al., 1973; Mort and Lamport, 1977). Therefore, EXT have been shown to interact with various cell wall components like pectins via β-(3,6)-galactan residues (Fong et al., 1992; Qi et al., 1995; Cassab, 1998).

EXTs are posttranslationally modified on proline residues catalyzed by prolyl 4-hydroxylases (P4Hs). These define subsequent O-glycolysation sites. Biochemical inhibition or genetic disruption of P4Hs results in an underarabinosylation of EXTs, which in turn blocks polarized root hair growth (Lamport et al., 2011; Velasquez et al., 2011). Therefore, EXT modifications affecting cell wall development contribute to the various functions of the cell wall. Mutations in individual *EXT* genes only rarely lead to significant phenotypes. The Arabidopsis lethal *root-, shoot-, hypocotyl-defective* (*rsh*) mutant is affected in embryogenesis. RSH, a structural Hyp-rich glycoprotein is located in nascent and mature cell walls and consists of amphiphilic peptide motifs representing potential sites of hydrophobic isodityrosine crosslinks. *rsh* develops incomplete cross walls resulting in abnormal cell shapes. The positively charged EXTs form a scaffold that can interact with acidic pectin to build EXT-pectate aggregates. The latter is a possible target as a template for the further deposition of cross wall material in the process of cytokinesis (Cannon et al., 2008).

EXT can also occur in the context of chimeric proteins like leucine-rich repeat (LRR) extensins (Lind et al., 1994; Ringli, 2005). The chimeric LRR-extensin (LRX) proteins contain a N-terminal LRR and a C-terminal extensin domain, are localized extracellularly, and are involved in cell wall formation (Rubinstein et al., 1995a; Baumberger et al., 2001; 2003a). In maize, two pollen-specific genes *PEX1* and *PEX2* (*POLLEN EXTENSIN-LIKE*) are identified encoding multiple repeats of the extensin-like motif Ser-Hyp_4. *PEX1* contains a C-terminal extensin-like domain and an N-terminal LRR domain and may act as structural or recognition molecule required for pollen-pistil interactions (Rubinstein et al., 1995a). PEX1 is localized specifically in the inner callosic layer of the pollen tube wall and exhibits a high glycosylation state. The mechanism how PEX proteins

mediate pollen-pistil interactions is unclear, but they are excellent candidates mediating this process (Rubinstein et al., 1995b). Another LRR-extensin in Arabidopsis is *LRX1* that is expressed in root hairs and affects root hair morphogenesis. LRX1 is localized in the root hair cell wall were it becomes insolubilized during development. *lrx1* mutants develop root hairs that frequently swell or burst and it is thought to be a regulator of cell wall formation and assembly, but the exact function of LRX1 is unknown (Baumberger et al., 2001).

Expansion of the cell wall

Cell walls show acidic-induced expansion or loosening driven by active proteins called expansins. They have been discovered in many plants and are known to promote cell expansion, fruit tissue softening, germination, and stress response. Expansins are divided into several subclasses: α-expansins (EXPA), β-expansins (EXPB) and the expansin-like family EXLA and EXLB (Cosgrove, 2005). Expansins are known to weaken paper but a hydrolysis of hydrogen bonds does not occur (McQueen-Mason and Cosgrove, 1994). They are thought to synergistically enhance hydrolysis of crystalline cellulose mediated by cellulases. Since glucan accessibility is the rate-limiting step in cellulase action, it is assumed that expansins promote the release of glucans in cellulose microfibrils to gain access for enzymatic attack. It is also possible that expansins drive complex polysaccharide dissociation by avoiding microfibril linkage (McQueen-Mason and Cosgrove, 1994). The activation of expansins is mediated by acidification, which correlates with the fact that the pH of the cell wall is usually between 4.5 and 6 (Cosgrove, 1989). Biochemically, EXPA and EXPB are not fully understood. The most important function of expansins seems to be local cell wall expansion during growth.

Polysaccharides need to be synthesized and integrated into the cell wall to maintain local flexibility and functional properties and to allow cell growth. The extracellular matrix resists the turgor pressure under conventional circumstances and this rigid structure needs to be relaxed when expansion occurs to increase the cell volume. At this level, cell wall organization and structure are relatively well described. But it is not really clear how dynamic processes like cell wall assembly and modification during growth occur. Single cell

organisms are ideal objects to explore these important cellular events. Influence of other cells is reduced and experiments can be more specifically applied. Pollen tubes (PTs), for example, are single cells with a dynamic, fast growing cell wall exclusively at the very tip and can be described as a single-cell organisms (Hepler et al., 2001). Therefore, PTs are a perfect model to study the dynamics of cell wall expansion and development on the cellular level.

1.2 FERTILIZATION AND POLLEN TUBE GROWTH

A fundamental process, polarized cell growth, reaches from PT growth in plants, to axon outgrowth in animals, hyphal growth in fungi and budding/mating in yeast cells (Cheung et al., 2010a). The coordination of turgor pressure, vesicle trafficking, ion fluxes, cytoskeletal structure, and cell wall formation play a major role in these high dynamic fast growing systems (Cheung and Wu, 2008). Pollen grains emerge from the anthers of the flowers in angiopsperms. A diploid meiocyte undergoes a meiotic division, subsequently forms a megaspore, and after a mitotic asymmetric division, a generative cell within the vegetative pollen grain is produced (McCue et al., 2011). Overall, a haploid pollen is the product of meiosis were a single cell divides several times to produce multicellular gametophytes. The growing pollen is considered to be a single-cell organism and the cytological organization is similar to that of vegetative cells, except it contains two sperm cells and it exhibits directed tip growth (Fig. 6). Additionally, the PT is a highly specialized, very fast growing cell and elongates with an incredible speed of 0.5 µm/min in *A. thaliana* and between 100 nm/s up to > 500 nm/s in *Lilium longiflorum* (lily) (Pierson et al., 1999; Dardelle et al., 2010).

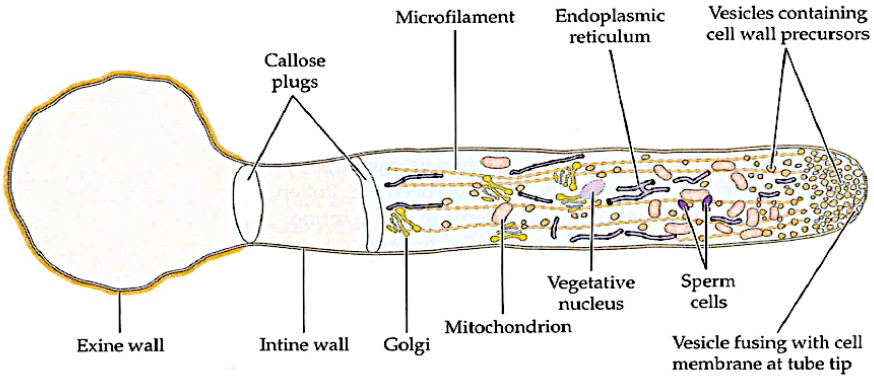

Figure 6: **Pollen tube structure and organization.** The pollen grain germinates and forms a pollen tube, which is essential for plant reproduction. Cellular organization of a PT after pollen germination is shown (Biochemistry & Molecular Biology of Plants: Buchanan, Gruissem, Jones, 2000).

Arabidopsis is a member of the angiosperms in the plant kingdom and plant reproduction occurs in general in the floral organ (Fig. 7A). The important unique process in plant development is the delivery of the two sperm cells by the male gametophyte through the process of PT growth to fertilize the egg cell. After penetrating the stigma surface in the closed style, PT growth occurs mainly in the transmitting tract (TT), were PTs must grow through various cell layers (Fig. 7B, C). PTs find their way from the surface of the stigma through the style, towards the micropyle of the female gametophyte (Lausser et al., 2010). Two different types of PT growth are generally recognized: (1) the short enclosed style of Arabidopsis described above (Fig. 7C) and (2) the open style of lily were the PT grow on the tissue surface in the open style to reach the ovary (Lennon et al., 1998).

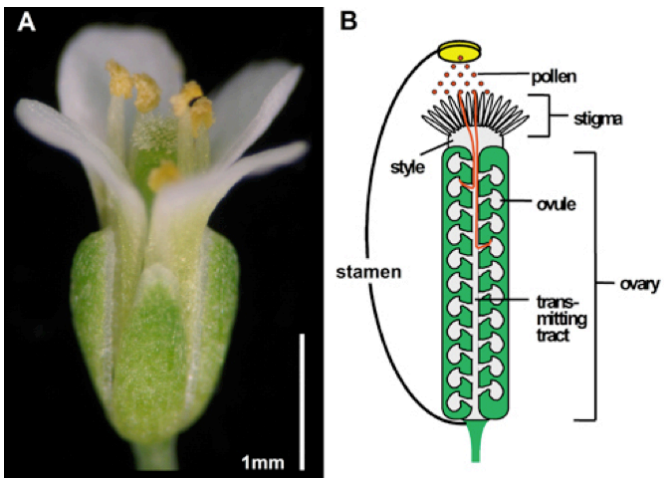

Figure 7: ***In vivo* fertilization and pollen tube growth.** (A) Arabidopsis wild-type flower (bar = 1mm). (B) Schematic principle of the fertilization process and PT growth. The pollen landing on the stigma, penetrates the papillar cells through the transmitting tract and grows towards the ovule to fertilize the egg. (C) *In vivo* callose staining shows PTs growing within the TT.

The longest growth phase of PTs in Arabidopsis *in vivo* occurs within the TT (Lennon et al., 1998; Crawford et al., 2007). PT elongation through the TT is not entirely clear. PT elongation is facilitated by the intercellular spaces and the cells of the TT undergo a breakdown when pollination takes place. It has been shown that PT growth supports programmed cell death (PCD) but the PT is apparently not required for the PCD of TT-cells (Lennon et al., 1998; Crawford et al., 2007). The movement of PTs within the TT is a not well understood non-random process. Factors supporting basal travel through the TT and lateral movement over epidermal surfaces towards the ovules are described rarely (Crawford et al., 2007). LUREs are species-specific cysteine-rich polypeptides (CRPs) and are known to be secreted by the synergid cells of the embryo sac of *Torenia fournieri*. In a morpholino antisense experiment (gene knock-down with synthetic antisense-RNA) LUREs were identified as diffusible chemoattractant(s) emitted by the egg cell to guide the PT in the last step of fertilization towards the micropyle (Okuda et al., 2009). Basically, movement of the PT is non-random and the whole path of fertilization involves two significant processes: (1) basal growth through the TT and (2) lateral movement towards the micopyle over epidermal surfaces. Species-specific differences in PT guidance increase tremendously the complexity of this very important field and a lot of work needs to be done to identify the exact mechanisms of fertilization.

1.3 POLLEN TUBE CELL WALL STRUCTURE

The exact structure of the cell wall depends on the type, function, and developmental stage of the cell. One of the best model systems to study cellular processes involved in polarity and directed tip growth are PTs (Boavida and McCormick, 2007). The PT is surrounded by a cell wall, which provides mechanical strength and allows expansion in one direction in the process of polar growth (Fig. 8A). PT tip growth is restricted to the extreme apex of the tube; it involves secretion at the plasma membrane and assembly of new cell wall components. The apical cell wall is plastic and incorporates new cell wall material. Especially pectic polysaccharides control the yielding mechanisms of tip growth (Bosch and Hepler, 2005). The PT cell wall shows mainly esterified pectins at the tip (Fig. 8B), which are presumed to provide a strong tensile surface that allows rapid cell expansion. During expansion, pectin in the more distal regions of the tube is demethylated by

pectin methyl-esterases (PMEs) leading to Ca^{2+} bridges and a stiffer pectin matrix. PME activity affects PT growth and leads to the assumption that PME regulation is essential for PT growth (Bosch et al., 2005; Cheung and Wu, 2008). Modified pectin of the PT is cross-linked to the cell wall, which consists of an outer cellulosic and an inner callosic layer. Callose and cellulose in the PT cell wall is mainly localized in the distal shank but absent in the tip (Fig. 8B; [Dardelle et al., 2010]).

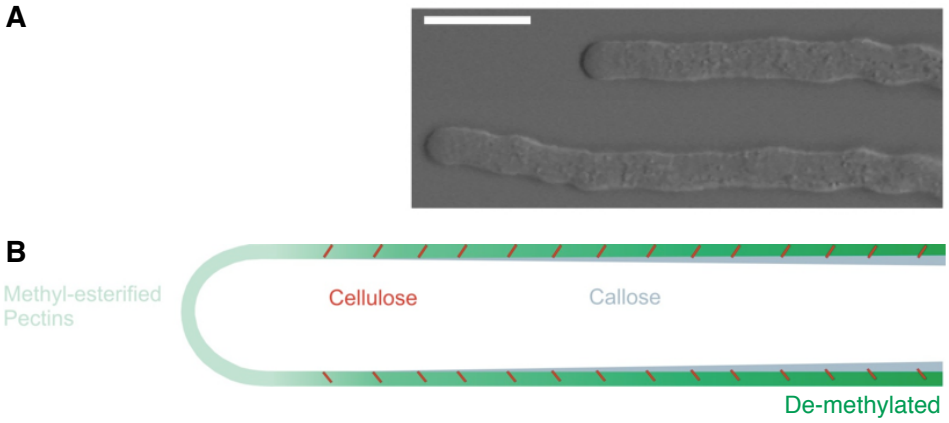

Figure 8: **Pollen tube cell wall structure.** (A) Arabidopsis wild-type PT tip growth observed over 10 min (bar = 10 µm). (B) Schematic picture of the PT cell wall. Methylation gradient from the tip towards the shank, cell wall pectin is mainly methylated in the growing zone and gets de-methylated during tube elongation. Adjacent to the tip, cellulose and callose is embedded to strengthen the cell wall (Chebli and Geitmann, 2007).

The cellulose content in PT cell walls is relatively low compared to walls of vegetative cells, a newly formed tube shows a high abundance of pectins, possibly to compensate for the reduced amount of cellulose (Geitmann and Parre, 2004). Therefore, a low cellulose content leads to the assumption that cellulose may not be the main stress-bearing component against turgor-induced tensile stress in circumferential direction (Ferguson et al. 1998; Aouar et al., 2009). Once the PT cell wall is part of the mature cylindrical region, no expansion in transversal or longitudinal direction is required. This leads to the assumption that the dynamic processes in the PT cell wall during tip growth are essential to withstand the internal turgor pressure and simultaneously maintain plasticity at the apex to allow directed tip growth. Both crucial factors, a highly

dynamic cell wall as well as the process of tip growth, remain to be investigated to evaluate the mechanisms involved in directed growth.

1.4 POLLEN TUBE PHYSIOLOGY

Cell wall dynamics during directed tip growth is a crucial factor in the process of PT elongation. Additionally, other processes contribute to PT tip expansion, which are not fully understand yet. For example, vesicle trafficking or streaming is dominant when directed PT tip growth is observed. New cell wall material and the factors required for tube elongation are delivered through this process to the tip. The vesicles form an "inverted cone" (also referred as clearing zone) seen by reverse cytoplasmic streaming (reverse fountain) back to the shank region of the PT (Fig. 9). The Golgi apparatus recycles cell wall precursors-containing vesicles through the endocytotic pathway, which derive from the subapical membrane and thereby contribute to the characteristic flow cycle pattern in a growing PT (Cheung et al., 2010b).

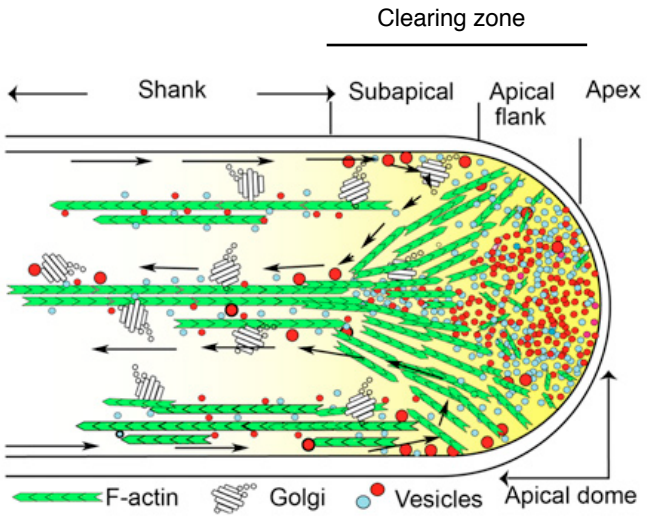

Figure 9: **Pollen tube vesicle flow and actin cytoskeleton organization in Tobacco.** Vesicles deliver precursors of cell wall material lateral to the apikal dome and build an "inverted cone" by reverse flow in the central region of the tube. Actin cytoskeleton is indicated green and follows the inverted retro-stream. Arrows trace the "reverse fountain" of the cytoplasmic streaming pattern (Cheung et al., 2010b).

Additionally, the subcellular structure in PTs reveal an elaborate and well organized dynamic actin cytoskeleton in the cytoplasm. Long lateral actin filaments (F-actin) reach the inverted cone region (Fig. 9) were short dynamic F-actin fibers aggregate and then are reorganized to long F-actin in the core cytoplasm (Vidali et al., 2001; Hwang et al., 2005; Cheung et al., 2010b). F-actin dynamics are regulated by F-actin-binding proteins. A pollen actin-binding protein LIM (L1LIM1) participates in PT elongation by stabilizing actin and simultaneously regulating of Ca^{2+} and H^{+} fluxes (Wang et al., 2008). The directed F-actin polymerization participates in PT elongation as a growth rate-limiting step, but the molecular mechanism of remodelling still remains to be elucidated (Vidali et al., 2001). Another cytoskeletal element, microtubules contribute to PT growth and support vesicle or organelle trafficking. PT organelles exhibit a clear ATP-dependent motor activity along microtubules similar to F-actin filaments in animal cells. It has been shown that motion of sperm cells and the vegetative nucleus are driven by cytoskeletal microtubuli (Astrom et al., 1995). Depending on the peripheral motor proteins, short-range movement of organelles along microtubuli occurs (Romagnoli et al., 2003). But the exact mechanism how microtubuli transport the generative cell, vegetative nucleus, and important organelles is far from established (Romagnoli et al., 2003). The cytoplasmic streaming of vesicles maintains an equilibrium of a membrane distribution between the cytoplasmic membrane and intracellular vesicles or organelles. This suggests that a very dynamic endocytotic vesicle recycling path is established during PT growth to facilitate rapid growth. However, reorganization and mechanisms of how crucial cytoskeletal elements contribute to polar PT growth are not completely elucidated yet.

1.5 POLLEN TUBE GROWTH REGULATION

Small ROP/RAC GTPases of the Rho-family are identified as signaling molecules playing a key role in cytoskeletal rearrangements in animal, plant, and yeast cells (Mucha et al., 2011). ROP GTPases (Rho of plants) or RACs promote downstream signalling and are identified as regulators of polarized PT growth. ROP/RACs are switching between GTP- and GDP-bound conformations by GTP-hydrolysis. The GTP-bound form is active and binding induces a conformational change, which allows the interaction with effectors to trigger the downstream signal (Mucha et al., 2011). Three classes of GTPase regulatory proteins are identified: (1) GEFs

(guanine nucleotide exchange factors) regulate the exchange of GDP to GTP for GTPase activation; (2) GAPs (GTPase activation factors) inactivate ROPs/RACs by converting the GTP- to the GDP-bound form; (3) GDIs (guanine nucleotide dissociation inhibitors) prevent from changing to the active GTP-bound form and avoid GEF binding (Wang, 2010). In PTs, GTP-bound ROP/RAC are localized at the tip and hydrolysis in the subapical region causes inactivation to maintain polarity. ROP-GDP is transported by GDIs from the plasma membrane into the cytoplasm to the extreme apex to close the cycle where GEF activates the ROP/RAC proteins again. ROPs/RACs induce apex-localized F-actin assembly and increase the cytoplasmic Ca^{2+} level to promote polar exocytosis of vesicles via different effectors (Mucha et al., 2011). FER (Feronia) a receptor-like kinase regulates female fertility by mediating PT reception, rupture, and sperm cell release (Escobar-Restrepo et al., 2007). FER is a potential upstream regulator of ROP/RAC-signalling during tip growth as shown for root hairs (Duan et al., 2010).

Ion fluxes are important aspects contributing to the elongation of PTs. The dynamics of ion signalling are controlled by influx (mediated by channels) and efflux (through pumps and antiporters) of ions through the PT plasma membrane. It is known that Ca^{2+} plays a role for the normal interaction between the PT and the female embryo sac in the fertilization process (Schiott et al., 2004). Ca^{2+} is considered to maintain a polar gradient in an elongating PT, which is restricted to the first 10-20 µm adjacent to the tip (Miller et al., 1992). Non-growing PTs do not show any Ca^{2+}-channel activity and Ca^{2+} gradients are absent (Malho et al., 1995). The Ca^{2+}-gradient is mediated by Ca^{2+} influx at the apex through putative strength-activated channels (Dutta and Robinson, 2004). It was also suggested that Ca^{2+} interacts with the cytoskeleton in the PT tip were it binds actin-binding proteins and regulates the structure or activity of F-actin (Cardenas et al., 2008). Arabidopsis mutants defective in the membrane associated Ca^{2+} activated ATPase revealed a reduced male fertility and show a reduced PT growth rate *in vitro* (Schiott et al., 2004).

PTs maintain a slight acidic tip based on increasing the pH around the base of the clear zone (Feijo et al., 1999). The PT tip pH is involved in actin remodelling and regulation in the subapical region were reverse cytoplasmic streaming occurs (Cheung and Wu, 2008). The tip-directed proton distribution is maintained by H^+ influx at the tip and efflux along the subapical membrane (Fig. 10).

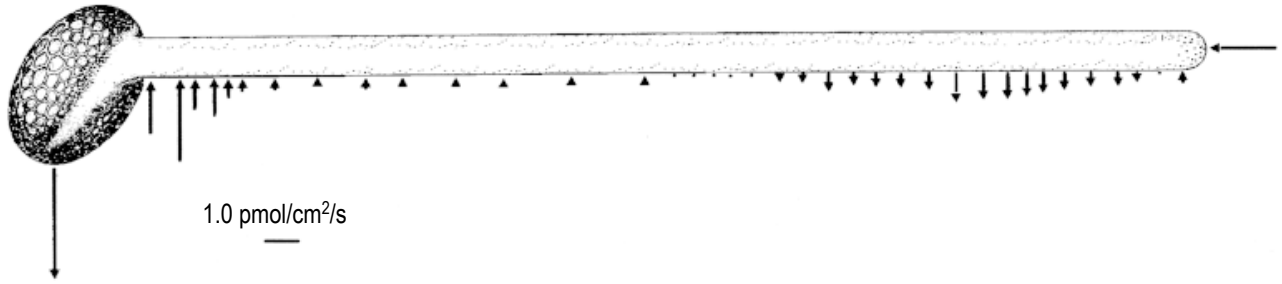

Figure 10: **Proton fluxes along the growing pollen tube (~800 µm long).** Proton effluxes driven by the PT membrane become a clear efflux in the behind the tip region. The influx domain is strong in the proximal 150-200 µm and characteristically strong at the tip (Feijo et al., 1999). Influx/efflux quantity indicated by bar = 1.0 pmol/cm^2/s

A notable process in tube elongation is the oscillatory pattern of *in vitro* grown PTs. The periodic oscillation of the growth rate is observed in lily PTs longer than 700 µm (Piersson et al., 1996). In lily PTs the period of growth oscillation is 20-50s and many of the underlaying processes also oscillate with the same period but in a different phase (Pierson et al., 1996; Chebli and Geitmann, 2007). Lateral H^+ fluxes are oscillating (Fig. 11 A) as well as the growth rate in PTs (Feijo et al., 1999). Intracellular Ca^{2+} (Fig. 11 B) at the apex of the PT may stimulate exocytosis (Fig. 11 C) and oscillates in a magnitude within the same period as the growth rate (Brewbacker and Kwack, 1963; Pierson et al., 1994; Roy et al., 1999; Cardenas et al., 2008). Anticipatory changes in cell wall material also contribute to the oscillatory growth pattern. Exocytosis and the amount of wall material are critical components and considered to predict and extend the rate of growth. Pectin secretion in the periplasmic space and turgor-driven embedding of the material in the cell wall matrix, together with Ca^{2+} chelation relaxes the cell wall and allows turgor-dependent PT extension. Therefore, exocytosis and incorporation of cell wall components emerge as potential regulators of the oscillation pattern in the rate of growth (McKenna et al., 2009).

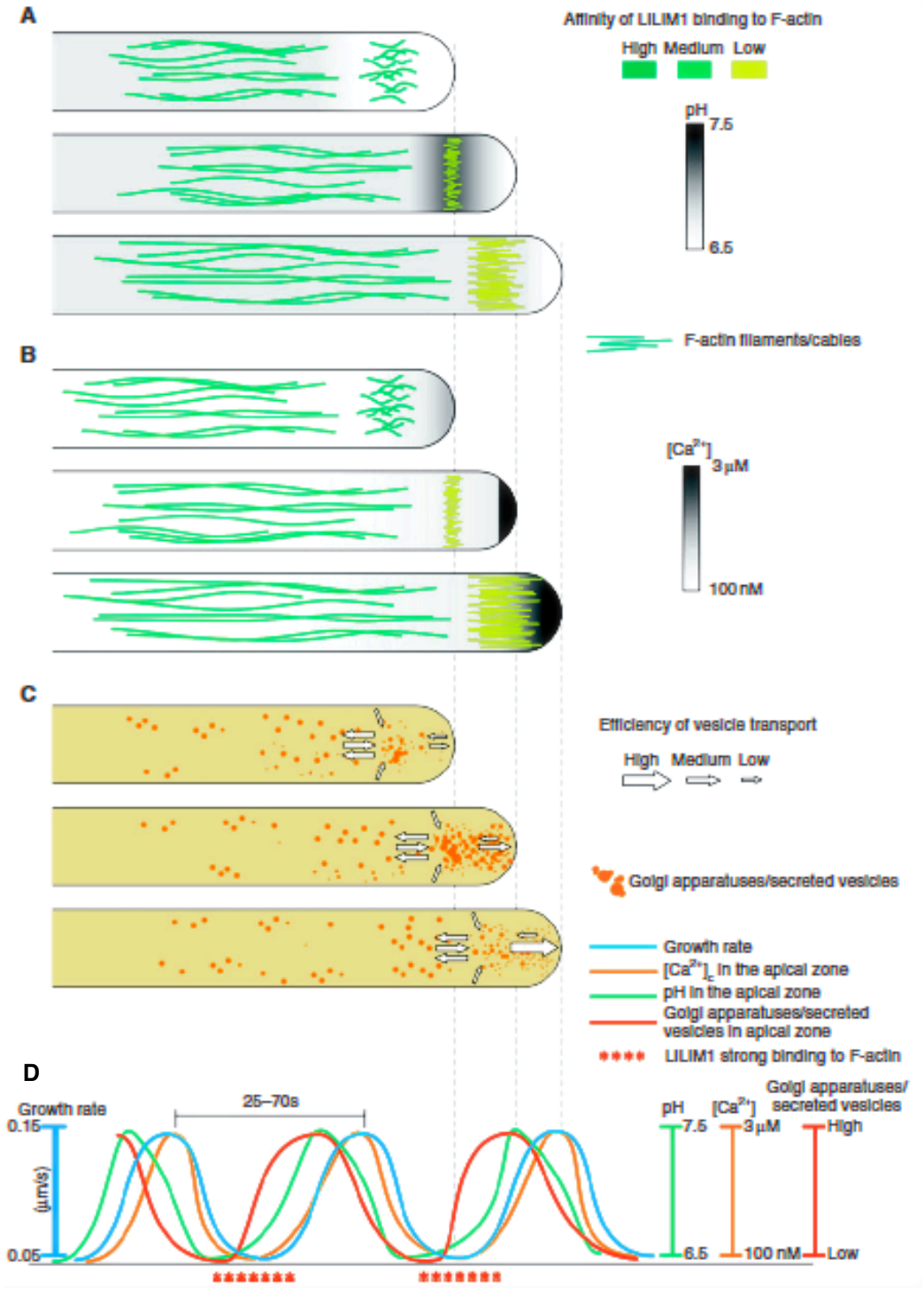

Figure 11: **Oscillatory patterns of calcium gradients, proton gradients, and exocytosis coupled with actin dynamics.** (A) and (B) Oscillatory patterns of the calcium and proton gradient coupled with actin dynamics regulated by L1LIM1 an actin-binding protein. Shown are three time points : (1) slow, (2) moderate and (3) fast growth. (C) Oscillatory pattern of vesicle transport. (D) Growth rate of the PT and apikal pH, calcium level and Golgi activity correspond to (A), (B) and (C). L1LIM1 mediates the Golgi apparatus and vesicle accumulation by actin binding at low pH and low calcium concentration. Increase of pH and calcium downregulates the L1LIM1 activity promotes tube elongation and actin filaments are generated for further fast growth. Vesicle stream towards the apex drives the fast growth rate and after exocytosis the decreased rate of vesicle streaming leads to slow growth. A decreased pH and a high calcium level follows a slow growth, which enhances L1LIM1 activity to strengthen actin filaments, and a new oscillatory period begins (Wang, 2010).

In summary, many different processes influence and contribute to PT elongation. The highly dynamic intracellular organization of PTs is a very complex system to elaborate and further experiments need to be done to identifiy the entire cellular regulation process of tip growth. Directed tip growth is a major event during fertilization and neither the “master regulator” nor the communication between the tip and the female tissue is clear. Many effectors like Ca^{2+}-gradient, pH-gradient, GTPases, cell wall components, cytoskeleton dynamics, PMEs, vesicle flow and oscillatory patterns contribute to the process of tip growth. It seems that a plethora of different contributors are necessary to perform the precise targeted process of fertilization.

1.6 POLLEN TUBE MECHANICS

Mechanisms involved in PT tip growth like vesicle transport, signalling, cell wall composition, and synthesis of the cell wall are relatively well described. For example, immunolocalization and cytochemical staining are methods to investigate the “steady state” of tip-growing cells. The turgor pressure is assumed to act as the driving force and must be maintained to allow cell enlargement (Eamus and Jennings, 1986). The results obtained from a pressure probe measuring the internal turgor pressure directly in a living PT revealed a relatively high pressure inside the PT. The pressure of a lily PT is constant about 0.2 MPa and the PT keeps the turgor pressure constant during elongation (Benkert et al., 1997). The correlation of the turgor pressure and embedding of new wall material seem to be determinants of PT extension (McKeena et al., 2009). Accordingly, cell morphogenesis depends on the process of deposition of new cell wall material at the cell surface and the mechanical deformation of this material by the stresses resulting from the turgor pressure (Dumais et al., 2006). When a force is applied to a polymeric substance, it undergoes a deformation (Cleland, 1972). In cell walls it is primarily shear deformation (change in shape but not in volume). The wall extends in the direction of the applied force and contracts in the other direction. Wall extension is considered to be elastic or reversible if the material reverts to its former size upon removal of the stress (Cleland, 1972). Therefore, a mechanical analysis starts with measurements of two types of variables: the relative elemental rates of wall expansion or strain rates (ε) and turgor-induced wall stresses (σ) described in Dumais et al. (2004). Stress is the force applied per unit area (1) and strain the deformation per unit length (2):

Tensile stress for a linear elastic material is:

$$\sigma = F / A \qquad (1)$$

Tensile strain for a linear elastic material is:

$$\varepsilon = (L - L_o) / L_o \qquad (2)$$

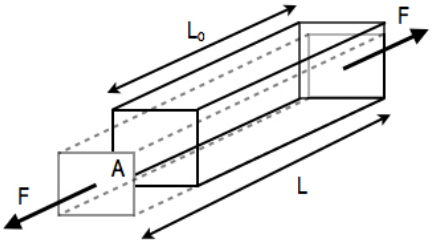

F : Force applied on an object under tension
A : Area through which the force is applied
L_o : Original length of the object
L : Length after the force is applied

The stress to strain ratio of an elastic is material follows Hooke's law (Hooke's law: the extension of a spring is in direct proportion with the load applied on it). Therefore, is σ direct proportional to ε in the stress-strain curve:

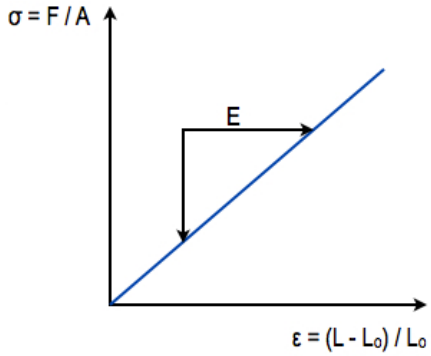

This extensibility is defined as the elastic modulus or Young's modulus (E). E describes the mechnical resistance of a material during elongation or compression. Therefore, E is a parameter to quantify the stiffness of a linear elastic material (Geitmann, 2006), it is calculated by dividing σ by ε:

$$E = \sigma / \varepsilon$$

Where E is the ratio of stress [Pa] to strain, which is dimensionless, therefore, E has the SI unit of pressure in pascal [Pa] or [N/m^2].

To characterize cell wall properties, mechanical principles, and to measure the Young's modulus of a living PT, a new method, the Cellular Force Microscope (CFM), was established. Novel methods need to be

applied on cellular systems to explore correlations and relationships between important processes during PT tip growth, which are difficult to describe with conventional methods.

1.7 CELLULAR FORCE MICROSCOPY

Several methods like Atomic Force Microscopy (AFM) or micro-indenter techniques have been described to measure the local elasticity of cell walls (Geitmann and Parre, 2004; Zhao et al., 2005; Zerzour et al., 2009; Peaucelle et al., 2011). The deflection of an AFM cantilever (100-400 µm in length and 10-50 nm in curvature) on a elastic sample is monitored and the deformation during a loading and unloading cycle gives a "force curve". The data show the relationship between deformation and applied force and are fitted into a mathematical model (i.e. finite elements), which is describing the mechanics to extract data to calculate the elastic properties of the material. The elasticity is later on described by the Young's modulus, which gives the mechanical resistance of a material during elongation or compression (Cleland, 1972; Zhao et al., 2005).

The new flexible, microrobotic system CFM is used to measure and apply defined forces on PTs and plant tissues (details see Felekis et al., 2011; Routier-Kierzkowska et al., 2012). A probe tip mounted on a Micro-Electromechanical System Sensor (MEMS) indents the cell wall, while the applied load and the displacement of the tip are observed. From the force-displacement curve, a slope is calculated and the stiffness values are extracted (Routier-Kierzkowska et al., 2012). The extracted force values in general depend on the MEMS sensor (5 nN to 10 mN) and the displacement values depend on the positioner (scanning range 27 mm in all directions with a resolution of 5 nm) mounted on the system (Chapter 2). The force applied on the material correlates with the stiffness of the material. The observed stiffness is not only reflecting the elastic properties of the cell wall. Additionally, the turgor pressure, the geometry of the probe tip, the cell itself, and mechanical stress prior to indentation influence the CFM measurements. This affects the actual stiffness of the cell wall and for that reason, it is referred to as "apparent stiffness" (Zamir and Taber, 2004; Routier-Kierzkowska et al., 2012). To measure the apparent stiffness of the PT cell wall, turgescent and plasmolysed PTs are measured by CFM. The measured data are processed and fitted into a PT finite element model to determine cell wall properties, turgor pressure and Young's modulus of the cell wall of living PTs.

1.8 AIM OF THESIS

The cell wall is a very complex dynamic structure and cell growth is a controlled very important process, which allows asymetric or directed cell expansion. A subset of numerous identified enzymes and polymers have been identified to be essential for cell wall synthesis and expansion. But the assembly of the complex cell wall network and the ongoing process of cell expansion is still not fully understood. Cell wall polysaccharides, proteins, and inorganic compounts contribute differently to cell wall flexibility. It is still a subject of ongoing discussion how a plant survives when fundamental structural cell wall elements are absent. Furthermore, synergistic effects that drive cooperative relationships of cell wall polymers during growth are not clear, yet. The aim of this thesis was to contribute to the understanding of the mechanism that affect cell wall expansion in pollen tubes (model organisms: *Lilium longiflorum, Arabidopsis thaliana*) by mechanical, genetical and biochemical characterization of parameters determing directed cell growth:

i. A novel microelectromechanical (MEMS) based system the Cellular Force Microscope (CFM) combined with a provided pollen tube model had to be established in an interdisciplinary environment. The relationship between turgor pressure, cell wall thickness, and cell wall expansion of a living elongating pollen tube is a very important issue.

ii. Cell wall mutants provide a base to investigate biochemically, genetical, and cytomechanically relevant compensatory effects that facilitate cell wall expansion in a disordered system. The effect of the absence of XyG on PTs was investigated.

iii. Identification and biochemical analysis of cell wall-related proteins and modifiers affecting cell wall development. The importance of LRX-type proteins in PTs and their contributions to tip growth is investigated.

iv. Another objective was the study of cell wall-related proteins involved in cell wall development and their contributions to cell wall regulation. To analyze the effect of LRX-type proteins on cell walls, *lrx3*, *lrx4*, and *lrx5* mutant lines were used as a model system and changes in the cell wall structure were investigated.

This systems biology approach is based on the combination of mechanical with experimental data of PTs to investigate growth and cell wall development. Biomechanical insights explain properties of growth by incorporating physiological data into a model to calculate the Young's modulus a value, which describes quantitatively physical properties of the wall. This thesis focuses on the relevance of mechanical properties of cell walls, synergistic effectors in cell development, and cell wall growth regulators in PT growth.

2. THE POLLEN TUBE: A SOFT SHELL WITH A HARD CORE (SUBMITTED)

Authors

Hannes Vogler[1], **Christian Draeger**[1], Alain Weber[2], Dimitris Felekis[3], Christof Eichenberger[1], Anne-Lise Routier-Kierzkowska[2], Aurélien Boisson-Dernier[1], Christoph Ringli[1], Bradley J. Nelson[3*], Richard S. Smith[2*] and Ueli Grossniklaus[1*]

Addresses

[1]Institute of Plant Biology and Zürich-Basel Plant Science Center, University of Zürich, Zollikerstrasse 107, CH-8008 Zürich, Switzerland

[2]Institute of Plant Sciences, University of Bern, Altenbergrain 21, CH-3013 Bern, Switzerland

[3]Institute of Robotics and Intelligent Systems, ETHZ, Tannenstrasse 3, CH-8092 Zürich, Switzerland

* Corresponding authors

Contributions to the submitted manuscript were performed in collaboration with Dr. Hannes Vogler:

Handling and germination of lily pollen tubes (PTs) *in vitro*. Stiffness measurements of PTs were performed to establish the Cellular Force Microscope (CFM). Osmotic treatmens to characterize the elastic properties of the cell wall. Cell wall staining and confocal microscopy to measure the cell wall thickness of a living lily PT. Measurement of cell wall thicknesses and diameters important for data implementation into the Finite Element Model (FEM). Communication of data important for the developmental process of the CFM software and the FEM of lily PTs.

2.1 SUMMARY

Cell expansion is controlled by a fine-tuned balance between intracellular turgor pressure, cell wall loosening, and cell wall biosynthesis. To understand these processes, it is important to gain in-depth knowledge of cell wall mechanics. Pollen tubes are tip-growing cells that provide an ideal system to study mechanical properties at the single cell level. With available approaches it was not easy to measure important mechanical parameters such as the turgor pressure and the elasticity of the cell wall. We used the novel Cellular Force Microscope (CFM) to measure the apparent stiffness of lily pollen tubes in combination with a mechanical model, based on the Finite Element Method (FEM), to calculate turgor pressure and cell wall elasticity, which we found to be around 0.3 MPa and 20-90 MPa, respectively. Furthermore, and in contrast to previous reports, we showed that the difference in stiffness between the pollen tube tip and the shank can be explained solely by the geometry of the pollen tube. CFM in combination with a FEM-based model provides a powerful method to evaluate important mechanical parameters of single, growing cells. Our findings indicate that the cell wall of growing pollen tubes has mechanical properties similar to rubber. This suggests that a fully turgescent pollen tube is a relatively stiff, yet flexible cell that can react very quickly to obstacles or attractants by adjusting the direction of growth on its way through the female transmitting tissue.

2.2 INTRODUCTION

Mechanical properties of cells and tissues have become an important aspect in understanding biological processes. During morphogenesis, mechanical stimuli were recently shown to be involved in the induction of embryonic development (Fernandez-Sanchez et al., 2010) and in the control of growth processes in both animals and plants (Martin, 2010; Mirabet et al., 2011).

Here, we study the mechanical properties of pollen tubes, which are extremely fast growing cells that cover large distances to deliver the male gametes to the female gametophytes in the ovary of flowering plants. Since growth is restricted to the tube tip, the cell wall in this area must be deformable and is subject to a highly dynamic integration of new cell wall and membrane material, whereas in the distal part (shank), the wall is more static to resist turgor pressure. A lot is known about the molecular regulation of pollen tube growth

(reviewed in (Qin and Yang, 2011; Hepler et al., 2012)), but only recently the instrumentation to study the mechanical aspects of cell expansion *in vivo* has become available (Geitmann and Parre, 2004; Parre and Geitmann, 2005; Zerzour et al., 2009).

Turgor pressure is the driving force of plant cell expansion, a process that is limited by the capability of the cell wall to extend. The plant cell wall is a complex composite material composed of cellulose microfibrils that are connected by a hemicellulose network and embedded in a pectin matrix containing structural proteins (reviewed in (Cosgrove, 2005; Burton et al., 2010)). Precise control of the internal pressure and stress relaxation in the cell wall allows for cell expansion.

From a mechanical point of view, the cell wall is under tensile stress created by turgor pressure (Wei and Lintilhac, 2007). Because growth depends largely on the in-plane extension of the cell wall, it is important to directly measure in-plane elasticity. Several methods have been described to measure the Young's modulus, which is a measure of the stiffness of a linear elastic material (Geitmann, 2006). Tensile tests have been applied to isolated cell wall compounds, intact isolated cell walls, or entire pieces of tissue using extensiometers (Chanliaud and Gidley, 1999; Edge et al., 2000; Cosgrove, 1993; Kutschera, 1996; Wei et al., 2006). However, experiments on single, living cells are rare, mainly because it is difficult to isolate individual cells from tissues without damaging the cell wall. Furthermore, tensile tests have the disadvantage that it is not possible to measure local differences in the mechanical properties of the cell walls of individual cells.

Pressure probes have been used to identify elastic properties of single cells by applying changes in turgor pressure. However, the method is invasive and, thus, does not allow the experimenter to make several measurements in different areas of the same cell. As a consequence, as in the case of tensile tests, it is not possible to find local differences in the mechanical properties of the cell wall (reviewed in (Tomos and Leigh, 1999)).

Nano- or micro-indentation approaches determine cellular stiffness by causing minute, local deformations of the cell and measuring the resulting forces. Atomic force microscopy (AFM) has proven to be instrumental for measuring the local elastic properties of single cells like fungal hyphae (Zhao et al., 2005) as well as of entire tissues, such as the shoot apical meristem (Milani et al., 2011; Peaucelle et al., 2011). Similar

in concept but using larger probes, micro-indentation techniques have been used to assess the mechanical properties of pollen tubes (Parre and Geitmann, 2005). Both methods do not damage the cell and are, therefore, suitable to measure the stiffness of single cells or tissues. While AFM offers a high degree of automation and resolution, it has a limited scanning area and the applied forces are too small to sufficiently indent the wall of fully turgid cells. Hence, the cell wall is compressed on a tiny surface rather than stretched, such that only conclusions about the elasticity perpendicular but not parallel to the surface can be drawn. The larger micro-indentation device provides more flexibility in the scanning range and is capable of measuring in-plane elasticity but lacks automation and is not commercially available. In all of these indentation methods the stiffness measured does not only reflect the mechanical properties of the cell wall. Additional parameters that contribute to the cellular stiffness are turgor pressure (Smith et al., 1998; Wang et al., 2004) as well as cell and indenter geometry (Bolduc et al., 2006). Therefore, obtained stiffness values are referred to as “apparent stiffness” (Zamir and Taber, 2004).

Despite of the huge amount of work that has been invested into the determination of the mechanical properties of pollen tubes, there are still considerable gaps in our knowledge. The values for turgor pressure vary by a factor of three or more, depending on the measuring method (Benkert et al., 1997). No values at all are available for the Young’s modulus, a measure of elastic properties, of the pollen tube cell wall. Here we use a Cellular Force Microscope (CFM), a novel, flexible microrobotic system in combination with osmotic treatments, to measure the mechanical properties of living and growing pollen tubes in a non-invasive manner. The CFM utilizes commercially available microelectromechanical system (MEMS)-based capacitive force sensors with a resolution of 5 nm and a wide force range from 5 nN to 10 mN (Felekis et al., 2011). The modular composition of the CFM provides great flexibility in the choice of microscope optics as well as micropositioners, depending on the needs for scanning range (up to several centimeters), precision of movement, and scanning amplitudes. Recent work showed that CFM is useful for stiffness mapping on both tissues and single cells. Combined with a mechanical model, CFM measurements revealed the mechanical effects of turgor pressure on the apparent stiffness of onion epidermal cells (Routier-Kierzkowska et al., 2012).

To compare and contrast the CFM approach with existing methods, we measured the stiffness of lily (*Lilium longiflorum*) pollen tubes. Previously published work allows for a direct comparison of our results with data produced with the micro-indentation technique. The CFM delivers apparent stiffness values that are in agreement with published data, showing that the pollen tube apex is apparently softer than the shank (Geitmann and Parre, 2004; Zerzour et al., 2009). Our interpretation of the data, however, is different. Using a modeling approach, we show that the difference in the apparent stiffness between the apex and the shank is not necessarily a result of different wall material properties in these regions but can be explained exclusively by the geometry of the pollen tube. Our mechanical model of the pollen tube, based on the finite element method (FEM), allows us for the first time to extract turgor pressure and the Young's modulus of growing lily pollen tubes by combining measurements of the apparent stiffness with changes in geometry that result from osmotic treatments.

2.3 RESULTS

Features of the Cellular Force Microscope (CFM)

For the automated micro-mechanical characterization of living and growing pollen tubes we developed a versatile system capable of characterizing living cells and organisms of highly diverse and changing morphology under different physiological conditions *in vivo*. By automating the measuring procedure, we were able to conduct multiple, high-resolution stiffness measurements over multiple samples in a small time interval on growing lily pollen tubes.

To achieve this goal, we designed and developed the experimental setup shown in Figure 1. The system consists of a commercially available MEMS-based force sensor attached to a three-axis positioning system with a scanning range of 27 mm and a resolution of 5 nm along each axis (boxed area in Figure 1a and Figure 1b) that was mounted on a custom-made stage on an optical, inverted microscope. Further components are a data acquisition system (DAQ card) and a position control unit (Figure 1a). For the control of automated tasks and data logging we designed a custom application in the LabVIEW software.

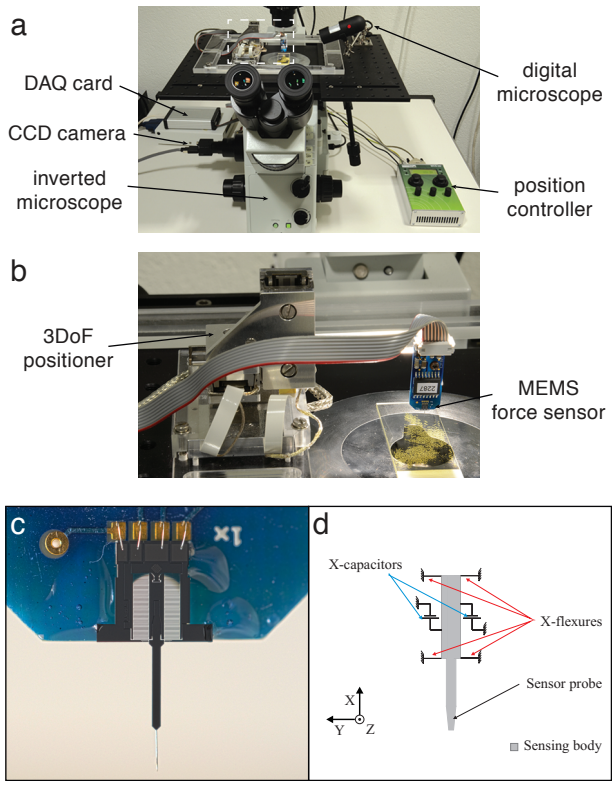

Figure 1: **The Cellular Force Microscope system**
a Overview of the CFM system showing the inverted microscope with a CCD camera and a digital microscope for MEMS sensor positioning enhancement, the data acquisition (DAQ) card, and the position controller to operate the three-degrees-of-freedom (3DoF) micropositioner (boxed area). **b** Magnification of the boxed area in **a,** showing the 3DoF micropositioner equipped with a MEMS force sensor. **c** Photograph of the MEMS sensor with a mounted 400 nm radius probe tip. **d** Schematic principle of a single axis MEMS-based capacitance microforce sensor without the attached tip.

The choice of the probe diameter depends on the properties to be characterized. In this work local elastic properties at the subcellular level were of interest, thus a sharp probe with a radius of 0.4 µm and 2 mm length was attached to the MEMS-based force sensor, which allows measurements in the sub-micronewton range (Figure 1c). The sensor probe is positioned vertically above the glass slide containing the lily pollen tubes to be measured. Figure 1d shows a schematic representation of the MEMS-based force sensor.

Apparent stiffness measurements on living pollen tubes

In order to measure the apparent stiffness of turgescent, growing lily pollen tubes we germinated pollen on glass slides. Good attachment of the tubes to the slide surface is crucial. Therefore, we tested several slide coatings and found that silane works best. After initial manual positioning of the sensor probe at the tip of the pollen tube, software-controlled measurements were taken every 5 µm along the tube axis.

As the pollen tubes continued growing during the experiment, we had to correct for the distance from the tip by taking into account an average growth rate of 135 nm/sec (± 21nm/sec, n=7), multiplied with the average time interval between two measurement points of 12.4 sec (± 0.9 sec, n=6). From this we calculated a relative movement of the sensor probe away from the tip of 6.7 µm per interval. We found a sharp increase in the apparent stiffness from 2.7 N/m to 3.8 N/m over the first 20 µm, after which a plateau was reached (Figure 2a and c, upper curve). This compares fairly well with previous micro-indentation experiments reporting 1.3 N/m at the tip to 1.9 N/m 50 µm behind the tip for lily (Zerzour et al., 2009), and a similar increase in apparent stiffness in the first 20 µm for pollen tubes of *Papaver rhoeas* (poppy) (Geitmann and Parre, 2004). Pollen from different anthers showed considerable variability in the apparent stiffness of the tubes, ranging from 1.8 N/m to 4.5 N/m in the plateau phase.

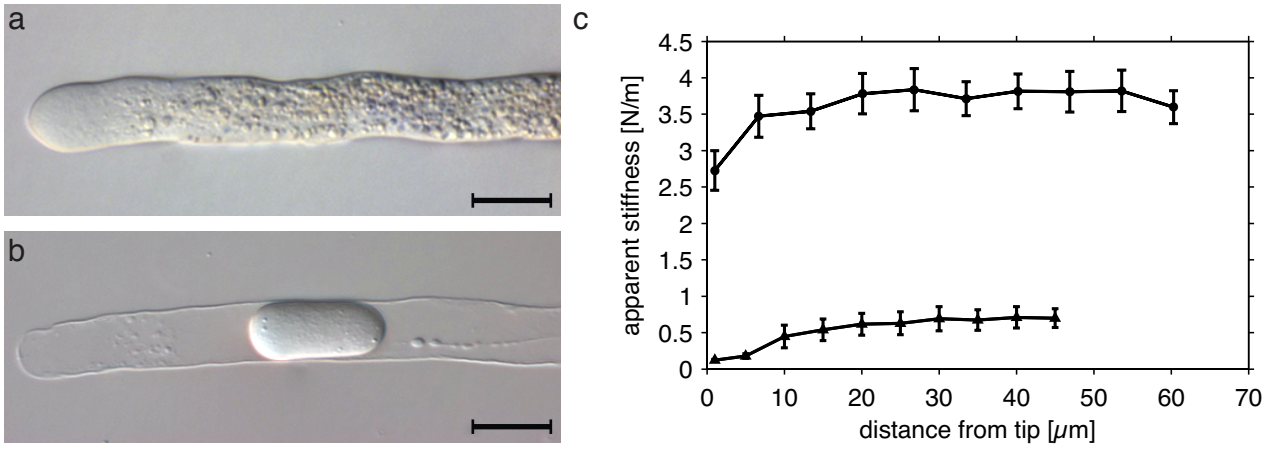

Figure 2: **Apparent cell wall stiffness of turgescent and plasmolysed lily pollen tubes**
a Turgescent and **b** plasmolysed lily pollen tube (size bar = 30 µm). **c** Cellular stiffness in the tip region of lily pollen tubes. The upper and lower curves represent the apparent stiffness of the turgescent and the plasmolysed pollen tube respectively.

In order to determine the contribution of turgor pressure to the measured stiffness, we released the pressure from the pollen tubes by replacing the growth medium with 15% mannitol to induce plasmolysis (Figure 2b). To ensure comparability, we used pollen from the same anther and germination experiment for the measurements on turgescent and plasmolysed pollen tubes, respectively. After decompression, we found a reduced apparent stiffness of 0.1 N/m at the tip, which gradually increased to 0.7 N/m (Figure 2c, lower curve). Osmotically treated pollen tubes stopped growing but were still alive as evidenced by the fact that they resumed growth after returning to normal osmotic conditions. Hence, the distance from the tip increased by 5 µm per measuring point. The difference between turgescent and plasmolysed samples implies that turgor pressure makes a large contribution to the apparent stiffness of growing tubes and, therefore, has to be considered as an important parameter for the estimation of the elastic properties of the pollen tube cell wall.

Determination of geometrical parameters

Since the cell wall is under tension induced by turgor pressure, release of turgor leads to shrinkage of the pollen tube. The magnitude of shrinkage can be used to characterize the elastic properties of the cell wall material. To quantify shrinkage after decompression we induced plasmolysis and determined the change in both length and the diameter along the pollen tube axis.

Measurements were taken at different distances from the tip over 200 µm, resulting in a mean diameter of 16.0 µm (± 0.7 µm, n=10). After plasmolysis, we found a reduction in the mean diameter to 13.4 µm (± 0.7 µm, n=10), which corresponds to shrinkage of the tube's diameter of 16.1 % (± 2.4 %, n=10; Figure 3a). In the longitudinal direction, the average shrinkage was 7.5 % (± 1.95 %, n=10), resulting in a ratio between circumferential and longitudinal shrinkage approximating 2:1. For cylindrical cells, the tensional stress in the surface plane of the cell wall is predicted to be twice as high in the circumferential as in the longitudinal direction (Schopfer, 2006). Thus, our data are consistent with a low degree of anisotropy in the wall material, which is expected for pollen tubes without an ordered arrangement of cellulose microfibrils (Anderson et al., 2002; Aouar et al., 2010).

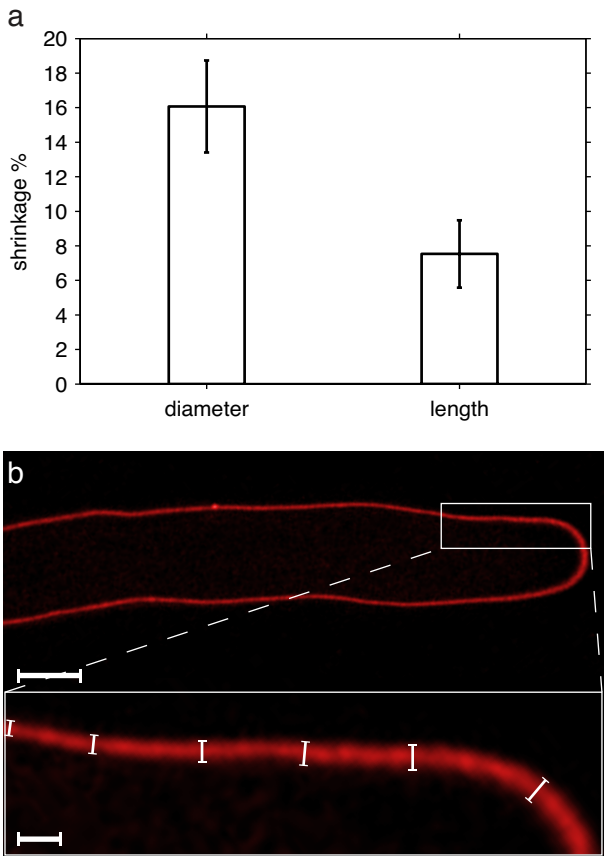

Figure 3: **Analysis of osmotic shrinkage and cell wall thickness**
a Relative shrinkage of lily pollen tubes after osmotic treatment. Pollen tube diameter and length from the tip to the pollen grain were measured before and after plasmolysis respectively (data are represented as mean ± SEM, n=10). **b** Confocal section of a PI stained lily pollen tube subjected to deconvolution to measure cell wall thickness (size bar = 10 µm). Multiple measurements were taken in the apical 50 µm of five pollen tubes (data are represented as mean ± SEM). The inlay shows a magnification of the boxed area with measurements in the tip region (size bar = 2 µm).

Another important parameter is cell wall thickness. The thinner the cell wall, the stiffer it needs to be to withstand a given tensional stress (Wang et al., 2004). Transmission electron microscopy (TEM) images suggested a wall thickness of 200-300 nm in the tip region of lily pollen tubes (Lancelle and Hepler, 1992; Lancelle et al., 1997). However, it cannot be excluded that these relatively thin walls are the result of shrinkage due to sample preparation as they were dehydrated for TEM. Differential interference contrast (DIC) images of plasmolysed pollen tubes under our conditions (Figure 2c) indicated a cell wall thickness of about 700 nm. Since it is not straightforward, however, to determine such small structures at the magnification we used from DIC images (McKenna et al., 2009), we also used confocal laser scanning microscopy (CLSM) to measure cell

wall thickness. We stained growing pollen tubes with Propidium Iodide (PI), a fluorescent dye that stains pectins in the cell wall without affecting cytoplasmic streaming and thus pollen viability (Tian et al., 2006). Confocal sections of PI stained tubes were deconvolved and measurements were taken at different positions of the cell wall within the apical 50 µm, giving an average value of 699 nm (± 65 nm, n=5; Figure 3b). Taking into account that this could still be an overestimation due to light scattering, we used 700 nm based on CLSM and 200 nm based on TEM as the upper and lower range limits, respectively, for the wall thickness parameter in a finite element model of the pollen tube.

Finite Element Model of the pollen tube

Apparent stiffness measurements reflect a combination of mechanical and geometrical properties. In order to separate the various influences on stiffness, it is essential to fit the data with a mechanical model that captures all of the relevant aspects. In the following section we present a quasi-static continuum mechanics model of a pollen tube, in which we reproduce our osmotic and CFM measurements. The model is subdivided into two steps: The first step describes the inflation of a pollen tube section due to osmotic water uptake. The second step simulates the contact of the inflated structure during indentation with a rigid probe, i.e. the MEMS-based force sensor.

The initial geometry of the pollen tube is represented by a cylindrical shell, which is attached to a hemispherical shell with radius and thickness based on microscopical data. The length of the section is chosen to be large enough to minimize the influence of boundary conditions, which are applied to the distal circular edge (Figure 4a).

Cellulose is thought to be the main load-bearing constituent in the cell wall. If it is deposited in an oriented manner, the cell wall is likely to show mechanical anisotropy (Fry, 1995; Erickson, 1976; Schopfer, 2006). Although our shrinkage experiment suggests rather isotropic properties of the pollen tube cell wall, we cannot exclude a certain degree of anisotropy. To allow for this possibility, we assigned the shell with an orthotropic, linear elastic material model. This constitutive model is able to capture different elastic behavior in longitudinal and circumferential direction. It is fully characterized by the compliance matrix, which relates

stresses and strains (see supplemental information), and three material directions that describe the structural anisotropy in each point. The parameters within the compliance matrix are called engineering constants. Three Young's moduli describe elasticity in one direction when the material is subject to loading in the same direction. Six Poisson's ratios, of which three are independent, describe how much the material stretches in one direction due to loading in a different direction (Poisson effect). Finally, three shear moduli describe shear flexibility.

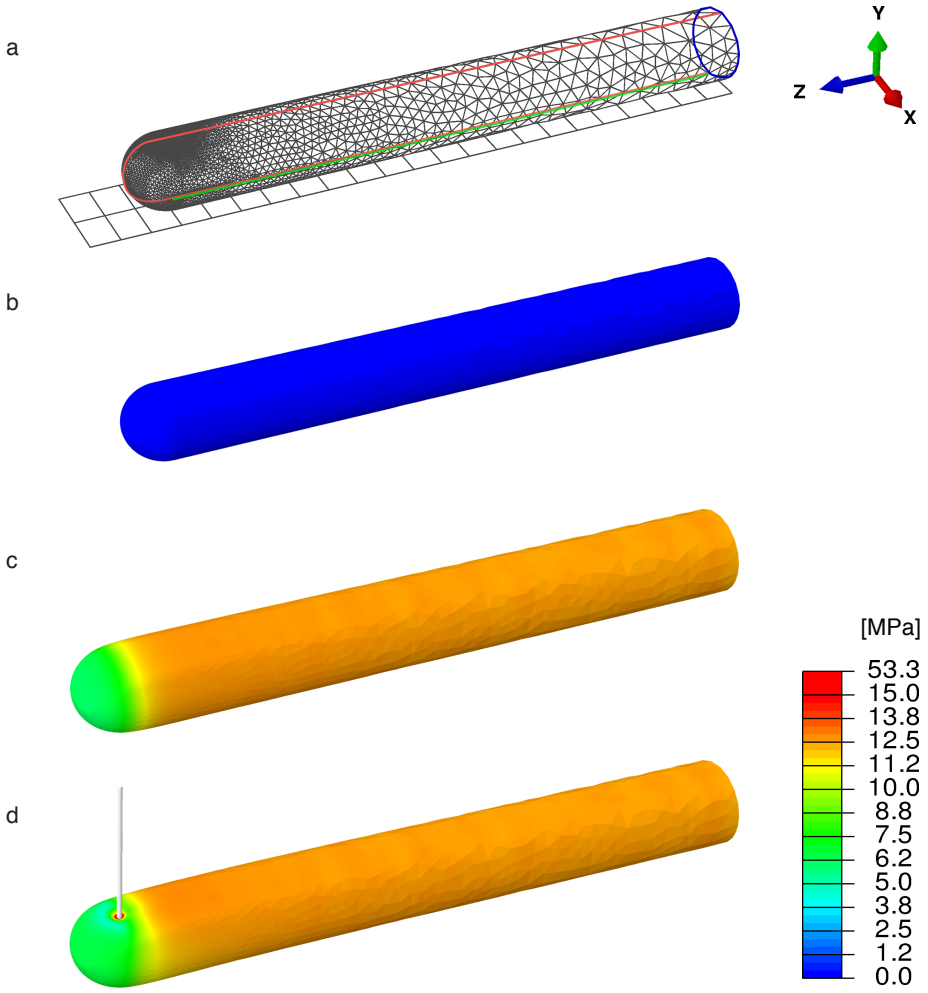

Figure 4: **Finite Element Model (FEM) of the pollen tube**
a Boundary conditions and mesh resolution of the FEM simulation. Boundary conditions were applied during the "inflation" and "indentation" step. Nodes on the red line were prevented to move in x-direction during both steps. Nodes on the green line were prevented to move in y-direction during both steps, and in z-direction only during the "indentation" step. Nodes on the blue line could not move in z-direction during both steps. The mesh was iteratively refined to provide higher accuracy near the contact patch. **b, c, d** Stress-distribution at three stages of the simulation. The stress-free reference configuration **b** was first pressurized **c**. Note the differences in maximum principal stress between the apex and the cylindrical part. In a second step, the pressurized structure was indented by a rigid probe in y-direction. This resulted in a local stress concentration **d**. Color code denotes the maximal principal stress in MPa.

Since we were not able to fit nine independent parameters, we made several assumptions on the mechanics of the cell wall. In particular we assumed that: (i) the material is fully compressible (i.e. all Poisson's ratios are zero); (ii) the first material direction is normal to the cell wall, the second one is pointing in circumferential and the third one in longitudinal direction (tangential to the wall surface); and (iii) all shear moduli equal $E_l/2$, where E_l denotes the longitudinal Young's modulus.

Assumption (i) implies that strain in any direction depends only on the stress in that direction. This is the most controversial assumption and its effects are discussed in the supplemental information. Assumption (ii) defines the local material orientation by assuming that a possible reinforcement would occur in circumferential direction. Finally, the choice of the shear moduli in assumption (iii) equals the one that we would expect for a fully compressible, isotropic material of stiffness E_l. This assumption is of low importance since shear stresses were significantly lower than principle stresses in all simulations.

The model includes two quasi-static steps. In a first step, the virtual pollen tube (Figure 4b) is inflated by a uniform pressure, which acts on the inside of the cell wall. As a result, the shell extends in circumferential and longitudinal direction (Figure 4c). The exact amount depends on the dimensions of the shell, the amount of turgor pressure, and the material coefficients. Since we chose the material to be fully compressible, extension in longitudinal and circumferential direction are independent. Although the geometry of the pollen tube is not perfectly cylindrical, the global deformation obeys quite closely the formula for stress distribution in a cylindrical pressure vessel. If the formula for stress distribution is combined with the material law, it reads:

$$\frac{Pr}{d} = \sigma_c = E_c \cdot \log(\lambda_c) \quad , \quad \frac{Pr}{2d} = \sigma_l = E_l \cdot \log(\lambda_l)$$

where P is the turgor pressure, r is the radius and d the thickness of the cylinder, σ_c (resp. σ_l) are Cauchy stresses, E_c (resp. E_l) are Young's moduli, and λ_c (resp. λ_l) are the initial stretch ratios in circumferential (resp. longitudinal) direction. It should be noted that the initial stretch ratios only depend on the dimensionless

quantity pressure over Young's modulus. This means that a certain stretch ratio can be reached by either having a soft material and little pressure or a stiff material and high pressure.

In the second step of the simulation, the pressurized shell is indented with a rigid probe, which has the shape of a hemisphere that is connected to a cylinder. The scanning mode of CFM is simulated by placing the probe at varying distances from the tip and by moving it vertically in small steps. Once the probe touches the pollen tube, a frictionless contact between the pollen tube and the probe (resp. the supporting plane) is simulated (Figure 4d). Depending on the surface geometry, the force exerted onto the probe by the pollen tube might not be aligned with the axis of indentation. Since the CFM sensor is designed to only measure forces in the direction of indentation, the vertical component is used for stiffness computations. The apparent stiffness is then calculated as the change in force over the change in vertical displacement. During both steps of the simulation, the same set of boundary conditions described in Figure 4a are applied.

Finite Element Model-based simulation reveals turgor pressure and Young's modulus of pollen tubes

To test our model we used the parameters summarized in Table 1. A point 40 µm behind the tip was fitted with the apparent stiffness data we measured before (Figure 2c, see supplemental information for details). The simulation revealed an apparent stiffness pattern very similar to what we found in our measurements (compare Figure 5 with Figure 2c, upper curve). Moreover, we did not find any notable differences in the apparent stiffness between model fits done with a cell wall thickness of 200 nm and 700 nm, respectively.

Table 1: **Model Parameters**
r_{ref} = reference radius, l_{ref} = length of reference modeling section, λ_c= circumferential stretch ratio, λ_l= longitudinal stretch ratio, r_i = indenter radius

Pollen tube parameters					Indenter parameters		Experimental parameters	
r_{ref} [µm]	l_{ref} [µm]	λ_c	λ_l	wall thickness [nm]	r_{ind} [µm]	indenter shape	target force [µN]	target stiffness [Nm^{-1}]
6.7	100	1.161	1.075	700 200	0.4	round	3.5	3.7

When we assumed a 200 nm thick wall, turgor pressure was 0.33 MPa, slightly higher than the 0.30 MPa determined for a 700 nm thick wall (Table 2). Indeed, a turgor pressure of around 0.3 MPa is in agreement with values measured with a pressure probe, but significantly different from 0.8 MPa calculated by the incipient plasmolysis method (Benkert et al., 1997).

Table 2: **Turgor pressure and Young's modulus depend on cell wall thickness**
P=turgor pressure, E_l= Young's modulus in the longitudinal direction, E_c=Young's modulus in the circumferential direction

	Cell wall thickness	
	200 [nm]	700 [nm]
P [MPa]	0.33	0.30
E_l [MPa]	89.31	22.77
E_c [MPa]	86.53	22.06

In addition to turgor pressure, our model reveals that the Young's modulus in the longitudinal (E_l) and the circumferential (E_c) direction are almost equal, reflecting our finding that circumferential and longitudinal shrinkage induced by plasmolysis occurred at a ratio of 2:1. As expected, we found considerably different Young's moduli for 200 nm and 700 nm thick cell walls with about 90 and 20 MPa, respectively. Both values, however, lie in the range of rubber, indicating that the cell wall of pollen tubes is very elastic.

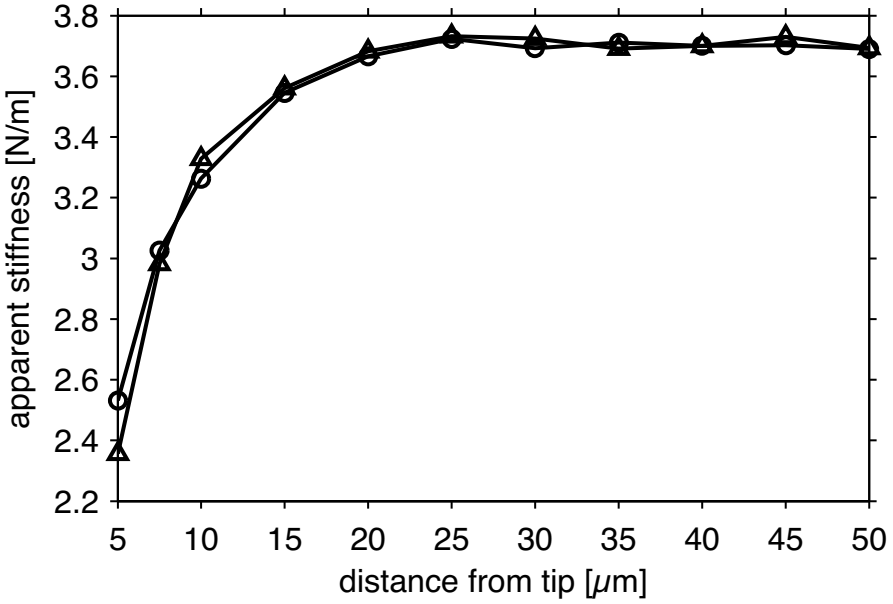

Figure 5: **Indentation simulation reveals the quality of the FEM model**
Indentation simulation with different cell wall thicknesses. The model was fitted with apparent stiffness data 40 µm behind the tip using the parameters shown in Table 1. The simulated apparent stiffness values along the entire length of 50 µm from the pollen tube tip are very similar to those obtained from measurements (Figure 2c, upper curve). Cell wall thickness has a negligible influence on the apparent stiffness. Triangles indicate the 200 nm and circles the 700 nm thick cell wall respectively.

2.4 DISCUSSION

Stiffness gradient in the pollen tube cell wall can be explained by geometry

The apparent stiffness pattern along the apical region resembles previous results, showing that the tip appears softer than the more distal regions of the shank. This has been interpreted as an indication that the cell wall properties must be different at the tip, which supports the assumption that expansion takes place exclusively at the tip of growing pollen tubes (Geitmann and Parre, 2004; Zerzour et al., 2009). In agreement with this idea, it has been suggested that new wall material is deposited near the tip (Chebli and Geitmann, 2007; Holdaway-Clarke and PK, 2003; Zonia and Munnik, 2008). Further evidence for the hypothesis of a softer tip came from observations showing that pectins are strongly methyl-esterified at the tip and become cross-linked by Ca^{2+} in more distal parts. Crystalline cellulose, as well as callose, is absent from the apical region of the pollen tube (Aouar et al., 2010; Geitmann, 2010). However, our results indicate that, assuming

uniform mechanical cell wall properties for the entire pollen tube, the reduction in apparent stiffness at the tip can be explained solely by the geometry of the pollen tube. Since we measure in vertical direction we have a gradually increasing angle of tilt between the direction of indentation and the surface towards the apex. This means that even if the forces were the same in magnitude we would expect microindentation methods to report lower values on the hemispherical part of the apex, because forces are measured only in the probe indentation direction. Geometry can also cause a gradient in stiffness near the apex in the cylindrical portion of the tube, due to turgor-induced pre-tension of the cell wall. In the cylindrical part, there is twice as much maximum principal tension than in the hemispherical apex. As a result of this difference, the cylindrical part acts like a guitar-string under high tension, which is harder to deflect than the same string under lower tension. This effect would also explain the qualitative difference between the prediction of our model and the one from Bolduc and colleagues (Bolduc et al., 2006). Albeit they also constructed an FEM model of the pollen tube, they did not include turgor pressure and, thus, did not observe the pre-tension effect. As a result, their model predicted the apex to appear stiffer than the shank based on geometry alone.

Despite the fact that our experimental data fit with a homogeneous material, we cannot exclude the possibility that there are gradients in cell wall properties. Firstly, we assume that the cell wall thickness does not change along the pollen tube. If, however, the cell wall would gradually get softer (e.g. by changing its composition) but also thicker towards the apex, we would expect it to behave similar to a homogeneous material of equal thickness. Secondly, in our model we have assumed that the cell wall is fully compressible, however, no data are available concerning the Poisson's ratio of pollen tube cell walls. The effect of a change of the Poisson's ratio between 0 (fully compressible) and 0.5 (low compressibility) could change the Young's moduli up to two-fold (Table S1). Thirdly, we are aware that the assumption of frictionless contact between pollen tube and CFM probe is arbitrary but that it may play a role at the apex since we observed that slippage can occur if we do not indent perpendicularly. This issue could be solved by adding rotational degrees of freedom to the micropositioner, which, on the other hand, would make the manual and automatic control of such a system a very demanding task. Another solution for this problem would be to use two-dimensional force sensors that are capable of measuring forces in the vertical as well as in the horizontal direction at the same

time. However, multi-axial force sensors are not currently commercially available for the force range and resolution we need.

CFM is a particularly well-suited to assess cellular stiffness

Compared with other microindentation methods, the CFM offers higher resolution and an increased level of automation and control of the experimental parameters. Although AFM offers higher resolution, it has smaller positioning and force ranges. The possibility to attach thin and long probes to the MEMS sensors allows the measurement of cells or tissue regions that are difficult to access by other methods. In addition, different mechanical properties of cells or tissues can be investigated by choosing a suitable probe shape and diameter.

The CFM has proven to be a versatile system to measure forces on living pollen tubes with high resolution, showing that this device can be used on fast growing cells with a very low apparent stiffness compared to previous applications (Routier-Kierzkowska et al., 2012). The wide force range that is covered by the possibility to mount different types of sensors makes it also suitable for animal cells and tissues. Indeed, the same type of sensor has been used previously to measure the mechanical properties of mouse oocytes pre- and post-fertilization (Sun and Nelson, 2007). In combination with fluorescence microscopy it may be possible to monitor intracellular responses to locally applied mechanical stress. The large scanning area makes it possible to get stiffness maps of entire organs and, thus, shed some light onto the interplay between mechanical and molecular effects during growth and development at unprecedented resolution.

A soft shell with a hard core

FEM modeling combined with our experiments revealed a Young's modulus of the pollen tube cell wall that approximately corresponds to rubber, equal to 20MPa and 90MPa for a cell wall thickness of 200 nm and 700 nm, respectively. To our knowledge, there is no reference value for the elasticity of pollen tube cell walls available and, generally, values for individual plant cells are sparse.

Wang and colleagues estimated the wall elasticity of suspension culture cells derived from root radicle calli of tomato to a value between 1.4 and 4.2 GPa, which depends on the chosen model assumptions, such as cell wall thickness, initial stretch ratio or the magnitude of cell deformation, as well as on experimental parameters like the pH value of the cultivation medium (Wang et al., 2004; Wang et al., 2008). A possible explanation for the remarkable difference in cell wall stiffness between cultured tomato cells and lily pollen tubes with a Young's modulus of 20 to 90 MPa could be the lower content of cellulose in the pollen tubes. It has been reported that pollen tube cell walls contain 2-10 % cellulose rather than 20-30 % found in other types of plant cells (Steer and Steer, 1989; Schlupmann et al., 1994).

Pollen tubes are fast growing cells. After germination they first have to penetrate the stigmatic tissue before reaching the transmitting tract. Attraction by the ovule forces the tubes to make sudden changes in direction and, in the process of fertilization, the pollen tubes need to push through the micropylar opening before penetrating a synergid cell. This may be easier for a relatively stiff cell with a flexible cell wall.

Our engineering style FEM mechanical model allows us to analyze the mechanical behavior of a pressurized pollen tube. By measuring the apparent stiffness, cell wall thickness, and the initial stretch ratio, we were able to calculate turgor pressure as well as the elasticity of the cell wall. This opens the door for further studies on cell wall mutants to investigate the influence of an altered cell wall composition on the mechanical properties of the pollen tube wall. It will be possible to correlate these data with growth rate, resistance to bursting, and fertilization success. Furthermore, it will be interesting to make use of genetic or molecular sensors to shed light on the effects of locally applied mechanical stresses on intracellular processes, such as calcium fluxes, the production of reactive oxygen species, or cytoskeleton dynamics, all of which play an important role in pollen tube growth.

2.5 EXPERIMENTAL PROCEDURES

Pollen tube growth

Anthers of lily (*Lilium longiflorum*) were frozen at −80°C until used. Frozen pollen was brushed on silane coated slides (Science Services GmbH, http://scienceservices.de/), incubated for 30 min in a moisture

chamber, subsequently covered with growth medium (10 % sucrose, 5 mM MES, 5 mM KNO_3, 0.13 mM $Ca(NO_3)_2$, 0.16mM H_3BO_3), and incubated at 22°C for 1.5-2.0 hours. The slides were washed thrice with growth medium to get rid of non-sticking pollen tubes and the remaining tubes were covered with growth medium for stiffness measurements. For osmosis experiments the growth medium was replaced with 15 % mannitol.

MEMS equipment

A commercially available single-axis capacitive MEMS-based microforce-sensing probe (FT-S540, FemtoTools GmbH, http://femtotools.com) was used for our experiments. Each sensor is individually precalibrated by the manufacturer following an SI-traceable calibration procedure that ensures the precision of the measurement system.

The working principle of the sensor is schematically shown in Figure 2d. The sensor consists of a movable body with an attached probe suspended by four flexures within an outer frame. A force applied to the probe in the x-direction results in a relative motion of the body and the outer frame, which can be measured by attached capacitive electrodes as a change in capacitance. Two capacitive changes with opposite signs are differentially measured using a capacitance-to-voltage converter (MS3110, Irvine Sensors Inc., http://www.irvine-sensors.com), resulting in a linear output.

Due to the symmetric design of this sensor with its four flexures, parallel motion of the movable body, as it is deflected, can be achieved, making this design superior to most cantilever-type sensors. Furthermore, due to its long sensing probe, the sensor can access three-dimensional structures, even in depressions, making the system suitable for measurements of organisms and tissues with diverse and changing morphology.

Software and data acquisition

For the integration of the components comprising the CFM system, presented in the system description paragraph above, we used a custom application developed in LabVIEW (National Instruments, http://

www.ni.com). The application performs the control of the automated tasks as well as the data logging. In addition, a user interface (UI) for the control of the experimental parameters was developed. The data acquisition is done using a National Instruments USB-6009 DAQ Card (National Instruments, http://www.ni.com). The sampling rate used is 100Hz for the coarse approach phase, and 50 Hz for the fine approach and the scanning mode. These values were chosen such that the desired force resolution, which is based on the noise signal, was achieved. The MEMS sensor is supplied with 5V power and the sensor's analog signal is acquired too. The data that are collected are the absolute X, Y and Z position of the microrobot, the sensor's analog signal (voltage), the calculated force sensed at the tip, the timestamp for each of the aforementioned values, and the type of movement performed at that timestamp, i.e. fine or coarse approach and scanning mode. All these data are logged for post-processing.

Except from the acquisition and logging there exists the thread for the control of the automated procedure. We use two different types of control methods. The first method is position feedback when we move from one measurement location to the next, when we position the end effector at a specific distance from the cell surface, and also when we perform the unloading phase. The second method is the control of the movement based on force feedback. This method is used in the actual measurement phase comprised of the coarse approach, the fine approach, and the loading phase.

All the experimental parameters such as contact and measurement force, step speed and size, scanning speed and amplitude, distance from the cell surface at starting position, and scanning mesh properties are defined at the beginning of the experiment.

Stiffness measurements

Lily pollen tubes that were adhered to silane-coated slides (Science Services, www.scienceservices.de) were focused at a 400x magnification with DIC optics on an inverted microscope (Olympus IX 71, http://www.olympus-global.com). After the sensor tip was positioned manually on the pollen tube at the starting point of the measurement series, control was taken over by the LabVIEW software. At each point we took four measurements with four scans (see below) from each of which we calculated the mean stiffness values.

Every individual measurement started with a “coarse approach” using the step mode of the actuator to identify the surface of the pollen tube. Then the sensor retracted from the sample by a previously defined distance before it started the “fine approach” to indent the tube until a threshold force (F_{max}) was reached. F_{max} values were 4 µN for turgescent and 2 µN for plasmolysed pollen tubes. The difference between coarse and fine approach is the step amplitude and frequency. Larger values for both parameters ensure faster movement and thus we use this approach to speed up the contact detection between the tip and the sample. At this point the movement switched to the scan mode and performed a number of loading and unloading cycles. The reason for using this positioning method for the measurements is that with the scan mode a smoother and continuous movement is achieved.

Data analysis was performed with Matlab (MathWorks, http://www.mathworks.ch). First, the contact point between the sensor probe tip and the pollen tube surface was estimated from the force-displacement curve acquired during the fine approach. Starting from the deepest point of indentation, the algorithm finds the first point for which the stiffness is below a predefined threshold. While indenting in liquid medium, the surface tension results in a positive force measured by the sensor before entering into contact with the sample. In consequence, the force at maximal indentation depth can differ from the user-defined maximal force threshold. Hence, we corrected the measured force such that the load at contact point is set to zero.

Stiffness values were determined from the slope of force-displacement curves acquired during scan mode by performing a least squares linear fit separately for each phase of the oscillations, as described previously (Routier-Kierzkowska et al., 2012).

Estimation of geometrical parameters

To measure the shrinkage of the pollen tubes, we took DIC images before and after plasmolysis. Diameter and length of the pollen tubes were measured with ImageJ (http://rsbweb.nih.gov/ij/). For the estimation of cell wall thickness we stained actively growing pollen tubes with growth medium containing 30 µM propidium iodide. After incubation for 3-5 min the staining solution was replaced with growth medium. Using a confocal laser scanning microscope (Leica SP2, http://www.leica-microsystems.com), we made

longitudinal optical sections with a thickness of 120 nm through the pollen tube. The image stacks where then deconvolved with the 3D Huygens deconvolution software (Scientific Volume Imaging, http://www.svi.nl). The stack slice showing the pollen tube section with the largest diameter was chosen to measure the thickness of the cell wall using ImageJ.

FEM implementation

The mechanical model was implemented in Abaqus Standard (Simulia, http://www.3ds.com/products/simulia/overview/) and solved based on finite deformation theory. For the representation of the pollen tube we choose linear triangular shell elements (S3). The discretization was individually computed for each indentation position, based on an iterative mesh refinement procedure. The contact problems between pollen tube and indenter, and between pollen tube and support, were solved by the node-to-node, augmented Lagrange algorithm.

Given our set of assumptions, there are three model parameters, which cannot be measured directly. These are the turgor pressure and the longitudinal and circumferential Young's moduli. In order to obtain quantitative estimates for those parameters we fitted our model to the experimental data. The quality of a fit was assessed based on two criteria. First, the model should show the same amount of stretch in longitudinal and circumferential direction as measured during the osmotic assays. Second, it should have the same apparent stiffness when indented 40 µm behind the apex.

ACKNOWLEDGEMENTS

We thank Simon Muntwyler and Felix Beyeler from FemtoTools for technical advice on the sensors, and Daniel Bollier for workshop support. This work was supported by the University of Zürich, the University of Bern, and the Research and Technology Development Project “Plant Growth in a Changing Environment” supported by SystemsX.ch, the Swiss Initiative in Systems Biology (to CR, BN, RSS, and UG).

2.6 REFERENCES

Anderson, J.R., Barnes, W.S. and Bedinger, P. (2002) 2,6-Dichlorobenzonitrile, a cellulose biosynthesis inhibitor, affects morphology and structural integrity of petunia and lily pollen tubes. *Journal of Plant Physiology* **159**, 61-67.

Aouar, L., Chebli, Y. and Geitmann, A. (2010) Morphogenesis of complex plant cell shapes: The mechanical role of crystalline cellulose in growing pollen tubes. *Sex Plant Reprod* **23**, 15-27.

Benkert, R., Obermeyer, G. and Bentrup, F.W. (1997) The turgor pressure of growing lily pollen tubes. *Protoplasma* **198**, 1-8.

Bolduc, J.F., Lewis, L.J., Aubin, C.E. and Geitmann, A. (2006) Finite-element analysis of geometrical factors in micro-indentation of pollen tubes. *Biomech Model Mechan* **5**, 227-236.

Burton, R.A., Gidley, M.J. and Fincher, G.B. (2010) Heterogeneity in the chemistry, structure and function of plant cell walls. *Nat Chem Biol* **6**, 724-732.

Chanliaud, E. and Gidley, M.J. (1999) *In vitro* synthesis and properties of pectin/*Acetobacter xylinus* cellulose composites. *Plant J* **20**, 25-35.

Chebli, Y. and Geitmann, A. (2007) Mechanical Principles governing pollen tube growth. *Functional Plant Science and Biotechnology* **1**, 232-245.

Cosgrove, D.J. (1993) Wall extensibility: Its nature, measurement and relationship to plant cell growth. *New Phytol* **124**, 1-23.

Cosgrove, D.J. (2005) Growth of the plant cell wall. *Nat Rev Mol Cell Biol* **6**, 850-861.

Edge, S., Steele, D.F., Chen, A., Tobyn, M.J. and Staniforth, J.N. (2000) The mechanical properties of compacts of microcrystalline cellulose and silicified microcrystalline cellulose. *Int J Pharm* **200**, 67-72.

Erickson, R.O. (1976) Modeling of plant growth. *Annu. Rev. Plant. Physiol.* **27**, 407-434.

Felekis, D., Muntwyler, S., Vogler, H., Beyeler, F., Grossniklaus, U. and Nelson, B.J. (2011) Quantifying growth mechanics of living, growing plant cells *in situ* using microrobotics. *Micro Nano Lett* **6**, 311-316.

Fernandez-Sanchez, M.E., Serman, F., Ahmadi, P. and Farge, E. (2010) Mechanical induction in embryonic development and tumor growth integrative cues through molecular to multicellular interplay and evolutionary perspectives. *Methods Cell Biol* **98**, 295-321.

Fry, S.C. (1995) Polysaccharide-modifying enzymes in the plant cell wall. *Annu. Rev. Plant. Physiol. Plant. Mol. Biol.* **46**, 497-520.

Geitmann, A. (2006) Experimental approaches used to quantify physical parameters at cellular and subcellular levels. *Am J Bot* **93**, 1380-1390.

Geitmann, A. (2010) How to shape a cylinder: Pollen tube as a model system for the generation of complex cellular geometry. *Sex Plant Reprod* **23**, 63-71.

Geitmann, A. and Parre, E. (2004) The local cytomechanical properties of growing pollen tubes correspond to the axial distribution of structural cellular elements. *Sex Plant Reprod* **17**, 9-16.

Hepler, P.K., Kunkel, J.G., Rounds, C.M. and Winship, L.J. (2012) Calcium entry into pollen tubes. *Trends Plant Sci* **17**, 32-38.

Holdaway-Clarke, T.L. and PK, H. (2003) Control of pollen tube growth: Role of ion gradients and fluxes. *New Phytol* **159**, 539-563.

Kutschera, U. (1996) Cessation of cell elongation in rye coleoptiles is accompanied by a loss of cell-wall plasticity. *J Exp Bot* **47**, 1387-1394.

Lancelle, S.A., Cresti, M. and Hepler, P.K. (1997) Growth inhibition and recovery in freeze-substituted *Lilium longiflorum* pollen tubes: Structural effects of caffeine. *Protoplasma* **196**, 21-33.

Lancelle, S.A. and Hepler, P.K. (1992) Ultrastructure of freeze-substituted pollen tubes of *Lilium longiflorum*. *Protoplasma* **167**, 215-230.

Martin, A.C. (2010) Pulsation and stabilization: Contractile forces that underlie morphogenesis. *Dev Biol* **341**, 114-125.

McKenna, S.T., Kunkel, J.G., Bosch, M., Rounds, C.M., Vidali, L., Winship, L.J. and Hepler, P.K. (2009) Exocytosis precedes and predicts the increase in growth in oscillating pollen tubes. *Plant Cell* **21**, 3026-3040.

Milani, P., Gholamirad, M., Traas, J., Arneodo, A., Boudaoud, A., Argoul, F. and Hamant, O. (2011) *In vivo* analysis of local wall stiffness at the shoot apical meristem in *Arabidopsis* using atomic force microscopy. *Plant J* **67**, 1116-1123.

Mirabet, V., Das, P., Boudaoud, A. and Hamant, O. (2011) The role of mechanical forces in plant morphogenesis. *Annu Rev Plant Biol* **62**, 365-385.

Parre, E. and Geitmann, A. (2005) More than a leak sealant. The mechanical properties of callose in pollen tubes. *Plant Physiol* **137**, 274-286.

Peaucelle, A., Braybrook, S.A., Le, G., L, Bron, E., Kuhlemeier, C. and Höfte, H. (2011) Pectin-induced changes in cell wall mechanics underlie organ initiation in *Arabidopsis. Curr Biol* **21**, 1720-1726.

Qin, Y. and Yang, Z. (2011) Rapid tip growth: Insights from pollen tubes. *Semin Cell Dev Biol* **22**, 816-824.

Routier-Kierzkowska, A.L., Weber, A., Kochova, P., Felekis, D., Nelson, B., Kuhlemeier, C. and Smith, R.S. (2012) Cellular force microscopy for *in vivo* measurements of plant tissue mechanics. *Plant Physiol* **158,** 1514-1522.

Schlupmann, H., Bacic, A. and Read, S.M. (1994) Uridine Diphosphate glucose metabolism and callose synthesis in cultured pollen tubes of *Nicotiana alata* Link et Otto. *Plant Physiol* **105**, 659-670.

Schopfer, P. (2006) Biomechanics of plant growth. *Am J Bot* **93**, 1415-1425.

Smith, A.E., Moxham, K.E. and Middelberg, A.P.J. (1998) On uniquely determining cell wall material properties with the compression experiment. *Chemical Engineering Science* **53**, 3913-3922.

Steer, M.W. and Steer, J.M. (1989) Pollen tube tip growth. *New Phytol* **111**, 323-358.

Sun, Y. and Nelson, B.J. (2007) MEMS capacitive force sensors for cellular and flight biomechanics. *Biomed Mater* **2**, S16-S22.

Tian, G.W., Chen, M.H., Zaltsman, A. and Citovsky, V. (2006) Pollen-specific pectin methylesterase involved in pollen tube growth. *Dev Biol* **294**, 83-91.

Tomos, A.D. and Leigh, R.A. (1999) The Pressure Probe: A versatile tool in plant cell physiology. *Annu Rev Plant Physiol Plant Mol Biol* **50**, 447-472.

Wang, C.X., Wang, L., McQueen-Mason, S.J., Pritchard, J. and Thomas, C.R. (2008) pH and expansin action on single suspension-cultured tomato (*Lycopersicon esculentum*) cells. *J Plant Res* **121**, 527-534.

Wang, C.X., Wang, L. and Thomas, C.R. (2004) Modelling the mechanical properties of single suspension-cultured tomato cells. *Ann Bot* **93**, 443-453.

Wei, C., Lintilhac, L.S. and Lintilhac, P.M. (2006) Loss of stability, pH, and the anisotropic extensibility of *Chara* cell walls. *Planta* **223**, 1058-1067.

Wei, C. and Lintilhac, P.M. (2007) Loss of stability: A new look at the physics of cell wall behavior during plant cell growth. *Plant Physiol* **145**, 763-772.

Zamir, E.A. and Taber, L.A. (2004) On the effects of residual stress in microindentation tests of soft tissue structures. *J. Biomech. Eng.* **126**, 276.

Zerzour, R., Kroeger, J. and Geitmann, A. (2009) Polar growth in pollen tubes is associated with spatially confined dynamic changes in cell mechanical properties. *Dev Biol* **334**, 437-446.

Zhao, L., Schaefer, D., Xu, H., Modi, S.J., Lacourse, W.R. and Marten, M.R. (2005) Elastic properties of the cell wall of *Aspergillus nidulans* studied with atomic force microscopy. *Biotechnol Prog* **21**, 292-299.

Zonia, L. and Munnik, T. (2008) Vesicle trafficking dynamics and visualization of zones of exocytosis and endocytosis in tobacco pollen tubes. *J Exp Bot* **59**, 861-873.

2.7 SUPPLEMENTAL DATA

Table S1: Estimated pressure and elasticity for varying "in-plane" Poisson's ratio.

The supporting information describes the influence of the chosen Poisson's ratio on the Young's moduli and turgor pressure resulting from our simulated experiment. We present the mathematical background and a Table S1 that shows the change in turgor pressure and the Young's moduli for different "in-plane" Poisson's ratios. Table S1 is related to Table 2 in the main manuscript.

3. SYNERGISTIC INTERACTION OF XYLOGLUCAN AND EXTENSINS IN POLLEN TUBE CELL WALLS

Authors

Christian Draeger[a], Hannes Vogler[a], Paul Knox[b], Ueli Grossniklaus[a], and Christoph Ringli[a*]

Addresses

[a]University of Zurich, Institute of Plant Biology, Zollikerstrasse 107, Switzerland;

[b]Centre for Plant Sciences, University of Leeds, Leeds LS2 9JT, UK

* Corresponding author

3.1 SUMMARY

Xyloglucans (XyGs), the major hemicellulose of dicotyledonous plants, and cellulose undergo a strong interaction and are thought to form a tension-bearing network. Due to this important function, XyG-deficient plants are expected to develop a severe growth phenotype, a hypothesis that was challenged by the XyG-xylosyltransferase double mutant *xxt1 xxt2* of *Arabidopsis thaliana*, which develops only a moderate growth phenotype. Here, pollen tubes (PTs) were used as a model system to investigate the function of hemicelluloses in cell walls. The *xxt1 xxt2* mutant PTs exhibit a strong growth defect, resulting in reduced fertilization efficiency. The reduction in XyG not only affects elongation of the PTs both *in vitro* and *in vivo*, but also causes loss of growth orientation, resulting in entangled PTs in the female tissue. Cell wall-specific monoclonal antibodies revealed an increase of extensin epitopes in the *xxt1 xxt2* pollen grain and the PT. Extensins are a class of structural proteins shown to strengthen the cell wall in different tissues. The mutant *xeg113* is affected in extensin formation and revealed to be particularly sensitive to enzymatic removal of XyG. Increased extensin epitopes in a plant lacking XyG (*xxt1 xxt2*) and an extensin deficient plant (*xeg113*) is sensitive to XyG removal suggest that there might be a synergistic function between these two cell wall components. Therefore, the triple mutant *xxt1 xxt2 xeg113* was produced, which revealed a strong phenotype in growth speed and morphology of Arabidopsis PTs. Additionally, *xxt1 xxt2 xeg113* PTs revealed an increased cell wall stiffness when measured by Cellular Force Microscopy (CFM). These results indicate that extensins can partly compensate for XyG deficiency and thus might be involved in a mechanism to compensate for the reduced hemicellulose content in PTs.

3.2 INTRODUCTION

A distinct feature of plants cells is the cell wall which is formed mainly by polysaccharides and structural glycoproteins. During cell growth, this rigid yet flexible structure is in a constant flow of remodeling, increasing its surface by the incorporation of new cell wall material in a coordinated fashion.

In the primary cell wall, mechanical strength is primarily provided by a cellulose-hemicellulose network [1]. Pectineaous polysaccharides are embedding this network, provide further support, and regulate porosity of the cell wall which influences fluxes of cell-wall modifying enzymes [2]. In dicotyledonous plants, xyloglucan (XyG) is the most abundant type of hemicellulose, representing 10-20% of the dry weight of cell walls. Due to the strong noncovalent interaction with cellulose, XyG was postulated to link cellulose microfibrils to form a network. Alternatively, XyG might also be required to provide correct spacing of cellulose microfibrils. XyG is composed of a (1→4)-β-glucan backbone regularly substituted by xylosyl residues to which Fucose (Fuc) and/ or Galactose (Gal) can be attached. To allow cell-wall expansion to take place, XyG linkages must be constantly broken and reestablished by the activity of XyG hydrolases and –transglycosylases present in the cell wall [3]. For *de novo* biosynthesis, Xyloglucan Xylosyltransferases (XXTs) present in the golgi are essential, substituting glucan with xylose residues. In *Arabidopsis thaliana*, an *xxt1 xxt2* double mutant shows a strong reduction of XyG by at least 95%. The double mutant is largely unaffected in the general development, raising the question about the significance of XyG or a possible compensatory mechanism that would balance out this significant change in cell wall composition [4]. Glycome profilig data have shown that the lack of detectable XyG does not cause significant compensatory changes in other polysaccharides and changes of non-XyG polysaccharide amounts cannot be ruled out [Zabotina et al., 2012].

Structural cell-wall proteins have been shown to influence the mechanical properties of cell walls. Hydroxyproline-rich glycoproteins (HRGPs) including extensins and arabinogalactan proteins (AGPs) are well studied structural cell-wall proteins. AGPs represent highly diverse glycopeptides and are involved in a number of developmental processes such as cell expansion or signaling [5]. Extensins are characterized by Ser-Pro_4 repetitive motifs and are strongly glycosylated [6]. The Pro residues are posttranslationally hydroxylated to hydroxyproline (Hyp) and glycosylation takes place at these Hyp and at Ser residues with Gal and Ara, respectively [7]. Extensins have been shown to be expressed in tissues under mechanical stress, upon pathogen attack or after cessation of growth [8] in order to strengthen the cell wall. They form rod-like structures that are able to self-aggregate into a three-dimensional network [9] and build linkages between polysaccharides through their sugar moieties, exemplified by extensin-pectin interaction [10]. Extensins can be

covalently crosslinked in the cell wall [11, 12, 13] further emphasizing a role of extensins in modifying cell wall mechanical properties. This was shown with *xeg113* a mutant, which exhibits elongated hypocotyls due to an underarabinosylation of extensins [14].

A model system to investigate the process of cell (wall) growth is the pollen tube (PT). PTs are isolated cells that show expansion only in the tip region [15]. During the fertilization process, pollen grains attach to the papillar cells of the stigma, germinate, and form a tube that penetrates the stylar transmitting tract to eventually reach the ovule [16]. This process requires rapid growth and hence a constant and effective enlargement of the cell wall at the tip. The composition of the tube cell wall not only differs compared to vegetative cells by e.g. considerable amounts of callose [17], but also strongly depends on the position along the tube. The tip region is a highly dynamic area that constantly expands. In contrast, the lateral walls forming the shank of the tube are much more pressure-resistant and do not expand [18, 19]. Due to the fast growth process, PTs are sensitive to changes in the cell wall that disturb the fine balance between providing stability and allowing fast expansion.

A lot is known about the molecular regulation of Arabidopsis PT growth, but tools for a mechanical characterization *in vitro* arose only recently [20; 21]. Cellular Force Microscopy (CFM) is an high-resolution micro-indentation system, which allows the measurement of cell wall elasticity. Local deformation experiments were used to measure the apparent stiffness (influence of turgor pressure, mechnical stress, cell, and indenter geometry). This CFM approach provides insights into the mechnical properties of cell walls [22].

In this work, the effect of the *xxt1 xxt2* double mutant on PT growth was investigated. PT growth in the *xxt1 xxt2* double mutant is affected in both *in vitro* and *in vivo*. The treatment of wild-type pollen with a fungal XyG endoglycosylase (XEG) leads to a comparable phenotype, supporting the assumption that it is the consequence of a degenerated XyG network. *In vivo*, *xxt1 xxt2* PTs frequently get entangled, suggesting that XyG is important for directed PT growth. Immunolabeling of *xxt1 xxt2* mutant PTs and XEG sensitivity tests suggest that extensins are part of a compensatory network partially substituting for XyG in the *xxt1 xxt2* mutant. The triple mutant plant *xxt1 xxt2 xeg113* corroborates the evidence of a compensatory mechanism by exhibiting a strong phenotype. CFM analysis was used to measure effects of *xxt1 xxt2* and *xeg113* on the

mechanical properties of the PT cell wall. Additionally, CFM provides micro-mechanical data, which change in *xxt1 xxt2 xeg113* PTs and facilitate the evidence that a compensation effect might be partially lost in the triple mutant.

3.3 RESULTS

XyG deficiency affects PT growth *in vivo* and *in vitro*.

The impact of xyloglucan on PT growth was investigated using the xyloglucan-deficient double mutant *xxt1 xxt2*. PTs revealed significant differences in the morphology between the wild type and the *xxt1 xxt2* mutant *in vitro*. The latter developed aberrant structures in 87.3% of all PTs. Multiple growing tips appeared (1.6%) or the tubes burst (58.7%). PTs frequently showed locally bulging (27.0%) up to a diameter of 9.7 ± 4.4 µm adjacent to the tip compared to the wild-type 5.6 ± 0.4 µm (Fig. 1A, B). Occasionally, *xxt1 xxt2* PTs discontinued growth and released cellular content prior to resuming elongation. This material revealed to be enclosed by membranes as indicated by FM4-64 staining (Fig. 1C-E), suggesting vesicle budding. This is likely to transiently reduce internal turgor pressure, which first needs to be built up prior to allow growth to resume, resulting in the observed cessation of tube elongation.

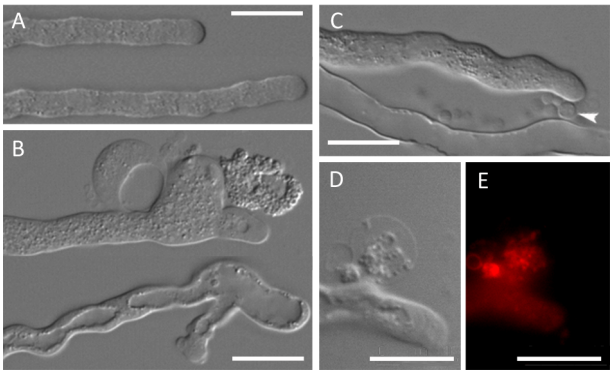

Figure 1: ***In vitro* growth of PTs.** Wild-type (A) PTs and *xxt1 xxt2* (B) PTs 6 h after germination. (C) Vesicle released from *xxt1 xxt2* PTs (arrowhead). Detail on vesicle release by DIC (D) and fluorescence (E) microscopy to visualize FM4-64 staining (Scale bars: 10 µm).

In a segregating population population of a *xxt1* x *xxt2* cross, *xxt1 xxt2* double mutants were rarely found [4], indicating an effect of the mutations on the fertilization process. To identify the cause of this defect, fertilization efficiency was compared between wild-type and mutant pollen. Pollination of wild-type pistils with mutant pollen led to the formation of shorter siliques as compared to pollination with wild-type pollen. Opening of the siliques revealed fewer fertilized ovules after pollination with mutant versus wild-type pollen (7.0% and 79.3%, respectively), suggesting reduced fertilization efficiency of mutant pollen (Table 1; Fig. 2A, B). In a reciprocal cross, fertilization of the *xxt1 xxt2* mutant with wild-type pollen was comparable to the wild-type (Table 1). Hence, the major defect of *xxt1 xxt2* mutants in the fertilization process is with the male gametophyte, i.e. PT development, which is in agreement with the *in vitro* growth defect observed for *xxt1 xxt2* mutant PTs.

Table 1: **PT ovule targeting at different time points after pollination**. For the crosses (top lane) genotype of female is shown first.

hours post germination	wt x wt	wt x *xxt1 xxt2*	*xxt1 xxt2* x wt
6 h	27.4%	10.4%	25.2%
24 h	56.1%	13.5%	58.4%
1 week	79.3%	7.0%	64.4%

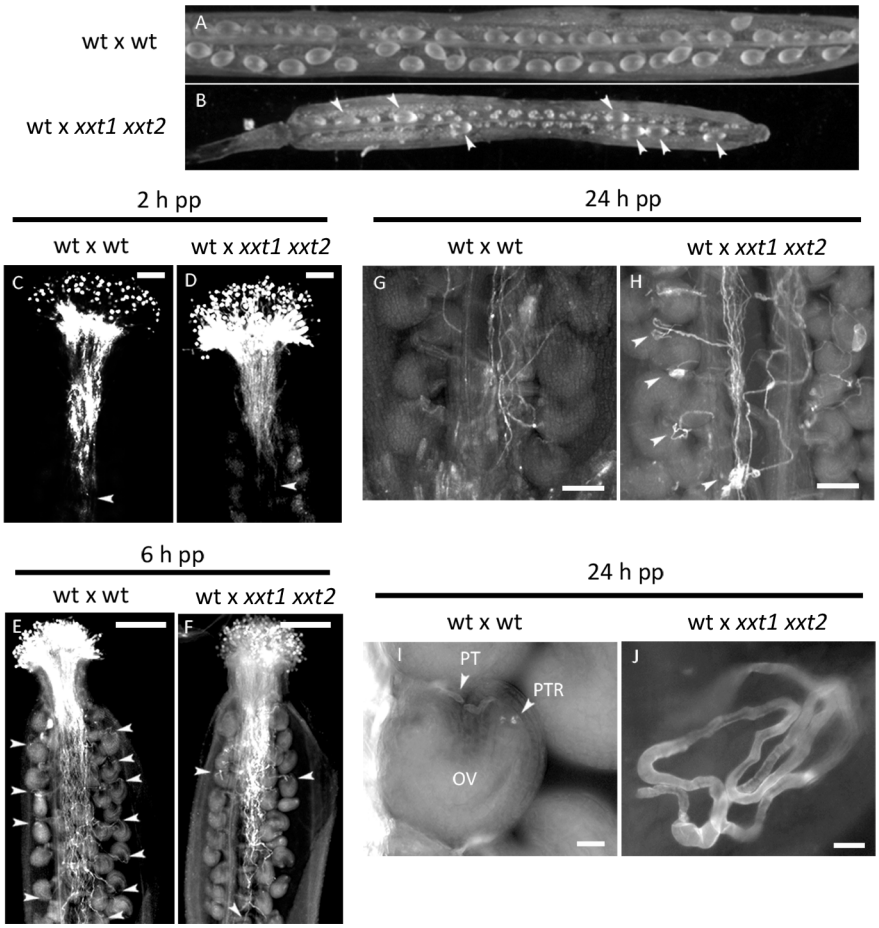

Figure 2: ***In vivo* PT ovule targeting of *xxt1 xxt2* double mutants is affected.** Wild-type siliques one week after fertilization with wild-type (A) and *xxt1 xxt2* (B) pollen revealed reduced fertilization efficiency with mutant pollen and shortened siliques (arrowheads: fertilized ovules). (C, D) Two h after pollination wild-type and *xxt1 xxt2* pollen tubes initially showed comparable germination and tube growth (arrowheads: longest pollen tubes; Scale bars: 100 µm). Differences in fertilization became apparent 6 h after pollination with wild-type (E) and *xxt1 xxt2* (F) pollen (arrowheads indicate fertilized ovules; Scale bars: 300 µm). After 24 h, wild-type PTs (G, I) effectively grew towards the ovules, while *xxt1 xxt2* PTs (H) frequently lost orientation (indicated by arrowheads) and grew in circles (J). (OV: ovule; PT: pollen tube; PTR: pollen tube rupture; (G, H) Scale bars: 100µm; (I) Scale bar: 25 µm; (J) Scale bar: 10 µm)

To investigate the PT growth properties *in vivo*, wild-type pistils were pollinated with wild-type and *xxt1 xxt2* mutant pollen and PT growth was followed over time. Germination and initial phase of PT elongation was comparable between wild-type and mutant pollen, as visualized in longitudinal sections of stylar tissue 2 h post pollination (pp) (Fig. 2C, D). First differences became apparent 6 h pp, where 27.4% of the ovules were targeted by wild-type pollen compared to only 10.4% with mutant pollen (Fig. 2E, F; Table 1). After 24 h pp, the frequency of targeted ovules increased to 56.1% with wild-type pollen, but remained low at 13.5% with mutant pollen (Table 1). In sections of stylar tissue, a striking growth phenotype became apparent in mutant pollen.

While wild-type PT grew through the transmitting tract and towards the ovule (Fig. 2G, I), *xxt1 xxt2* mutant PTs frequently got entangled. PTs grew in circles, either in the transmitting tract or close to the ovule (Fig. 2H, J). In a reciprocal cross using *xxt1 xxt2* as the female, wild-type PT grew normal (Table 1). In summary, reduced fertilization of the *xxt1 xxt2* mutant is due to an impaired development of the male gametophyte, particularly a loss of growth directionality of PTs.

Immunocytological characterization of *xxt1 xxt2* pollen tubes and somatic tissue.

The influence of the *xxt1 xxt2* mutations on cell wall structures was investigated by monoclonal antibodies (mAbs) directed against cell-wall epitopes. To detect XyG moieties, anti-XyG mAbs LM15 and CCRC-M1 were used [23, 24]. Immunolabeling with both mAbs was uniform in wild-type but absent in *xxt1 xxt2* PTs (Fig. 3) an expected consequence of the *xxt1 xxt2* mutations with causes loss of detectable amounts of XyG [4].

Homogalacturonan (HG), a component of the pectic matrix, is recognized by the mAbs JIM5 and JIM7 [25], which detect partially and strongly methylesterified HGs, respectively. With JIM5, wild-type PTs showed a specific ring-shaped staining behind the tip, whereas JIM7 epitopes were detected in the tip region (Fig. 3). In *xxt1 xxt2* PTs the localization of the labeled epitopes differed from the wild type. The distribution of JIM5 epitopes were disarranged, probably due to the aberrant shape of mutant PTs. Secondary tips showed an increased fluorescence signal with JIM7 (Fig. 3), in line with strongly methylated pectin accumulation in expanding cell walls [26]. Rhamnogalacturonan I (RGI) is recognized by LM5 and LM6, which bind galactan and arabinan side-chains, respectively [27, 28]. While no labeling was observed with LM5, the RGI-associated arabinan epitopes recognized by LM6 showed a uniform labeling in wild-type PTs. Massive bulges in *xxt1 xxt2* PTs showed a strong staining with LM6 (Fig. 3).

LM14 recognizes the glycan moiety of AGPs [29], resulting in a uniform labeling along the wild-type PT. In the *xxt1 xxt2* double mutant, LM14 labeling was increased close to sites of bursting (Fig. 3), suggesting local rearrangements of cell wall structures during this process.

Extensins were detected with JIM12 [30] and JIM20 [31]. Wild-type PTs showed a regular staining along the cell wall with JIM20. In *xxt1 xxt2* PTs, this labeling was redistributed to bulges at the tip (Fig. 3). With JIM12, immunostaining was not detectable in wild-type, but clearly present in the *xxt1 xxt2* PTs (Fig. 3). The increased extensin labeling was also observed in otherwise normal looking PTs. This is in contrast to the other mAbs, where changes in labeling were associated with aberrant structures in *xxt1 xxt2* PTs. A similar increase in extensin-labeling was observed in whole seedling extracts of *xxt1 xxt2* mutants (SI, Fig. S1).

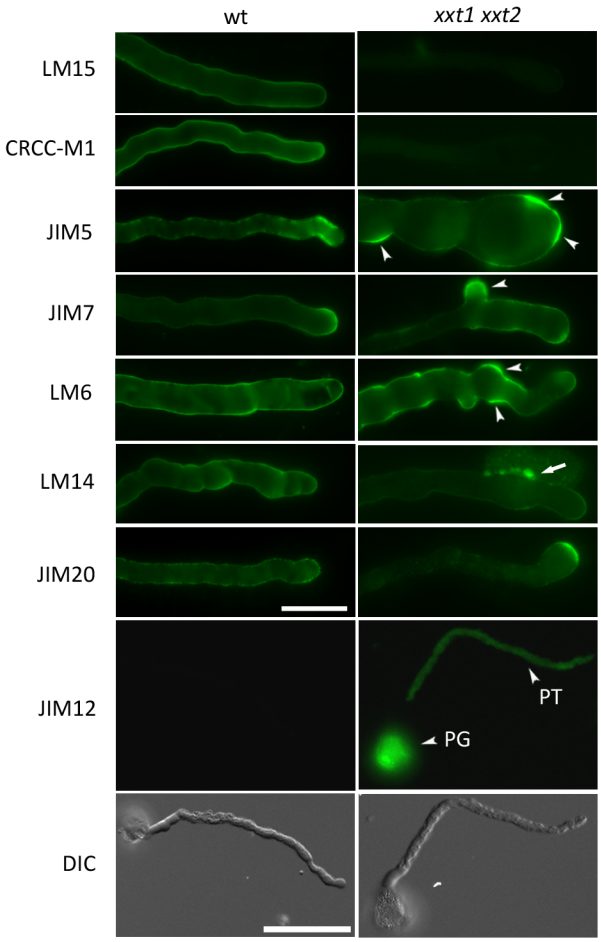

Figure 3: **Immunolabeling of wild-type and *xxt1 xxt2* mutant pollen tubes with cell wall-specific mAbs.** Arrowheads indicate aberrant structures in mutant pollen tubes. LM15, CRCC-M1: anti-XyG; JIM5, JIM7: anti-homogalacturonan (low and highly methylated form, respectively); LM5, LM6: anti-RGI (anti-Gal and anti-Ara sidechains, respectively); LM14: anti-AGP; JIM20, JIM12: anti-extensin. JIM12 labeling and DIC of a germinated pollen grain (PG) with PT (Scale bars: 20 µm; JIM12, DIC: 50 µm)

XEG treatment of Arabidopsis pollen tubes.

Next, it was investigated whether the phenotypic alterations in *xxt1 xxt2* mutant PTs were indeed induced by the reduction in XyG content. To this end, a recombinant fungal xyloglucanase (XEG [32]) was used to digest XyG in *in vitro* grown PTs. In wild-type PTs, XEG treatment induced a similar situation as monitored in *xxt1 xxt2* PTs. After approximately 4-6 min, the wild-type PTs began to release vesicle-like structures in the tip region (Fig. 4A).

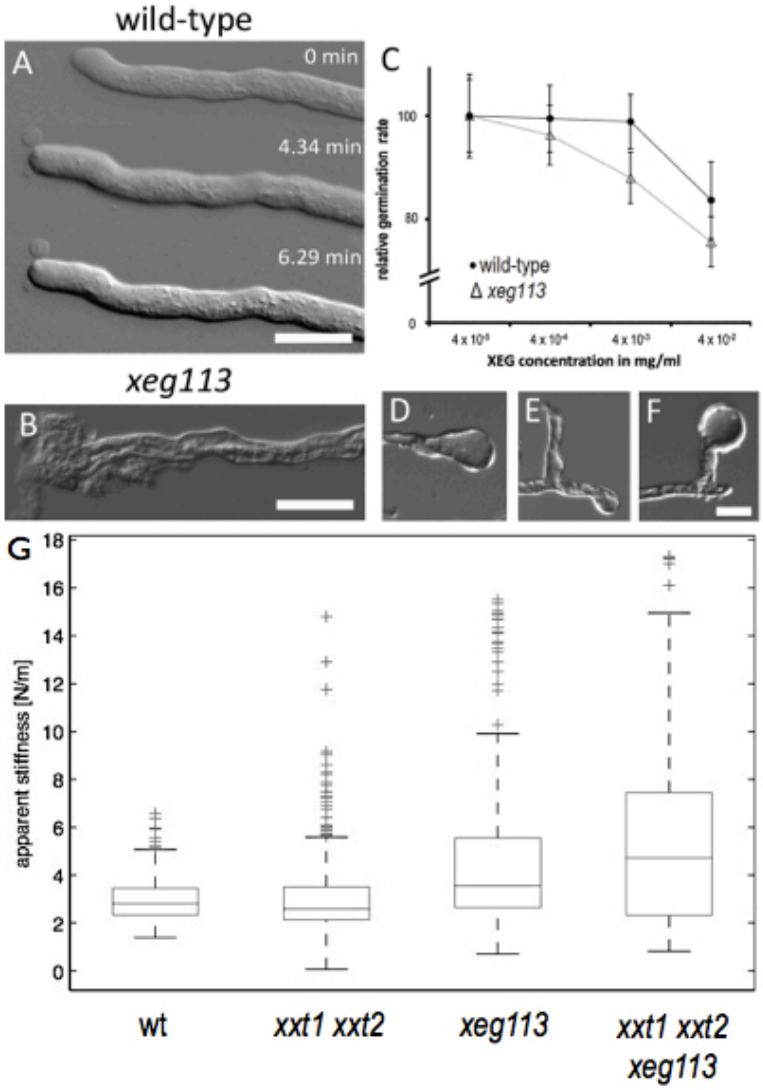

Figure 4: **XEG treatment of wild-type and *xeg113* PTs.** (A) XEG treatment of wild-type PTs results in the release of vesicles (Scale bar: 10 µm). (B) *xeg113* PT phenotype (Scale bar: 10 µm). (C) Relative germination rate of wt and *xeg113* PTs during XEG treatment. Wild-type (D) and *xeg113* (E, F) PTs after 16 h of XEG treatment (Scale bar: 10 µm). (G) Apparent stiffness measurements of wt, *xxt1 xxt2, xeg113*, and *xxt1xxt2 xeg113*.

Hence, XEG treatment of wild-type PTs caused growth defects comparable to those observed in *xxt1 xxt2* PTs, suggesting that in both instances, they are due to degradation of XyG. The apparent overrepresentation of extensins suggests that they might be part of a compensatory mechanism as a response to a lack of XyG. This point was followed by analyzing the effect of XEG-treatment on PTs in the extensin mutant *xeg113*. *In vitro* grown *xeg113* PTs, 72.3% did show a phenotype such as bursting (20.0%), bulging (49.2%) or infrequently secondary tips (Fig. 4B). *xeg113* PTs were treated with XEG and their sensitivity to XyG removal was assessed. To quantify the sensitivity of *xeg113* PTs to XEG treatment pollen grains were *in vitro* germinated in a concentration row of XEG containing germination medium. *xeg113* single mutant PTs showed a reduction of the germination rate after XEG treatment compared to wild-type PTs (Fig. 4C). Additionally, four hours post germination XEG was added and PTs were observed after two hours and only vesicle release could be observed. Six hours post germination, XEG was added and the effect on PT growth was investigated 16 h later. While wild-type PT tips formed drop-like structures, *xeg113* tips became spherical and often burst at the tip (Fig. 4D, E, F). In total, 71.9% of *xeg113* PTs and 52.2% of wild-type PTs showed aberrant structures. These results suggest that *xeg113* PTs are hypersensitive to XEG treatment compared to the wild-type.

The triple mutant *xxt1 xxt2 xeg113*.

Immunolabeling revealed higher extensin content in the *xxt1 xxt2* double mutant and XEG treatment showed a hypersensitivity against XyG removal in *xeg113*. Therefore, a triple mutant *xxt1 xxt2 xeg113* was produced (SI, Fig. S2) to investigate the effect of underarabinosylated extensins in *xxt1 xxt2* double mutants. Pollination of wild-type plants with mutants homozygous for *xxt1 xxt2* and heterozygous for *xeg113* showed a transmission of 19.5% of the *xeg113* mutation. Thus, the reduction of the fertilization of triple mutant *xxt1 xxt2 xeg113* pollen is suggesting that extensin deficiency affects plants missing XyG and leads to a synergy between these two cell wall components. Adult triple mutants show a massive reduced growth in terms of plant size, growth speed and silique size (SI, Fig. S3). This leads to the conclusion that a XyG lacking plant is

affected in extensin arabinosylation and a synergistic effect occurs, therefore, extensins might play a role in compensating the lack of XyG.

Cellular force microscopy (CFM) of *xxt1 xxt2, xeg113,* and *xxt1 xxt2 xeg113.*

Turgescent growing Arabidopsis PTs were germinated and measured by CFM. Single point PT measurements were accomplished 20 µm adjacent to the PT tip. A 1 µm probe-tip mounted on a MEMS sensor was positioned manually. Measurements (n=20) were repeated 5 times at the same position. Wt PTs showed a median stiffness of the PT tip of 2.88 N/m. The double mutant *xxt1 xxt2* revealed a slight decreased median stiffness of 2.58 N/m. *xeg113* the extensin mutant showed an increased median stiffness of 3.55 N/m, and the XyG/extensin triple mutant *xxt1 xxt2 xeg113* was 4.33 N/m (Fig. 4G). Thickness measurements on DIC pictures revealed in wt, *xxt1 xxt2*, and *xeg113* a cell wall of approximately 860 nm, respectively. *xxt1 xxt2 xeg113* showed a reduced cell wall thickness of 730 nm in average.

3.4 DISCUSSION

Arabidopsis PT cell walls are bilayered with a fibrillar outer layer and a weakly electron-dense inner layer. The amount of XyG is rather low compared to walls of vegetative cells but has a higher degree of galactosylation, fucosylation, and acetylation of Gal [33], indicating that XyG in PT cell walls are structurally distinct from the one of vegetative cells and might serve particular purposes. XyG show a strong interaction with cellulose [1] and have been shown to contribute to the mechanical strength of cell walls [34, 35]. Despite this apparent importance, it was surprising to find that the *xxt1 xxt2* double mutant, containing strongly reduced amounts of XyG, only show mild growth phenotypes [4]. The data presented here demonstrate that this mutant line develops a strong PT growth phenotype. PTs elongate by tip-growth [14] as do root hairs [36], and the *xxt1 xxt2* mutant as well as the xxt5 mutant develop a root hair phenotype [4, 37]. Hence, it seems that XyG is of particular importance in tip-growing cell types. There is increasing evidence for cell wall enlargement rather than solely turgor pressure being a main determinant in elongation growth in PT [38]. Considering the particular composition of XyG in PTs [33] and the strong mutant phenotype of the *xxt* mutants, it can be

speculated that XyG plays a significant role in the cell wall growth process in tip-growing cells. The observed release of vesicles in PTs with a degenerated XyG suggests that hemicelluloses are important not only for the mechanical strength but also for the integrity of the cell wall. The budding process *per se* is likely to be turgor-driven, which explains the concomitant but transient interruption of tube elongation. This phenomenon is most likely a direct cause of XyG-deficiency as it is also observed in wild-type PTs within minutes of XEG application.

Despite the strong growth phenotype, XyG deficiency seems not deleterious to cell growth and produces fertile plants. This raises the question as to whether there is a structural compensation for this major change in cell wall composition. Defects in cell wall structure can cause secondary changes to cope with the resulting stress [39] and mutants with cell wall formation defects can be suppressed by the introduction of secondary changes in cell wall structures [40]. Pectic polysaccharides and arabinoxylans are assumed to be candidates that compensate by sharing the mechanical load of the wall [41]. Recently, it has been shown that a lack of detectable XyG does not cause significant changes in the amount of other polysaccharides. It has been suggested that it is likely that they undergo rearrangements without changing synthesis of other cell wall components to compensate for XyG deficiency [42]. Nevertheless, our results support a picture were structural cell wall proteins playing a major role. It has been shown that glycoproteins are involved in the early cell wall formation and their contributions to cell wall mechanics are not described yet. The data presented here suggest that extensins may be involved in a possible compensatory mechanism in the *xxt1 xxt2* double mutant. These structural hydroxyproline-rich glycoproteins form rod-like structures that are able to link different wall components [10, 43]. Extensins can self-assemble into larger structures [44] and insolubilize in the cell wall [11-13]. Insolubilization can be induced by tension stress or pathogen attack [45, 46] and is likely to increase mechanical strength. Based on these characteristics, extensin might indeed be able to fortify XyG-deficient cell walls in order to maintain wall integrity. The *xeg113* extensin mutant used in this study is particularly useful since arabinosylation of extensins in general is affected in this line. Extensin single mutants in most cases do not develop a striking phenotype, which can be explained by genetic redundancy among the many extensin genes in the Arabidopsis genome [47]. The *xeg113* mutant was identified in a chemical genetic

screen aiming at identifying mutants with altered responses to changes in the XyG content. In the presence of XEG, *xeg113* seedlings developed longer hypocotyls and petioles than the wild type. In the absence of XEG, no difference in seedling growth was observed [32]. These results show that extensins contribute to limit cell growth when XyG is enzymatically removed. Apparently, PTs are more sensitive to changes in extensin content, reflected by the strong growth phenotype of the *xeg113* mutant. This points towards a particular importance of XyG and extensins for the cell wall of this particular cell type.

The analysis of *xxt1 xxt2* mutant PTs with mAbs revealed several changes in the cell wall structure. Apart from those with anti-extensin antibodies, these changes in labeling are related to changes in PT shape. For example JIM7, detecting the highly methylesterified homoglacturonan labeled also secondary tips, which mirrors the necessity of expandable pectin at the growing tip [48]. The AGP-epitope recognized by LM14 appears particularly abundant at the site of vesicle emergence. AGPs have been shown to be expressed in pollen and have an important function in PT growth [49, 50]. Evidently, the release of vesicles in XyG-deficient PTs is concurrent with dramatic changes in cell wall structure and the data indicate that AGPs are involved in this process. Whether they are necessary for vesicle release to take place or rather represent a repair mechanism induced by local disruption of the cell wall remains to be shown.

In addition to the effect on PT elongation, the reduction in XyG also affects growth directionality. *xxt1 xxt2* mutant PTs initially grow into the transmitting tract but then seem to loose orientation, leading to the observed entanglement. This often occurs in the transmitting tract but sometimes, PTs grew as far as to the ovule where they fail to enter the micropyle, a prerequisite for successful fertilization to take place. Entanglement has also been observed in other mutants. *feronia* PTs grow into one synergid cell where they fail to burst and keep growing in a disoriented fashion [16]. In this case, growth orientation and direction are not affected but rather the signaling process that leads to rupture of the PT [15]. PTs are guided through the transmitting tract by attractants and nutrients provided by this tissue [51]. The cell wall integrity of PTs also is a crucial factor in this complex process. A lack of XyG and underarabinosylation of extensins does not only affect PT growth, as shown in the transmission efficiency experiments with *xxt1 xxt2* heterozygous *xeg113*. The triple

mutant plant *xxt1 xxt2 xeg113* revealed massive reduction in plant size and growth speed, which is related to the essential role of extensins in building and maintaining of the growing primary cell wall [44].

Here, is shown that the mechanical properties of Arabidopsis PTs change when cell wall biochemistry varies. Mechanical micro-indentation of Arabidpopsis PTs was performed by Cellaular Force Microscopy (CFM). The obtained data revealed that the measured apparent stiffness increases or decreases when XyG and extensins are affected. XyG deficient PTs were slight softer when measured by CFM this implies that XyG may partly contribute to cell wall stiffness. The findings are consistent with the observed *xxt1 xxt2* PT phenotype and the hypothesis that XyG remodelling maintains tensile strength of the cell wall and plays a role during cell elongation [1, 35]. *xxt1 xxt2* cell walls have been shown are mechanically weaker (more extensible) in breaking strenght assays [41]. *xeg113* PTs show a growth phenotype and CFM results demonstrate that the stiffness is significantly increased. Extensins were reported to insolubilize in the cell wall by an unknown mechnism by covalently cross-linking cell walls [8, 13]. They are proposed to be assocciated in the cell wall with the cessation of growth [8]. The phenotype described in *xeg113* is most probable caused by the underarabinosylation of extensins. Less cross-links would implicate to weaken or destabilize the cell wall. But the produced XyG/extensin mutant (*xxt1 xxt2 xeg113*) revealed stiffer PTs that often burst. It is likely that a putative expanding zone at the tip needs extenins to initiate tip growth or XyG rearrangements in *xeg113* to accomplish cell wall expansion. A less flexible cell wall in *xxt1 xxt2 xeg113* PTs leads to the assumption XyG and extensins may synergistically interact. This would strenghten the hypothesis that XyG and extensins compensate each other in a situation were one of the components is lacking.

In conclusion, the process of cell wall expansion and elongation is a crucial and important process for plant growth, and its incomplete network of responsible factors leads to dramatic changes in plant morphology. It was shown the first time that the extensins might compensate the effect of the missing cell wall component XyG and that plants have and engage mechanisms to balance the complex cell wall network when a component is removed.

3.5 EXPERIMENTAL PROCEDURES

Plant Material. *Arabidopsis thaliana* (ecotype Col-0) *xxt1 xxt2* seeds [4] were obtained from the NASC European Arabidopsis stock center. *xeg113-2* was provided by M. Pauly. Plants were grown in growth chambers with 16 h light, 8 h dark cycles at 22°C.

***In vitro* PT Growth and FM4-64 Staining.** Flowers were collected and incubated in a moisture chamber, for 30 min at 22°C. Liquid growth medium was prepared as described [52]. Pollen grains were brushed on Biobond (BBI International) and covered with liquid growth medium, germinated, and grown in a moisture chamber, first at 30°C, 30 min and then at 22°C for 6 h. For germination on solid medium, 1.5% low melting agarose was added to liquid growth medium. For CFM measurements PTs were germinated on silane coated slides. Living PTs were stained with 5 µM FM4-46, added to the liquid germination medium. For XEG digestion, 140 U/mL recombinant xyloglucanase (XEG; EC 3.2.1.151; Novozymes [31]; 1 U releases 1 µmol of XyG oligosaccharides per minute) was added to PT growth medium. DIC on a Leica DM6000 microscope was used for documentation of PTs. Fluorescence staining of FM4-64 was detected with a Leica DM6000 microscope. To analyze the length of the PTs, ImageJ (http://rsbweb.nih.gov/ij/) was used.

***In vivo* Pollination.** Flowers were emasculated at stage 6.5 [53] and left for 24 h prior pollination. Pollinated pistils were collected after 2 h, 6 h, and 24 h. Pistils were mixed with ethanol/acetic acid and incubated overnight at 4°C. Pistils were dehydrated in a dilution series of ethanol from 30-70%, cleared with chloral hydrate/clearing solution [15] for 5 min at 60°C, and washed with 0.1 M sodium phosphate buffer, pH 8.0. The washed pistils then were incubated in 5 M NaOH at 60°C for 10 min and washed with sodium phosphate buffer twice. Tissue was stained with 0.1% Methyl Blue (Sigma) in sodium phosphate buffer prior to microscopic analysis.

Immunocytological Analysis. Immunolabeling of PTs was carried out as described [54]. PTs were incubated with a 10-fold dilution of primary mAbs in PBS/MP for 1 h. Samples were washed in PBS and incubated with a

100-fold dilution of fluorescein isothiocyanate-labeled secondary Ab (Sigma) in PBS/MP for 1 h in darkness. The samples were washed three times and mounted in a glycerol-based anti-fade solution (Citifluor AF1) and fluorescence was detected on a Leica DM6000 microscope.

Cellular Force Microscopy. Arabidopsis PTs that were adhered to silane-coated slides (Science Services, www.scienceservices.de) were focused at a 400x magnification with DIC optics on an inverted microscope (Olympus IX 71, http://www.olympus-global.com). After the sensor tip was positioned manually on the PT at the starting point of the measurement series, control was taken over by the LabVIEW software. At one point five measurements with four scans were taken. From each point the mean stiffness values were calculated. Sensor movement and data analysis is described in Chapter 2 (EXPERIMENTAL PROCEDURES).

Acknowledgements

We would like to thank K. Schnorr (Novozymes) for provding XEG and M. Pauly for *xeg113-2* seeds, A. Meury for technical assistance, H. Vogler and A. Boisson-Dernier for critical reading of the manuscript. This work was supported by the SystemsX program of the Swiss National Science Foundation.

3.6 REFERENCES

[1] Cosgrove DJ (2005) Growth of the plant cell wall. *Nat Rev Mol Cell Biol* 6:850-861.

[2] Willats WGT, McCartney L, Mackie W, Knox JP (2001) Pectin: cell biology and prospects for functional analysis. *Plant Mol Biol* 47:9-27.

[3] Hayashi T (1989) Xyloglucans in the primary cell wall. *Annu Rev Plant Physiol Plant Mol Biol* 40:139-68.

[4] Cavalier DM, et al. (2008) Disrupting two *Arabidopsis thaliana* Xylosyltransferase genes results in plants deficient in xyloglucan, a major primary cell wall component. *The Plant Cell* 20:1519-1537.

[5] Showalter AM (2001) Arabinogalactan-proteins: structure, expression and function. *Cell Mol Life Sci* 58:1399-1417.

[6] Wilson LG, Fry JC (1986) Extensin: A major cell wall glycoprotein. *Plant Cell Environ* 9:239-260.

[7] Liang Y, Faik A, Kieliszewski M, Tan L, Xu WL, Showalter AM (2010) Identification and characterization of in vitro galactosyltransferase activities involved in arabinogalactan-protein glycosylation in tobacco and Arabidopsis. *Plant Physiol* 154:632-642.

[8] Cassab GI (1998) Plant cell wall proteins. *Annu Rev Plant Physiol Plant Mol Biol* 49:281-309.

[9] Cannon MC, Terneus K, Hall Q, Tan L, Wang YM, Wegenhart BL, Chen LW, Lamport DTA, Chen YN, Kieliszewski MJ (2008) Self-assembly of the plant cell wall requires an extensin scaffold. *Proc Natl Acad Sci USA* 105:2226-2231.

[10] Qi XY, Behrens BX, West PR, Mort AJ (1995) Solubilization and partial characterization of extensin fragments from cell walls of cotton suspension-cultures - evidence for a covalent cross-link between extensin and pectin. *Plant Physiol* 108:1691-1701.

[11] Fry SC (1982) Isodityrosine, a new cross-linking amino acid from plant cell-wall glycoprotein. *Biochem J* 204:449-455.

[12] Held MA, Tan L, Kamyab A, Hare M, Shpak E, Kieliszewski MJ (2004) Di-isodityrosine is the intermolecular cross-link of isodityrosine-rich extensin analogs cross-linked in vitro. *J Biol Chem* 279:55474-55482.

[13] Ringli C (2010) The hydroxyproline-rich glycoprotein domain of the Arabidopsis LRX1 requires Tyr for function but not for insolubilization in the cell wall. *Plant J* 63:662-669.

[14] Gille S, Hänsel U, Ziemann M, Pauly M (2009) Identification of plant cell wall mutants by means of a forward chemical genetic approach using hydrolases. *Proc Natl Acad Sci USA* 106:14699-14704.

[15] Yang Z (1998) Signaling tip growth in plants. *Curr Opin Plant Biol* 1:525-530.

[16] Huck N, Moore JM, Federer M, Grossniklaus U (2003) The Arabidopsis mutant *feronia* disrupts the female gametophytic control of pollen tube reception. *Development* 130:2149-2159.

[17] Ferguson C, Teeri TT, Siika-aho M, Read SM, Bacic A (1998) Location of cellulose and callose in pollen tubes and grains of *Nicotiana tabacum*. *Planta* 206:452-460.

[18] Cai G, Moscatelli A, Cresti M (1997) Cytoskeletal organization and pollen tube growth. *Trends Plant Sci* 2:86-91.

[19] Martin C, Bhatt K, Baumann K (2001) Shaping in plant cells. *Curr Opin Plant Biol* 4:540-549.

[20] Geitmann A, and Parre E (2004) The local cytomechanical properties of growing pollen tubes correspond to the axial distribution of structural cellular elements. *Sex Plant Reprod* 17, 9-16.

[21] Parre E, and Geitmann A (2005) More than a leak sealant. The mechanical properties of callose in pollen tubes. *Plant Physiol* 137, 274-286.

[22] Routier-Kierzkowska AL, Weber A, Kochova P, Felekis D, Nelson B, Kuhlemeier C and Smith RS (2012) Cellular force microscopy for *in vivo* measurements of plant tissue mechanics. *Plant Physiol*

[23] Puhlmann J, et al. (1994) Generation of monoclonal antibodies against plant cell wall polysaccharides. *Plant Physiol* 104:699-710.

[24] Marcus SE, et al. (2008) Pectic homogalacturonan masks abundant sets of xyloglucan epitopes in plant cell walls. *BMC Plant Biol* 8:60.

[25] Clausen MH, Willats WGT, Knox JP (2003) Synthetic methyl hexagalacturonate hapten inhibitors of anti-homogalacturonan monoclonal antibodies LM7, JIM5 and JIM7. *Carbohydr Res* 338:1797-1800.

[26] McKenna ST, et al. (2009) Exocytosis precedes and predicts the increase in growth in oscillating pollen tubes. *Plant Cell* 21:3026-3040.

[27] Jones L, Seymour CB, Knox JP (1997) Localization of pectic galactan in tomato cell walls using a monoclonal antibody specific to (1→4)-β-D-galactan. *Plant Physiol* 113:1405-1412.

[28] Willats WGT, Marcus SE, Knox JP (1998) Generation of a monoclonal antibody specific to (1→5)-α-L-arabinan. *Carbohydr Res* 308:149-152.

[29] Moller I, et al. (2008) High-throughput screening of monoclonal antibodies against plant cell wall glycans by hierarchial clustering of their carbohydrate microarray binding profiles. *Glycoconjugate J* 25:37-48.

[30] Smallwood M, et al. (1994) Localization of cell-wall proteins in relation to the developmental anatomy of the carrot root apex. *Plant J* 5(2):237-246.

[31] Smallwood M, Martin H, Knox JP (1995) An epitope of rice threonine- and hydroxyproline-rich glycoprotein is common to cell wall and hydrophobic plasma membrane glycoproteins. *Planta* 196:510-522.

[32] Pauly M, et al. (1999) A xyloglucan-specific endo-β-1,4-glucanase from Aspergillus aculeatus: expression cloning in yeast, purification and characterization of the recombinant enzyme. *Glycobiol* 9:93-100.

[33] Dardelle F, Lehner A, Ramdani Y, Bardor M, Lerouge P, Driouich A, Mollet JC (2010) Biochemical and immunocytological characterizations of Arabidopsis pollen tube cell wall. *Plant Physiol* 153:1563-1576.

[34] Ryden P, Sugimoto-Shirasu K, Smith AC, Findlay K, Reiter WD, McCann MC (2003) Tensile properties of Arabidopsis cell walls depend on both a xyloglucan cross-linked microfibrillar network and rhamnogalacturonan II-borate complexes. *Plant Physiol* 132:1033-1040.

[35] Pena MJ, Ryden P, Madson M, Smith AC, Carpita NC (2004) The galactose residues of xyloglucan are essential to maintain mechanical strength of the primary cell walls in Arabidopsis during growth. *Plant Physiol* 134:443-451.

[36] Dolan L et al. (1994) Clonal relationships and cell patterning in the root epidermis of Arabidopsis. *Development* 120:2465-2474.

[37] Zabotina OA, van de Ven WTG, Freshour G, Drakakaki G, Cavalier D, Mouille G, Hahn MG, Keegstra K, and Raikhel NV (2008) Arabidopsis *XXT5* gene encodes a putative α-1,6-xylosyltransferase that is involved in xyloglucan biosynthesis. *Plant J* 56:101-115.

[38] Winship LJ, Obermeyer G, Geitmann A, Hepler PK (2010) Under pressure, cell walls set the pace. *Trends Plant Science* 15:363-369.

[39] Bosca S, Barton CJ, Taylor NG, Ryden P, Neumetzler L, Pauly M, Roberts K, Seifert GJ (2006) Interactions between MUR10/CesA7-dependent secondary cellulose biosynthesis and primary cell wall structure. *Plant Physiol* 142:1353-1363.

[40] Diet A, Link B, Seifert GJ, Schellenberg B, Wagner U, Pauly M, Reiter WD, Ringli C (2006) The Arabidopsis root hair cell wall formation mutant *lrx1* is suppressed by mutations in the *RHM1* gene encoding a UDP-L-rhamnose synthase. *Plant Cell* 18:1630-1641.

[41] Park YB, Cosgrove DJ (2012). Changes in cell wall biomechanical properties in the xyloglucan-deficient *xxt1/xxt2* mutant of Arabidopsis. *Plant Physiology* 158:465-475.

[42] Zabotina OA, Avci U, Cavalier D, Pattathil S, Chou Y, Eberhard S, Danhof L, Keegstra K, Hahn MG (2012) Mutations in multiple *XXT* genes of Arabidopsis reveal the complexity of xyloglucan biosynthesis. *Plant Physiol* 159:1367-1384.

[43] Iiyama K, Lam TBT, Stone BA (1994) Covalent cross-links in the cell wall. *Plant Physiol* 104:315-320.

[44] Lamport DTA, Kieliszewski MJ, Chen Y, Cannon MC (2011) Role of the Extensin Superfamily in Primary Cell Wall Architecture. *Plant Physiol* 156:11-19.

[45] Shirsat AH, Bell A, Spence J, Harris JN (1996) The Brassica napus *extA* extensin gene is expressed in regions of the plant subject to tensile stresses. *Planta* 199:618-624.

[46] Brisson LF, Tenhaken R, Lamb C (1994) Function of oxidative cross-linking of cell wall structural proteins in plant disease resistance. *The Plant Cell* 6:1703-1712.

[47] Showalter AM, Keppler B, Lichtenberg J, Gu DZ, Welch LR (2010) A Bioinformatics approach to the identification, classification, and analysis of hydroxyproline-rich glycoproteins. *Plant Physiol* 153:485-513.

[48] Bosch M, Cheung AY, Hepler PK (2005) Pectin methylesterase, a regulator of pollen tube growth. *Plant Physiol* 138:1334-1346.

[49] Mollet JC, Kim S, Jauh GY, Lord EM (2002) Arabinogalactan proteins, pollen tube growth, and the reversible effects of Yariv phenylglycoside. *Protoplasma* 219:89-98.

[50] Pereira LG, Coimbra S, Oliveira H, Monteiro L, Sottomayor M (2006) Expression of arabinogalactan protein genes in pollen tubes of *Arabidopsis thaliana*. *Planta* 223:374-380.

[51] Johnson MA, Lord E (2006) Extracellular guidance cues and intracellular signaling pathways that direct pollen tube growth. *In The Pollen Tube eds Malho (Springer-Verlag)* pp 223-242.

[52] Boavida LC, McCormick S (2007) Temperature as a determinant factor for increased and reproducible in vitro pollen germination in *Arabidopsis thaliana*. *Plant J* 52:570-582.

[53] Boyes DC, Zayed AM, Ascenzi R, McCaskill AJ, Hoffmann NE, Davis KR, Gorlach J (2001) Growth stage-based phenotypic analysis of Arabidopsis: a model for high throughput functional genomics in plants. *Plant Cell* 13:1499-1510.

[54] McCartney L, Steele-King CG, Jordan E, Knox JP (2003) Cell wall pectic (1→4)-β-D-galactan marks the acceleration of cell elongation in the Arabidopsis seedling root meristem. *Plant J* 33:447-54.

3.7 SUPPLEMENTAL DATA

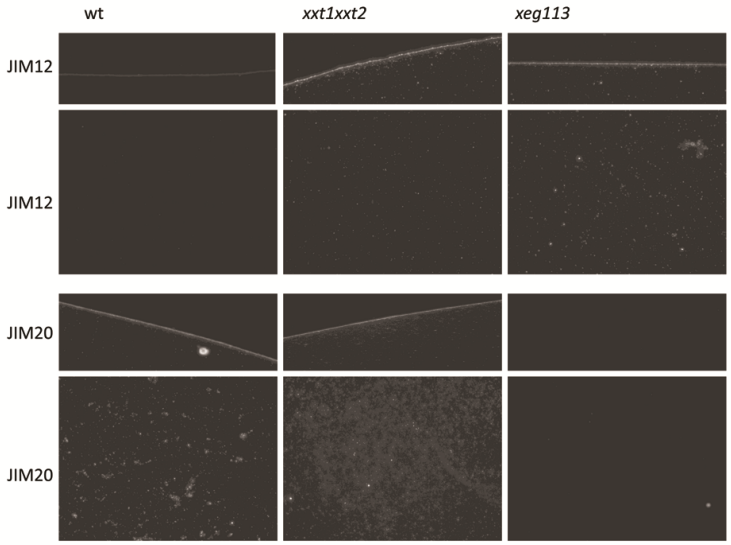

Figure S1: **Immuno-dot blot analysis of crude seedling extracts.** Extensins are labeled with JIM12 and JIM20 mAbs. The upper picture shows the outer edge of the spotted extract, the lower shows the inner area.

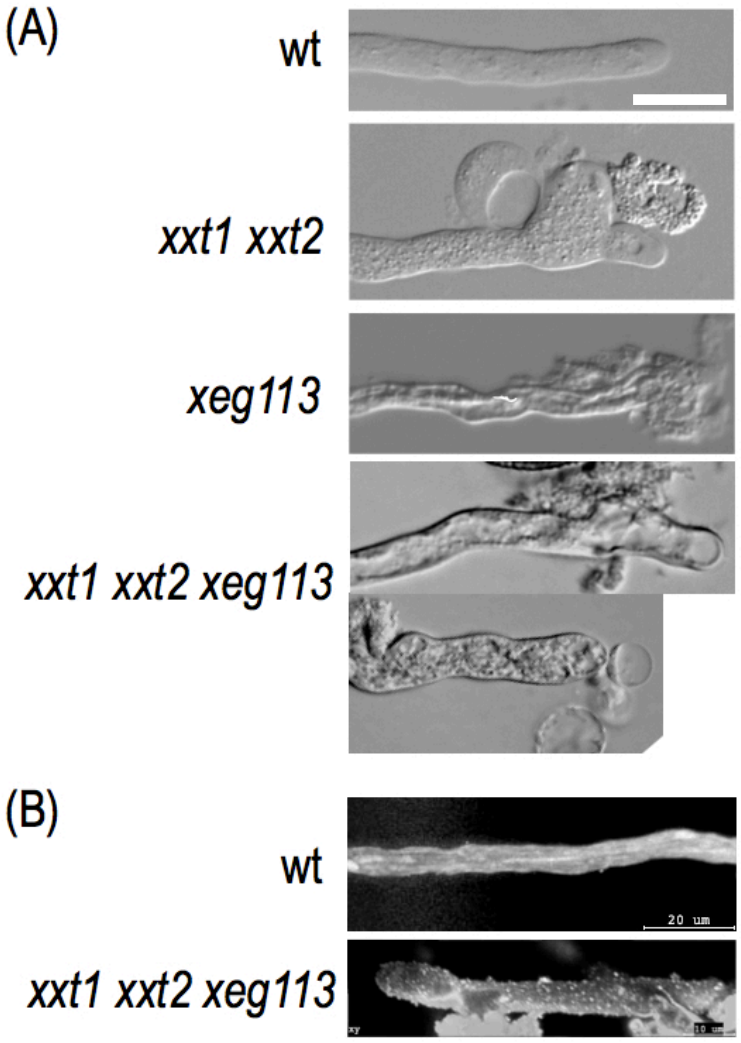

Figure S2: **Pollen tube phenotype of *xxt1 xxt2 xeg113*.** (A) DIC pictures of the phenotypes of wt, *xxt1 xxt2*, *xeg113*, and *xxt1 xxt2 xeg113*. (B) Confocal image of wt and *xxt1 xxt2 xeg113*. wt revealed a smooth cell wall surface whereas *xxt1 xxt2 xeg113* showed a uneven rough surface. (Scale bars: (A) = 10 µm; (B, wt) = 20 µm; (B, *xxt1 xxt2 xeg113* = 10 µm)

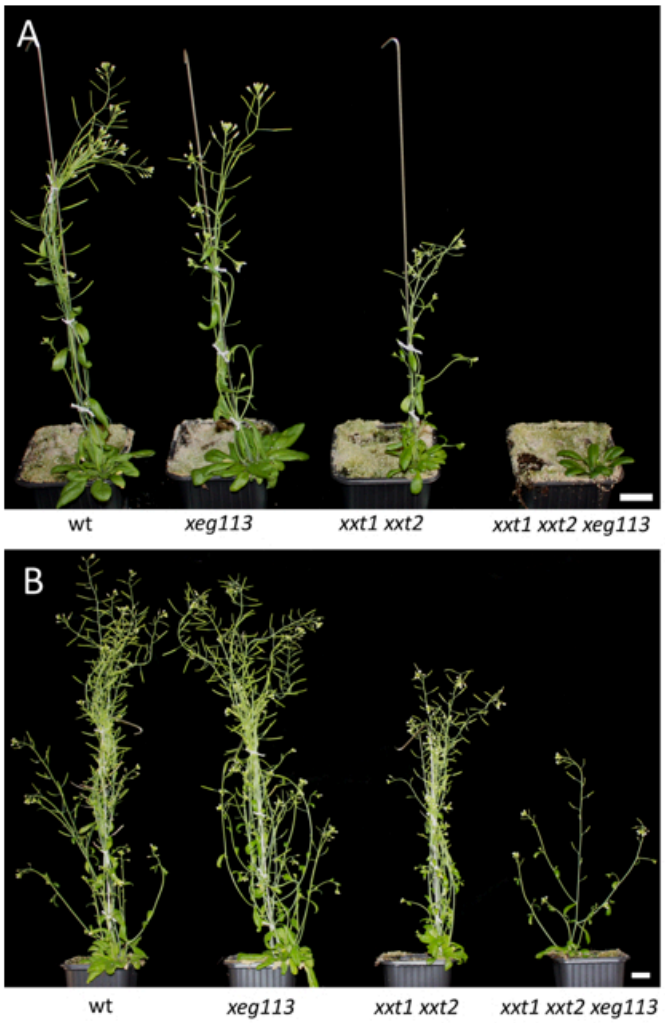

Figure S3: **The triple mutant *xxt1 xxt2 xeg113*.** Three weeks (A) and five weeks (B) old Arabidopsis plants of wt, *xeg113*, *xxt1 xxt2* and *xxt1 xxt2 xeg113*. (Scale bars: 2 cm).

4. LOSS-OF-FUNCTION EFFECT OF LRR-EXTENSINS (*ATPEX*) ON POLLEN TUBE GROWTH

During a mutant screen, LRR-extensin mutants were identified showing a growth phenotype in pollen tubes (PTs). LRR-extensin (LRX) proteins are involved in cell wall development but their function remains elusive. *LRX1* and *LRX2* have overlapping functions and regulate cell wall morphogenesis during Arabidopsis root hair development (Baumberger et al., 2001; Baumberger et al., 2003a).

A pollen-specific maize (*Zea mays*) LRX (PEX1) occurs in the intine layer of the pollen grain and the callosic sheath of the pollen tube (PT). The PEX1 protein revealed a typical chimeric structure containing an extensin-like and an LRR domain. Proteins of the extracellular matrix play an important role in cell-cell recognition, like pollen-pistil interaction during pollination by mediating an active interaction between male and female tissues (Rubinstein et al., 1995a; 1995b). The PEX1 protein is proposed to be involved in reproduction, either as structural recognition molecule deposited in the PT wall or as a sexual recognition molecule interacting with molecules in the pistil (Rubinstein et al., 1995a). *PEX1* is a maize gene and the function of the pollen-specific *LRX* homologs in Arabidopsis (*AtPEX*) is not determined yet. Therefore, an analysis of *AtPEX* may help to characterize to the function of LRX proteins in the process of cell wall development.

Segmental gene duplication in the *LRX* gene family generated gene pairs (*AtPEX1/AtPEX2* and *AtPEX3/AtPEX4*), which are considered to be paralogs. Members of the *LRX* family *ATPEX1, ATPEX2, ATPEX3,* and *ATPEX4* are only expressed in pollen (Baumberger at al., 2003b). PTs and root hairs are the only cells in the plant kingdom which exhibit directed tip growth. It is not known whether *atpex1, atpex2, atpex3,* and *atpex4* mutants are affected in PT growth. Therefore, a mutant screen of the *LRX* familiy members *atpex1, atpex2, atpex3,* and *atpex4* was performed. T-DNA insertion lines of *atpex1* (At3g19020; SALK_001367), *atpex2* (At1g49490; SALK_136073), *atpex3* (At2g15880; SALK_087083), and *atpex4* (At4g33970; SALK_030664) were confirmed by PCR or Southern blot (Fig. 1). Except for *atpex3*, homozygous mutants were isolated and characterized. Technical problems delayed the analysis of the *atpex3* mutant.

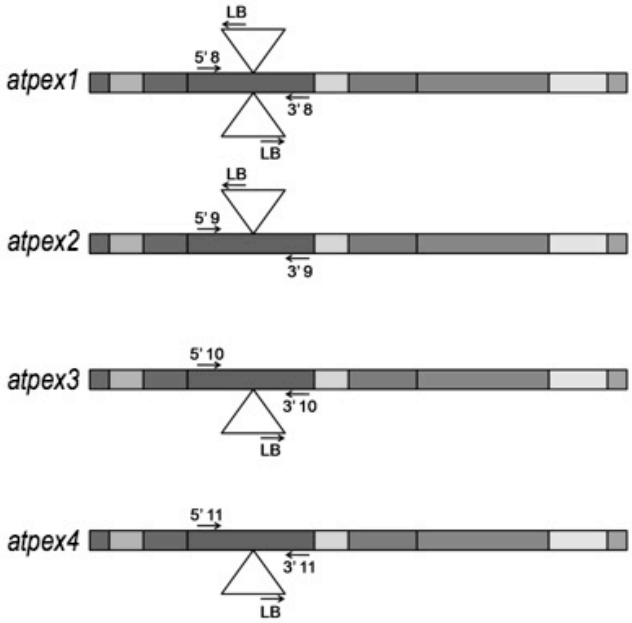

Figure 1: **T-DNA insertion lines *atpex1-4*.** Mutants were confirmed by PCR or Southern blot.

PTs of *atpex1, atpex2* mutants revealed generally a normal growth when grown 2-3h *in vitro* compared to wt (Fig. 2 A, C, D). The double mutant *atpex1 atpex2* revealed untypical high frequently secondary tips compared to wt (Fig. 2 E). *atpex1 and atpex4* PTs showed bulging structures in regular intervals of (10-50 µm) in the single mutants when grown longer than 6h (Fig. 2 F, G).

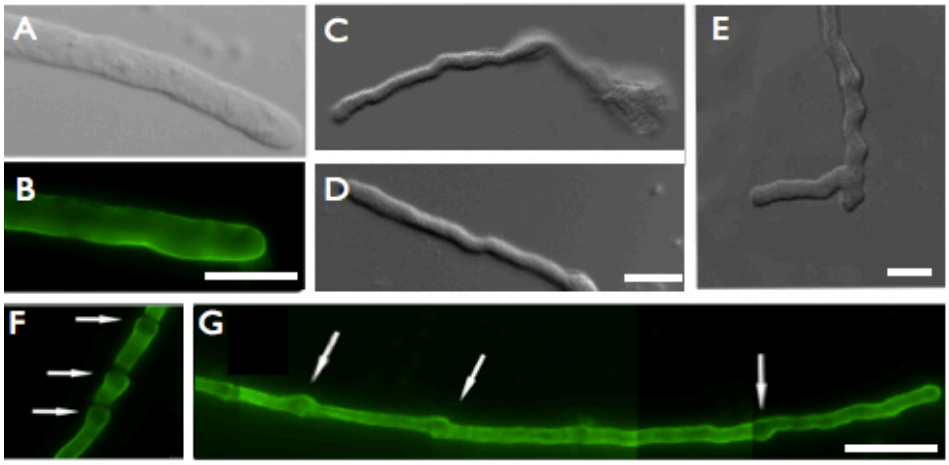

Figure 2: **Pollen tube phenotype of knock-out mutants of pollen expressed *LRX*s.** (A) wild-type Arabidopsis PT. (B) XyG staining with LM15 shows uniform labeling in wild-type PTs. (C) *atpex1* and (D) *atpex2*. LM15 uniform staining, bulging structures indicated by arrows. (E) *atpex1 atpex2* double mutants reveal frequently PT branching. (F) *atpex4* (E) *atpex1* LM15 uniform staining, bulging structures indicated by arrows. (A), (B): bars = 10 µm; (C), (D): bar = 25 µm; (E): bar = 20 µm; (F), (G): bar = 50 µm.

Mutants were screened with different mAbs against different cell wall structures as described in Chapter 3. The immunocytological analysis revealed no differences compared to the wild-type with LM15 a XyG mAb (Fig. 2 B, F, G), LM2 (recognizes glucoronic acids in AGPs; Smallwood et al., 1996; Yates et al., 1996), and CRCC-M1 (recognizes fucosylated XyG) Puhlmann et al. (1994). *atpex1* and *atpex4* revealed an increased signal at the described bulges labelled with LM6. LM6 mAbs recognize arabinan epitopes and may also bind AGPs (Fig. 3). The *LRX* mutant *atpex3* and the combinations *atpex3 atpex4, atpex1 atpex2 atpex3, atpex1 atpex3 atpex4, atpex1 atpex2 atpex4, atpex2 atpex3 atpex4, atpex1 atpex2 atpex3 atpex4* remain to be established.

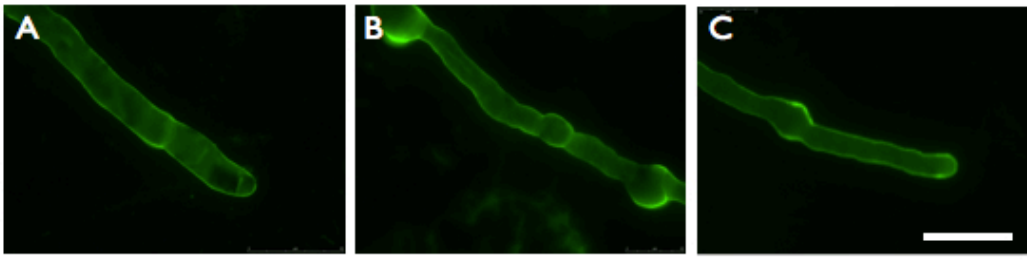

Figure 3: **LM6 labeling of *atpex1* and *atpex4* mutant pollen tubes.** (A) wild-type Arabidopsis PT labeled with LM6. (B) LM6 immunolabeling of *atpex1* and (C) *atpex4* PTs shows an increased signal at bulging structures. (A), (B), (C): bar = 25 µm.

The *atpex1, atpex4, and atpex1 atpex2* mutant lines show a growth phenotype in PTs, hence LRX proteins are important for PT growth.

Cell wall analysis is difficult in Arabidopsis PTs, due to the small amounts of cell wall material available. A change to a tissue where the biological material is not the limiting factor would be ideal to elucidate changes in the cell wall due to mutations in *LRX* genes. *LRX3, LRX4, LRX5* are expressed in leaves and they are chosen with the assumption that the amount of material in these mutants is not limited for a biochemical cell wall analysis. To analyze further contributions of *LRX* genes to cell wall development, *lrx* mutants *lrx3, lrx4, lrx5* were used.

5. LRX3, LRX4, AND LRX5 AFFECT PECTIN STRUCTURE AND ARE IMPORTANT FOR CELL WALL DEVELOPMENT

5.1 SUMMARY

LRR-extensins (LRX) are a family of structural cell wall proteins involved in cell wall morphogenesis. In *Arabidopsis thaliana* the analysis of *LRX1* and *LRX2* has shown that they are paralogs, mainly expressed in roots, and are involved in cell wall formation. The gene family members *LRX3, LRX4,* and *LRX5* are mainly expressed in the aboveground organs. Using complementation as a parameter for the protein function, our experiments indicate that LRX3, LRX4, and LRX5 have a similar function and the *lrx* mutants revealed changes in the biochemical composition of the cell wall. Scanning electron microscopy (SEM) revealed that the pavement cells of leaves show a phenotype in *lrx3, lrx4, lrx5, lrx3 lrx4,* and *lrx3 lrx4 lrx5* single, double, and triple mutants. Comprehensive Microarray Polymer Profiling (CoMPP) analysis showed a reduced amount of xylan/arabinoxylan, arabinan, and extensins in double and triple mutants. Analysis of the monosaccharide composition of the cell wall in double and triple mutants shows a decrease in rhamnose and galactose contents. The results obtained indicate that *LRX3, LRX4,* and *LRX5* may be involved in cell wall development, where they might be contributors to the modification or regulation of pectin in the cell wall.

5.2 RESULTS

LRX3, LRX4, and LRX5 protein structure

The Arabidopsis gene family members *LRX3, LRX4,* and *LRX5* (Table of *LRX* gene nomenclature, Supplementary data, S1) are located on chromosomes III and IV of the Arabidopsis genome. A Segmental genome duplication in Arabidopsis generated gene pairs including *AtLRX3/AtLRX4*, which are considered to be paralogs. The remaining gene *LRX5* is a homologous single gene (Baumberger et al., 2003b). The N-terminal LRR domain and a C-terminal extensin domains are characteristic for LRR-extensins (Fig. 1).

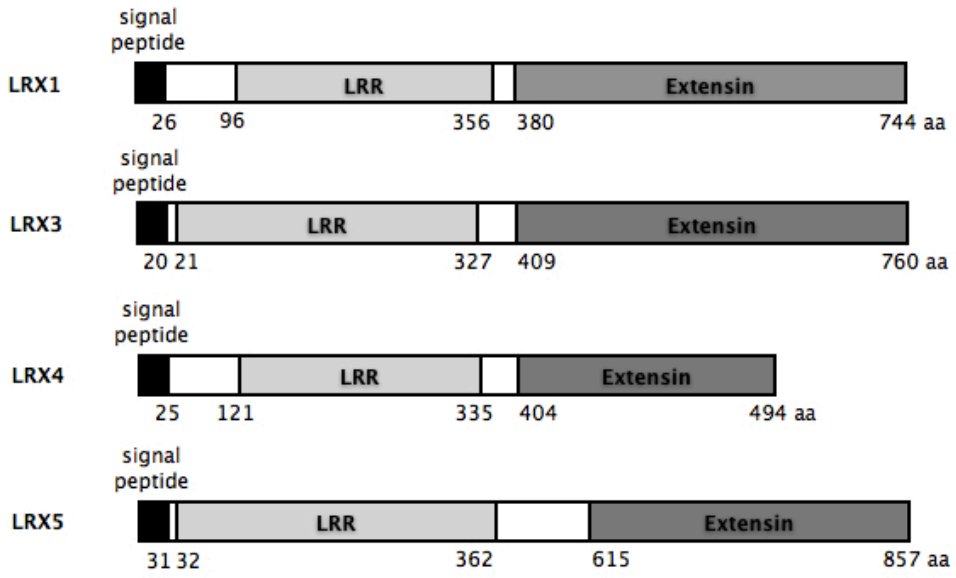

Figure 1: **Schematic structure of the deduced LRX3, LRX4 and LRX5 proteins.** LRX1 protein sequence compared with the LRR-extensin family members LRX3, LRX4 and LRX5. Indicated is the hydrophobic putative signal peptide (black), the LRR domain (LRR), and the extensin-like domain (Baumberger et al., 2001).

The *LRX3, LRX4,* and *LRX5* genes are intronless and encode an approximately 30 amino acid-long signal peptide, an LRR-domain, and an extensin-like domain. LRX4 shows the shortest extensin domain when compared to the other LRX proteins. The LRR domain of LRXs are highly conserved and show similarities up to 73% (Zhou et al., 1992; Rubinstein et al., 1995a; Baumberger et al., 2001). The LRR-domain of LRX1 aligned with the LRR domains of LRX3, LRX4 and LRX5 revealed a very high similarity with 144 identical and 113 similar aa positions (Supplementary data, (SI); Fig. S2). This is consistent with the previously published data (Baumberger et al., 2003b). Previous reports described an expression of *LRX3, LRX4* and *LRX5* in roots of seedlings, but mainly in the aboveground tissues of adult plants (Baumberger et al., 2003b).

Gene analysis and phenotypes of *lrx* mutants

The importance of of *LRX3, LRX4,* and *LRX5* was assessed by analyzing T-DNA insertions lines. T-DNA insertions of *lrx3, lrx4,* and *lrx5* are located at the position 752 (Salk_094400), 1173 (GABI_017A08), and

898 (Salk_013968) bp from the start codon, respectively (Fig. 2). The T-DNA insertion lines *lrx3*, *lrx4* and *lrx5* were crossed to generate the double mutant of the paralogs *lrx3* and *lrx4* and the triple mutant *lrx3 lrx4 lrx5*.

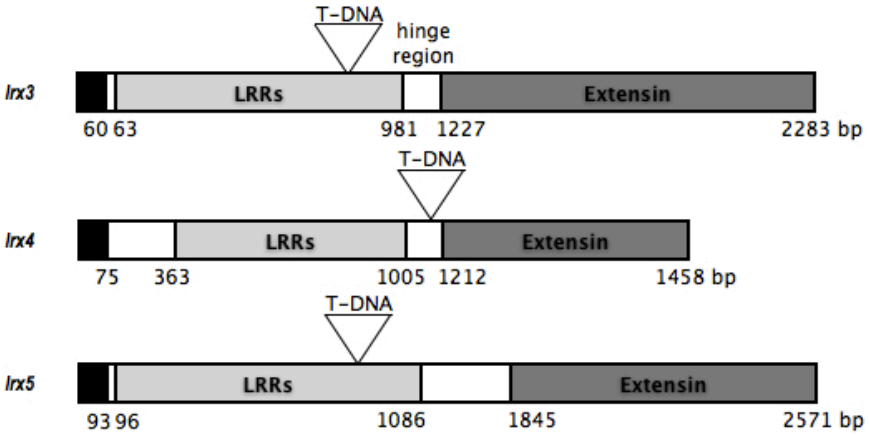

Figure 2: **Schematic structure of *lrx3, lrx4* and *lrx5* insertion lines.** T-DNA insertion lines of *lrx3, lrx4* and *lrx5*, triangels indicate the location of the T-DNA insertion in the coding sequence of the particular gene (black: signal peptide; light grey: LRR domain; dark grey: Extensin domain).

The single mutants showed a weaker phenotype. *lrx3* and *lrx4* infrequently revealed abberant pavement cells (SI, Fig. S3). *lrx5* revealed wild-type (wt) pavement cells (SI, Fig. S3). Root length of *lrx3, lrx4*, *lrx5,* double, and triple mutants was measured in 6 days-old plants (Fig. 3). *lrx3 lrx4 lrx5* roots were shorter than wt roots, and t-test revealed a statistically significant reduction in root length.

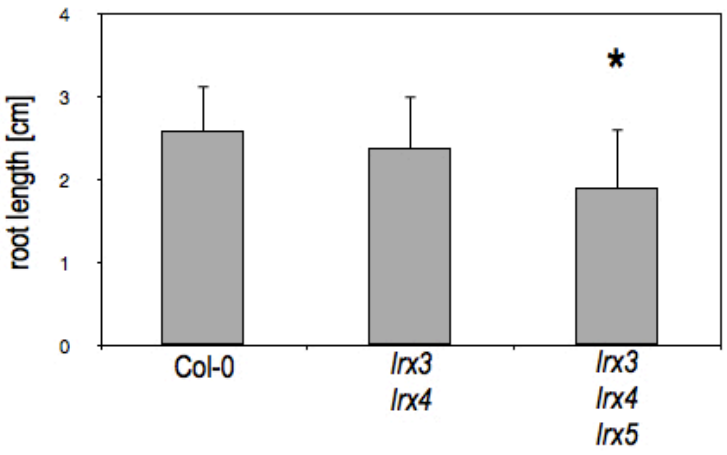

Figure 3: **Root length of *lrx3, lrx4*, *lrx5,* double, and triple mutants.** Length measurements revealed a significant difference in the *lrx3 lrx4 lrx5* triple mutant. Asteriks indicates significant difference in length.

Seedlings of *lrx3 lrx4* double mutants revealed a frequent reduction in size of cotyledons if compared to the wt 6 days-old seedlings, while the triple mutant *lrx3 lrx4 lrx5* showed consistently smaller and less epinastic cotyledons (Fig. 4 A). Analysis of adaxial pavement cells in normal-size cotyledons of *lrx3, lrx4* and *lrx3 lrx4* revealed jigsaw puzzle-like cells which have the same size as in wt cotyledons. In small cotyledons of *lrx3 lrx4,* and in *lrx3 lrx4 lrx5* triple mutants the pavement cell shape is disturbed. *lrx* mutants showed pavement cells with a partial loss of lobes and indentations in smaller cotyledons (Fig. 4 B). SEM pictures of *lrx3 lrx4* revealed a sinuous leaf surface in cotyledons and rosette leaves which is not observed in the wt. *lrx3 lrx4 lrx5* showed massive crater-like structures and a reduced leaf growth in cotyledons and rosette leaves (Fig. 4 C; SI, Fig. S3).

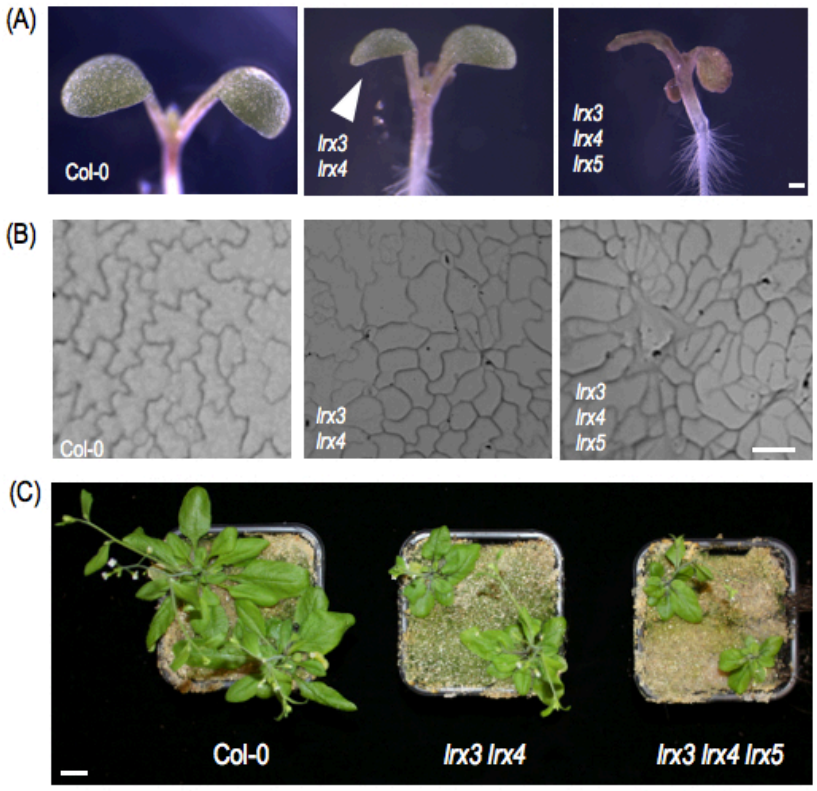

Figure 4: **Phenotype of the *lrx3, lrx4* and *lrx5* mutants.** (A) *lrx* mutant seedlings (6 days old). The arrowhead indicates small cotyledons of the *lrx3 lrx4* double mutant. (B) Pavement cells of the *lrx* mutants did show a phenotype in small cotyledons.(C) Adult plants revealed a growth phenotype with reduced plant size and small rosette leafs. Bars = 0.5 mm (A), 40 µm (B), 1 cm (C).

lrx3 and *lrx4*, the double mutant *lrx3 lrx4* and the triple mutant *lrx3 lrx4 lrx5* revealed a phenotype of reduced growth of cotyledons, rosette leaves, and shoots (Fig. 4C; SI, Fig. S4 A, B). To confirm whether these phenotypes are induced by the T-DNA insertions, complementation experiments were performed with single and double mutants.

Complementation constructs for *lrx* mutants

The genes *LRX3* and *LRX4* were amplified including the native promotor and terminator. The wt copies of *LRX3, LRX4,* and *LRX5* were unstable in *E. coli* strains. In particular, the extensin coding region was frequently truncated. It was shown by complementation experiments with *LRX1* and *LRX2* that the extensin domains are interchangable (Baumberger et al., 2003b). Therefore, the fragment containing promotor and the

LRR-coding domain was amplified from LRX3 and LRX4 and fused with the LRX1-extensin domain and terminator resulting in the chimeric complementation constructs *LRX3:LRR3_EXT1* and *LRX4:LRR4_EXT1*, respectively. For *LRX5* this alternative cloning approach was unsuccessful and forced us to abandon complementation of the *lrx5* mutant.

Complementation of *lrx3, lrx4* and *lrx3 lrx4*

LRX3:LRR3_EXT1 was transformed into *lrx3* and *LRX4:LRR4_EXT1* into *lrx4* plants. *lrx3 lrx4* was transformed with either *LRX3:LRR3_EXT1* or *LRX4:LRR4_EXT1*. Due to the strong phenotype of *lrx3 lrx4 lrx5*, the triple mutants could not be used for plant transformation. T2 progeny segregating for BASTA resistance in a ratio of 3:1 were used for assessment of complementation. Cotyledon imprintings of complemented *lrx3* and *lrx4* mutants revealed normal shaped pavement cells, complemented *lrx3 lrx4* double mutants complemented with *LRX3:LRR3_EXT1* and *LRX4:LRR4_EXT1* showed a *lrx3* and *lrx4*-like single mutant phenotype, respectively (SI, Fig. S5 A). Adult plants also showed a complementation of the *lrx3 lrx4* growth phenotype (SI, Fig. S5 B). Hence, the phenotypes of the mutant lines indeed are induced by the mutations in the *LRX* genes. Complementation was performed with the native promotors of *LRX3* and *LRX4*, explaining why single mutant phenotypes were observed in the double mutant complemented with one construct. Complementation with *LRX3:LRR3_EXT1* or *LRX4:LRR4_EXT1* under a very strong constitutive promotor may lead to a complete reversion of the *lrx3 lrx4* phenotype to a wild type-like phenotype.

Immunocytological CoMPP analysis of *lrx* mutants

To elaborate the cell wall composition of the double and the triple mutant, a screen with monoclonal antibodies (mAbs) against different cell wall components may indicate potential cell wall glycans changed in *lrx* mutants. Therefore, a high throughput characterization using Comprehensive Microarray Polymer Profiling (CoMPP) was performed on leaf and stem extracts (Moller et al., 2007), which both shared reduced growth in the mutants. Plant tissue extracts were washed with the pectin solubilizing solvents diamino-cyclo-hexane-tetra-acetic acid (CDTA) and NaOH, spotted on microarray plates, and the intensity of the spot signals was

quantified (SI, Fig. S6). CoMPP revealed significant changes in the relative intensities of JIM13 (recognizes arabinogalalactan proteins (AGPs; [Knox et al., 1991; Yates et al., 1996]), JIM20 (recognizes extensins [Smallwood et al., 1994; Knox et al., 1995]), LM11 (recognizes xylan; [McCartney et al., 2005]), and LM13 (recognizes arabinan; [Moller et al., 2008; Verhertbruggen et al., 2009]), (Table 2).

Table 2: **Relative intensity data of glycan profiling of wt, *lrx3 lrx4,* and *lrx3 lrx4 lrx5*.** Shown are the values, which differ significantly between wt and mutants.

washing	mutant	organ	AGP JIM13	extensin JIM20	xylan LM11	arabinan LM13
CDTA	wt	stem	90.04 ± 8.62	85.59 ± 8.41		97.44 ± 2.55
	lrx3 lrx4	stem	78.78 ± 0.48	75.97 ± 2.22		92.50 ± 2.05
	lrx3 lrx4 lrx5	stem	66.16 ± 13.46	58.93 ± 6.98		66.14 ± 4.35
NaOH	wt	leaves			95.54 ± 3.86	
	lrx3 lrx4	leaves			40.20 ± 2.80	
	lrx3 lrx4 lrx5	leaves			58.68 ± 16.16	
	wt	stem				49.91 ± 16.50
	lrx3 lrx4	stem				13.41 ± 7.81
	lrx3 lrx4 lrx5	stem				5.22 ± 5.17

Samples washed with CDTA and labeled with JIM13 and JIM20 revealed a reduction in labeling up to 32% in double and triple mutant stems compared to the wt. Samples washed with NaOH showed a reduced LM11 intensity up to 58% in the double mutant. LM13 epitopes were reduced up to 74% in *lrx3 lrx4* plants and up to 90% in *lrx3 lrx4 lrx5* mutants. In summary, the observed changes suggest an effect on the cell wall composition of *lrx* mutants.

Monosaccharide analysis

As an alternative biochemical approach, a monosaccharide analysis of *lrx3 lrx4* and *lrx3 lrx4 lrx5* was performed. Analysis of *lrx3 lrx4* and *lrx3 lrx4 lrx5* revealed a significantly reduced galactose content compared

to the wt (Fig. 7). The rhamnose content in *lrx3 lrx4* and *lrx3 lrx4 lrx5* is also reduced, but not significantly in *lrx3 lrx4 lrx5*. This leads to the suggestion that *lrx* mutants are affected in the assembly of galactose and rhamnose containing cell wall components. For most measurements the standard deviation values are highest in the *lrx3 lrx4 lrx5* triple mutant. This indicates that a process controlling cell wall formation might be affected rather than cell wall formation per se. This analysis suggests that the one possible target affected in *lrx3 lrx4* and *lrx3 lrx4 lrx5* cell walls are pectins due to their relatively high amount of rhamnose and galactose.

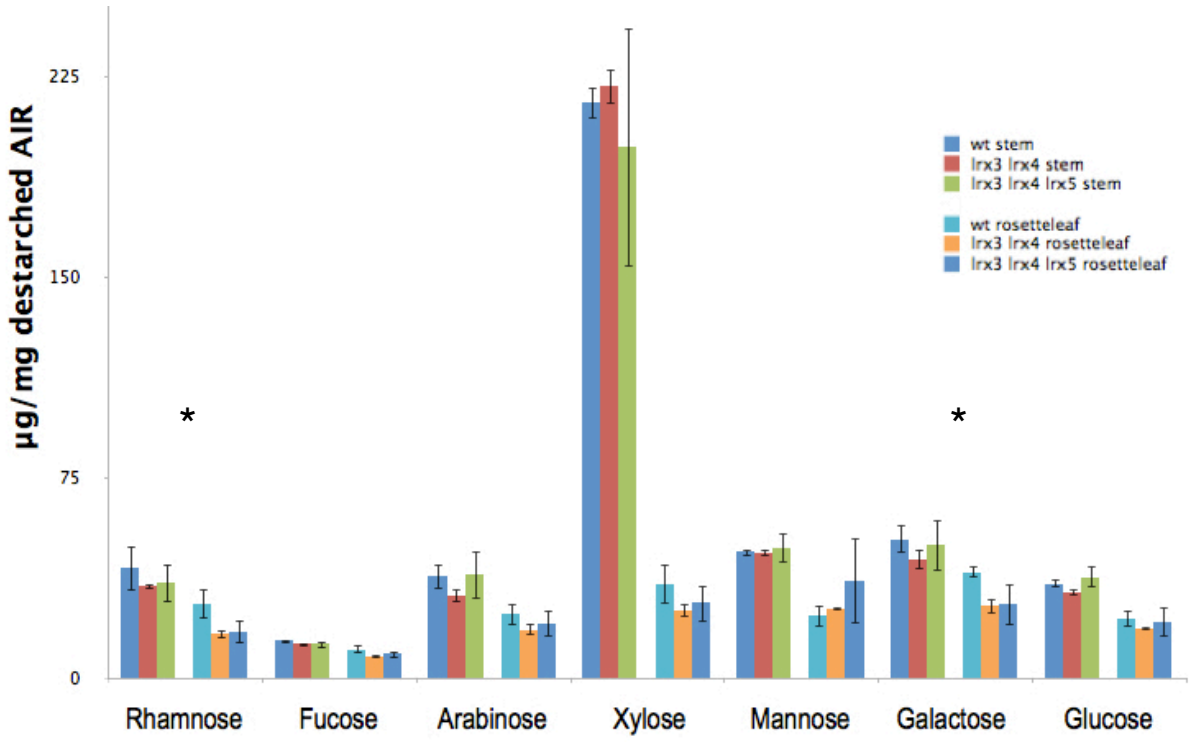

Figure 7: **Monosaccharide analysis of wt, *lrx3 lrx4,* and *lrx3 lrx4 lrx5* stem and rosette leaves.** Destarched AIR in µg/mg of rhamnose, fucose, arabinose, xylose, mannose, galactose and glucose is shown. Asteriks indicates the values of sugar contents, which differ significantly from wt plants.

5.3 EXPERIMENTAL PROCEDURES

Plant material and growth

The *Arabidopsis thaliana* wild type and mutants *lrx3* (At4g13340; Salk_094400), l*rx4* (At3g24480; GABI_017A08), and *lrx5* (At4g18670; Salk_013968) are of the ecotype Col-0. Seeds were obtained from the

NASC European Arabidopsis Stock Center. Seeds were surface sterilized (1% sodium hypochlorite, 0.03% TritonX-100) and stratified 2-4 days at 4°C. Seeds were plated on 1/2 strength Murashige and Skoog medium (supplemented with 100 mg/ml myo-inositol, 0.6% phytagel, and 2% sucrose) and grown in growth chambers with 16 h light, 8 h dark cycles at 22°C.

DNA primers, constructs and plant transformation

For the *LRX3* and *LRX4* complementation constructs *LRX3:LRR3_EXT1 and LRX4:LRR4_EXT1*, promotor and coding sequence (CDS) of *LRR3* and *LRR4* were amplified by PCR with the following primers: LRX3F: 5'-TCATATGTGCTGTAGATGATTGGG-3'; LRX3R: 5'-CTGCAGTTTACCGGCGGACGAGACAAAAACG-3'; LRX4F: 5'-ACCCTCTAGCCTTTATATATTTATAG-3'; LRX4R: 5'-CTGCAGTCCACCGAAGGCCGTGACAAGAAAG-3' and cloned into the *pSC* Vector (Stratagene). A *Pst*I site was introduced into the sequence coding for the hinge region between the LRR- and the EXT-coding region. After sequencing, these fragments were cut with *Apa*I and *Pst*I and cloned into a *pSC* vector containing the LRX1 sequence (hinge-coding region with a *Pst*I site, extensin domain and terminator (Baumberger et al., 2003a)). For plant transformation, the constructs were cloned by *Not*I into *pBART27* (Gleave et al., 1992) and plants were transformed as described (Diet et al., 2006). T_1 seeds were collected from transformed plants, sterilized, and plated on BASTA (50 µg/ml) containing selection medium to select for transformants. T_2 seeds obtained from the primary transformants were sterilized and sown on BASTA plates, resistant seedlings were transfered to soil for propagation. Transgenic T_2 lines that showed a 3:1 segregation ratio for resistance versus susceptibility were used for further experiments.

Pavement cell analysis and SEM analysis

Imprinting of pavement cells was done following Horiguchi et al. (2006) and observed with a Zeiss AX10 microscope. Scanning Electron Microscope (SEM) analysis of cotyledons was done as described (Baumberger et al., 2003b).

Comprehensive microarray polymer profiling (CoMPP) and monosaccharide analysis

Preparation of AIR (Alcohol insoluble residue): Plant tissue was grinded in liquid nitrogen, washed with 80% EtOH and subsequently washed in 100% acetone, and CoMPP was performed as described in Moller et al. (2007). For monosaccharide analysis plant tissue was freeze-dried and 60 mg of lyophilized cell wall material was analyzed by LC-MS as described in Moller et al. (2007).

5.4 Supplemental Data

Table S1: **Nomenclature of the described *LRX* genes.** Gene names regarding to the the BAC clones of the genes, accession number, and the old gene names. Gene names were used as described in Baumberger et al. (2003b).

Gene name	BAC	Accession number
LRX3	T9E8	At4g13340
LRX4	MXP5	At3g24480
LRX5	F28A21	At4g18670

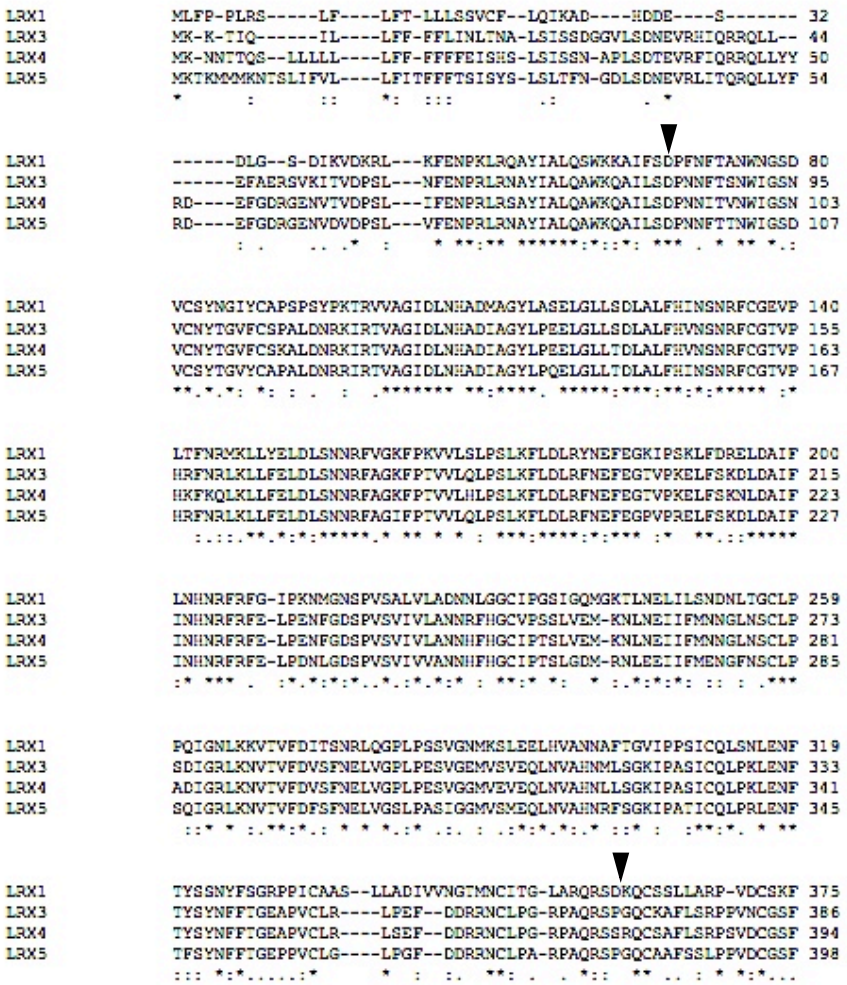

Figure S2: **Alignment of the deduced LRX1, LRX3, LRX4, and LRX5 proteins.** Alignment of the LRR domains of LRX1 (At1g12040), LRX3 (At4g13340), LRX4 (At3g24480) and LRX5 (At4g18670). Identity and similarity are indicated by the asteriks and the colons, respectively. The LRR domain is delimited by the arrowheads.

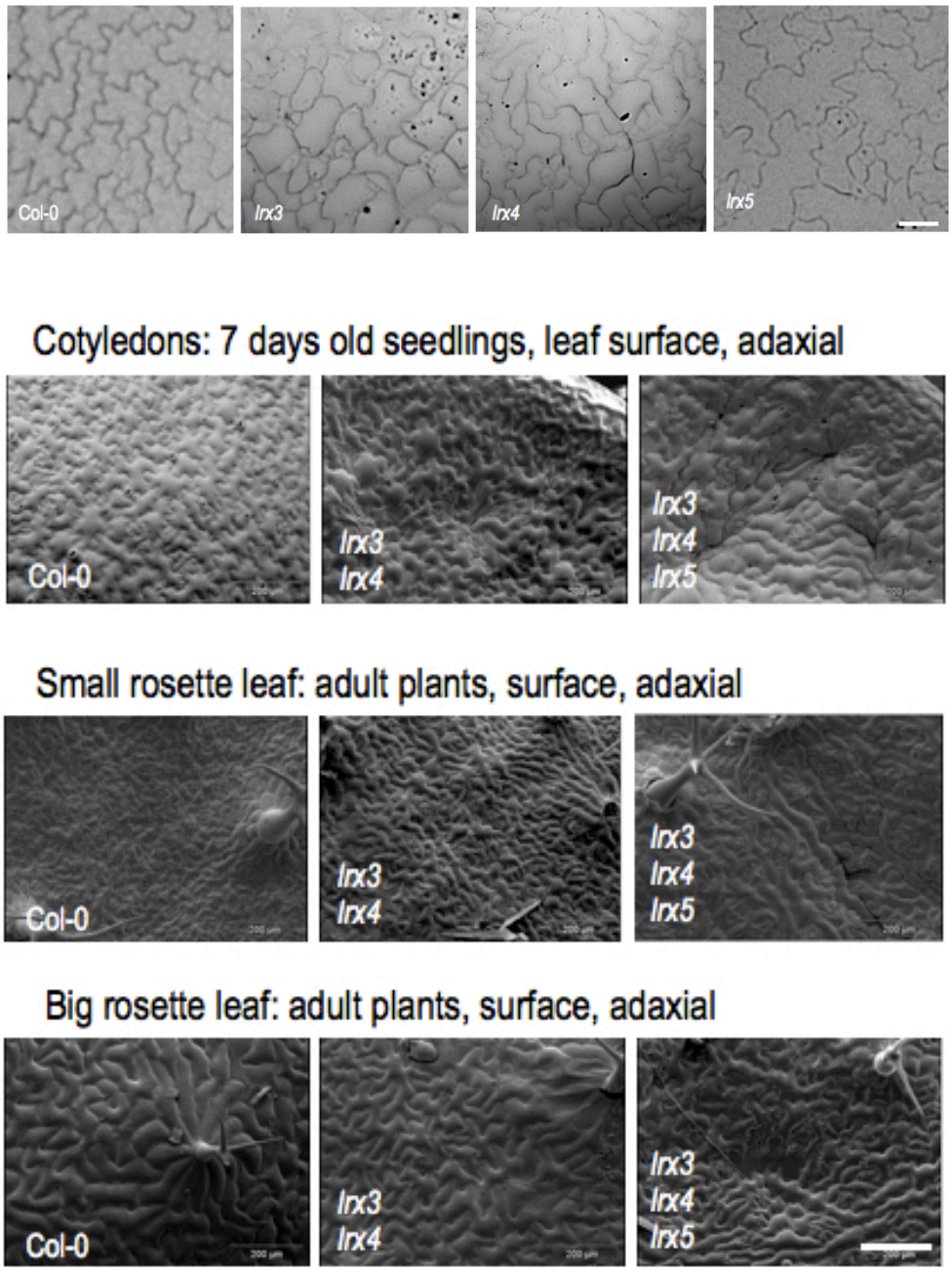

Figure S3: **Pavement cell phenotype of *lrx3, lrx4,* and *lrx5* mutants.** Upper row cotyledon imprintings of *lrx3*, *lrx4*, and *lrx5* single mutants. SEM pictures of cotyledons and rosette leaves revealed a pavement cell phenotype. The triple mutant *lrx3 lrx4 lrx5* revealed crater-like structures on the leaf surface. Bars = 40 µm; 200 µm

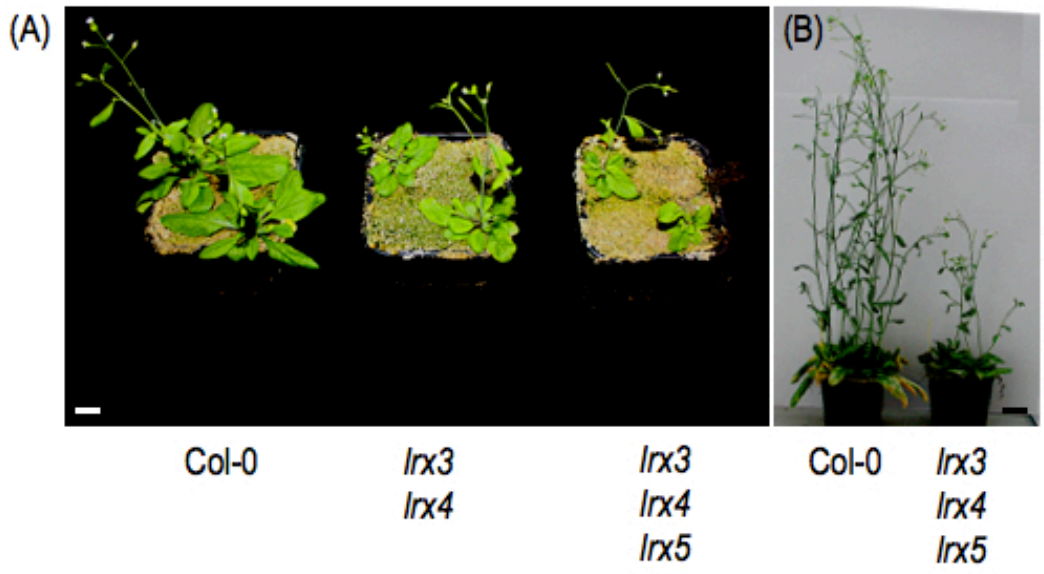

Figure S4: **Growth phenotype of *lrx3 lrx4* and *lrx3 lrx4 lrx5* mutants.** (A) Adult plants of *lrx3 lrx4* and *lrx3 lrx4 lrx5* after 2 weeks of growth. (B) Adult plants of *lrx3 lrx4 lrx5* (3-4 weeks). Bar = 1 cm (A), Bar = 3 cm (B)

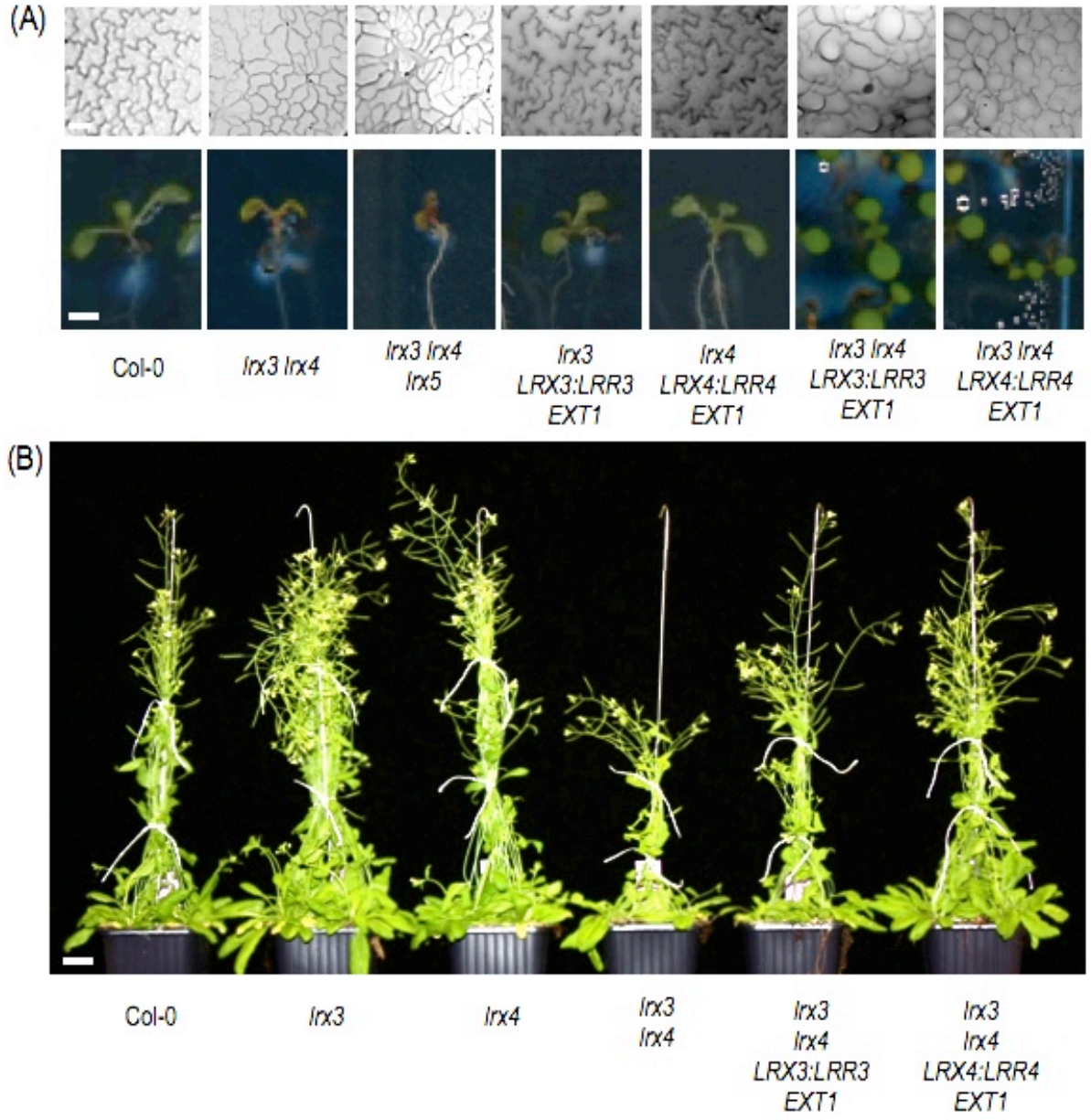

Figure S5: **Complemented plants of *lrx3 lrx4* and *lrx3 lrx4 lrx5* mutants.** (A) Cotyledon imprinting analysis of the complemented lines and growth phenotype of complemented 6 days old seedlings. (B) Adult plants of *lrx3 lrx4* complemented with *LRX3:LRR3 LRX1* and *lrx3 lrx4* complemented with *LRX4:LRR4 LRX1*. Bar = 40 µm (A, upper row), Bar = 2 mm (A, lower row), Bar = 2 cm (B)

Table S6: **CoMPP quantification data of glycan profiling of wt, *lrx3 lrx4*, and *lrx3 lrx4 lrx5*.** Indicated are the washing methods, the mutant lines *lrx3 lrx4* and *lrx3 lrx4 lrx5* used for measurements, plant organs, and the mAbs against the different cell wall structures.

Average

washing	mutant	organ	HG LM19	AGP JIM13	extensin JIM20	galactan LM5	arabinan LM6	xylan LM11	arabian LM13	xyloglucan LM15
CDTA	wt	leaves	87.60	0.00	54.85	59.81	7.06	0.00	18.41	6.06
	3,4	leaves	69.18	0.00	54.79	35.91	0.00	0.00	18.15	0.00
	3,4,5	leaves	72.99	3.97	64.18	43.90	2.33	0.00	31.35	2.99
	wt	stem	74.66	90.04	85.59	65.23	1.83	14.50	97.44	2.74
	3,4	stem	72.91	78.78	75.97	83.27	7.05	23.59	92.50	8.99
	3,4,5	stem	76.28	66.16	58.93	93.33	4.80	21.22	66.14	9.99
NaOH	wt	leaves	0.00	19.80	77.08	58.59	83.74	95.54	7.72	73.39
	3,4	leaves	7.74	22.29	71.68	64.05	76.04	40.20	7.47	63.60
	3,4,5	leaves	6.35	20.00	83.02	72.45	74.06	58.68	9.75	69.33
	wt	stem	0.00	40.86	30.43	58.03	87.15	52.43	49.91	82.47
	3,4	stem	0.00	53.30	36.55	43.83	68.14	37.98	13.41	60.50
	3,4,5	stem	0.00	35.84	34.28	47.98	72.72	45.01	5.22	62.76

Stdev

washing	mutant	organ	HG LM19	AGP JIM13	extensin JIM20	galactan LM5	arabinan LM6	xylan LM11	arabian LM13	xyloglucan LM15
CDTA	wt	leaves	13.96	0.00	7.71	2.29	6.89	0.00	2.86	5.66
	3,4	leaves	15.01	0.00	30.58	25.45	0.00	0.00	11.08	0.00
	3,4,5	leaves	3.62	6.88	9.98	10.08	4.04	0.00	6.38	5.19
	wt	stem	5.47	8.62	8.41	5.56	3.17	1.58	2.55	4.74
	3,4	stem	7.11	0.48	2.22	2.96	1.76	1.99	2.51	4.36
	3,4,5	stem	13.37	13.46	6.98	7.30	4.66	6.44	4.35	4.22
NaOH	wt	leaves	0.00	6.43	8.06	7.42	14.15	3.86	1.56	10.97
	3,4	leaves	2.18	13.14	17.67	5.37	0.58	2.80	1.91	6.37
	3,4,5	leaves	1.38	7.29	17.34	10.51	3.78	16.16	5.03	14.13
	wt	stem	0.00	3.93	9.59	0.77	7.46	3.09	16.50	15.46
	3,4	stem	0.00	4.81	13.51	4.41	7.24	6.49	7.81	3.38
	3,4,5	stem	0.00	0.86	16.03	19.19	11.41	6.70	5.17	10.48

6. GENERAL DISCUSSION

Systems Biology is combining genomics with the core sciences chemistry, mathematics, physics, and engineering. This relatively new field is shifting biology from a descriptive, qualitative to a predictive, quantitative science (Kitano, 2005). Novel technology, quantitative biological data, and mathematical models that simulate or predict the behaviour of biological systems are combined in the Swiss Initiative of Systems Biology (www.systemsx.ch) to describe properties of biological organisms.

In this thesis, the cell wall is in the focus of research and Systems Biology was used to investigate the mechnical properties quantitatively. The first achievement was the establishment of a new technology to gain quantitative data about cell wall mechanics. Here, the first time the mechanical properties of mutant Arabidopsis pollen tubes (PTs) were measured by Cellular Force Microscopy (CFM). An advantage of this system is the potentially wide applicability in various organisms. Arabidopsis as the model organism provides a great basis for further mechanical measurements of all different kinds of processes contributing to physical properties of the plant cell wall. For example, influence of mechanical stress on cell growth. With some modifications on the CFM setup, a huge variety of organisms can be investigated. Some preliminary tests with Venus Flytraps (*Dionaea muscipula*), for example, revealed forces which are necessary to activate its famous trapping mechanism triggered by the bending of tiny hairs on their inner surface.

6.1 Cellular Force Microscopy

Pollen tubes (PTs) are one of the fastest growing cell types and can be considered as a single cell organism, the male gametophyte. They are used as a model organism to investigate the cell wall development due to this unique characteristics. Biosynthesis of the PT cell wall is involved in the regulation of PT growth (Edlund et al., 2004) but molecular mechanisms, which control PT cell wall synthesis and expansion remain largely unknown. The aims of the thesis were the mechanical analysis, biochemical, and genetic characterization of the cell wall of living Arabidopsis PTs:

i. Quantitative mechanical characterization and analysis of PT cell walls

ii. Biochemical analysis of the PT cell wall

iii. Analysis of proteins involved in cell wall development

Cell wall analysis by a mechanical approach is a relatively new field of plant research. The challenge lies first of all in the establishment of a system providing data to describe the strength of the cell wall. Quantification of forces applied on living cells gives a new insight from a different angle of view when determining changes in cell wall mutants. Conventional methods used in molecular biology cannot give quantitative information about the stiffness of the cell wall. Here, a CFM setup was established to measure the cell wall stiffness on PTs to elaborate the dynamics of cell wall growth. CFM is a new easy-to-use microrobotic technology to determine mechanical properties of tissues and single cells. The flexibility of that system allows to use different types of sensors and a huge variety of sensor probe tips. Extremely precise local measurements on very stiff turgid tissue, cell walls, and other samples can be used to elaborate the strength of the measured system (Felekis et al., 2011; Routier-Kierzkowska et al., 2012). The CFM allows to measure the stiffnes of living PTs with high resolution over multiple samples in a small time interval. It provides a high level of automation and the results between the samples are comparable (Chapter 2).

Lily PTs were used as a model to establish the CFM sytem, since they have a very high germination rate as well as a decent tube size (20-25 µm) to perform measurements with a high sample number. In PT growth, important molecular and cellular mechanisms are involved including signalling, cellular differentation, and endomembrane trafficking. However, the dynamics of cell wall expansion in elongating PTs are not well understood. The CFM turned out to be a useful method to measure the apparent stiffness of the cell wall in lily PTs. Measurements were highly reproducible and were performed in relatively high numbers. Combined with incorporation of data into a PT finite elements model revealed to be a suitable system to calculate the stiffness (Young's modulus) and the turgor pressure of lily PTs.

CFM measurements described a gradient in stiffness from the tip to the apex. Micro-indentation another method to measure the cellular stiffness revealed that the tip of the tube is significantly softer than the PT shank and it provides comparable data with a similar measurement process (Zerzour et al., 2009; Aouar et al., 2010). These findings imply that the mechanical properties change during PT growth. This could be explained by callose deposition and pectin methylesterification towards the shank, which is changing the cell wall composition. However, lily PTs can not be gentically studied as the genome of lily is octaploid (http://www.cbs.dtu.dk/databases/DOGS/). Hence, there are no cell wall mutants available to test the influence of individual components on mechanical properties. Alternatively, lily treatments with cellulase or drugs to induce growth arrest were performed (Zerzour et al., 2009; Aouar et al., 2010). In respect to that Arabidopsis provides a much better system. Mutant lines are available and different changes or cell wall modifications are possible, as shown by the XyG knock out line *xxt1 xxt2* (Cavalier et al., 2008). Mutant Arabidopsis lines, with specifically affected cell wall components have not been measured yet in terms of their mechanical properties. Therefore, CFM analysis of Arabidopsis PTs provides an method to investigate the contributions of individual cell wall components to the mechanical behaviour of the cell wall. Here, the first CFM data of *xxt1 xxt2* and *xxt1 xxt2 xeg113* Arabidopsis PTs affected in the cell wall composition is shown. Hence, it was shown that the CFM system works on Arabidopsis PTs and differences in the PT cell wall stiffness were measured.

6.2 CFM measurements and Youngs Modulus of Arabidopsis pollen tubes

The first time micro-indentation experiments on Arabidopsis PTs was performed. The triple mutant *xxt1 xxt2 xeg113* revealed higher apparent stiffness. Apparent stiffness measurements reflect a combination of mechanical and geometrical properties. The next step will be the implementation of the experimental data into a Finite Element Model (FEM) to elaborate the turgor pressure and Youngs modulus of the PT cell wall. A crucial point for implementation is the thickness of the cell wall. Wild-type, *xxt1 xxt2*, and *xeg113* revealed a cell wall thickness of approximate 860 nm whereas the *xxt1 xxt2 xeg113* cell wall was 730 nm. The FEM model, established for lily PTs was adapted for Arabidopsis PTs. Arabidopsis revealed a ratio of PT radius (2.6-3.2 µm) to cell wall thickness of 3:1. Therefore, the triangular shell elements of the FEM model need to be

adjusted to calculate the Youngs modulus and the turgor pressure of Arabidopsis PTs to estimate the cell wall stiffness (A. Weber, personal communication). This adaptation is the next step for the analysis of the Arabidopsis cell wall stiffness and can be considered as an outlook for future work on *xxt1 xxt2 xeg113* PTs.

6.3 Pollen expressed LRR-extensins

ATPEXs are members of the LRX protein family and the mutants *atpex1-4* were analyzed. They revealed a slight pollen-specific growth phenotype in *atpex1, atpex2, atpex4,* and *atpex1 atpex2* mutant PTs. The *atpex3* mutant and the triple-/ quadruple mutants are not established yet. If the genetic redundance in these mutants is strong they probably exhibit a more intense growth phenotype. This was shown in Arabidopsis quadruple mutants deficient in multiple phytochromes, which revealed a strong plant growth phenotype (Franklin et al., 2003). *atpex1* and *atpex4* were labeled with LM6, an mAb raised against short-chain linear oligomers of galactan and arabinan (Jones et al., 1997; Williats et al., 1998). Arabinans are generally associated with the RGI backbone in the cell wall and are thought to be involved in pectin fluidity (Carpita and Gibeaut, 1993; Jones et al, 2003). A cell wall related function defect in pectins in *atpex* mutants may lead to cell wall bulges and secondary tips developed in these mutants.

Biochemical cell wall analysis may lead to cell wall components affected in *atpex* mutant PTs. But PTs are not an ideal candidate to gain a decent amount of material for a high throughput biochemical assay. Other members of the *LRX* gene family *LRX3*, *LRX4*, and *LRX5* displayed a cell growth phenotype in leaves when mutated. These are probably the better candidates for a biochemical cell wall analysis to identify contributions of LRXs to cell wall development.

6.4 Biochemical analysis of cell wall development in *lrx* mutants

LRXs are extracellular localized proteins and are important for cell-wall formation as shown for the *LRX* mutant *lrx1* (Baumberger et al., 2001). Genetic and morphological data of *LRX1 and LRX2* are available, but there are no biochemical data on their cell wall composition. *lrx1* mutants are affected in root hair formation

by developing abberrant root hairs (Baumberger et al., 2001). Small amounts of cell wall material in *lrx1* root hairs forced us to change to other *LRX* gene family members showing a cell growth phenotype. *LRX3, LRX4,* and *LRX5* expression in the aboveground organs and the mutants *lrx3, lrx4,* and *lrx5* show a phenotype in pavement cells of cotyledons, rosette leaves, and stems of adult plants. These tissues provide sufficient material for a biochemical analysis. Therefore, these mutants are ideal to elucidate biochemically the cell walls of *lrx* mutants and thus the functional effect of LRXs in cell wall development.

The paralogs *LRX3* and *LRX4* may have a similar function in cell growth development. The observed phenotypes in *lrx3, lrx4* and *lrx3 lrx4* lead to a synergistic effect as shown in *lrx1* and *lrx2* (Baumberger et al., 2003a). The homolog *LRX5* shows a synergistic interaction in *lrx3 lrx4 lrx5* triple mutants and may have a similar function as well. The EXT domain has been shown to be important for protein function but interchangeable between *LRX*s. This was shown by the replacement of *LRX1_EXT* domain by their equivalents *LRX2_EXT* (Baumberger et al., 2003a). Therefore, a possible function of the EXT domain may be anchoring of the protein. This is an assumption related to other extensins, which are proposed to interact with cell wall pectin (Cannon et al., 2008).

The observed cell growth phenotype in *lrx3 lrx4* and *lrx3 lrx4 lrx5* is similar to other mutants affected in cell wall development and may be explained by the observed changes in the cell wall composition. The Arabidopsis mutant *rsw1* (*root swollen1*) is important for cellulose synthesis and it was shown that cotyledons are smaller, have an uneven surface and the pavement cell pattern is disturbed (Williamson et al., 2001). *ROL1* (*REPRESSOR OF LRX1*) encodes a *RHM1* a rhamnose synthase and *rol1* mutants exhibit modifications in the pectin structure (Diet et al., 2006). The *rol1* mutant revealed brick-like pavement cells similar to the *lrx3 lrx4* and *lrx3 lrx4 lrx5* phenotype (Ringli et al., 2008).

lrx mutants are affected in cell wall formation or regulation of cell wall development. Cell wall pectin and especially rhamnogalacturonan I (RGI) contains rhamnose in the backbone and side chains decorated with galactose and arabinose (Somerville et al., 2004). They may contribute to RGI formation, which is a major pectin component containing arabinose, galactose, and rhamnose. LM11 a xylan/arabinoxylan recognizing mAb is decreased in the CoMPP experiment in leaves. Xylans are thought to cross-link cellulose microfibrils,

contribute to cell mechanical properties (McCartney et al., 2005), and are part of the xylogalacturonan backbone of pectin. Therefore, LRX proteins may regulate or are directly involved in the modification of pectin in the plant cell wall. Cell wall degrading enzymes like the endopolygalacturonase (PG) are known to degrade cell walls and are involved in plant tissue maceration. The PGs are controlled by specific PG-inhibiting proteins (PGIPs) containing an LRR domain. PGs as recognition factors are regulated by PGIPs (DeLorenzo et al., 2001). PGIPs show a close relationship with known plant LRRs (Protsenko et al., 2008). LRRs are highly conserved structural motifs, responsible for protein-protein interactions (Buchanan and Gay, 1996). In all LRR proteins, the consensus sequences for the LRR repeats are similar. PGIPs are known to modify cell wall pectin and high similarities in the LRR domain lead to the homology-based suggestion that LRX3, LRX4, and LRX5 may modify pectin. This hypothesis can be tested by identifiying the interaction partner of LRR-extensins.

7. OUTLOOK

The cell wall is a very complex and important structure of the cell. A lot is known about its structure and the biochemical composition, but there are missing links in terms of growth dynamics and assembly during growth. The new CFM method is a powerful tool to investigate mechanical properties of cell walls. It is a very flexible system and many different approaches on different tissues, mutants and organisms are possible. The CFM system was established and tested on lily PTs and showed a very high reproducibility of the results obtained, which are comparable to other micro-indentation systems. The CFM results in combination with immunocytological, biochemical, and genetical data revealed differences in the cell wall composition and the stiffness of the investigated Arabidopsis mutants. The next step would be the analysis of other cell wall mutants also affecting cell growth or cell wall development. The identified *atpex* or *lrx* mutants would be ideal to test whether they are affected in cell wall stiffness. Another possible target would be Arabidopsis cell wall mutants not showing any PT phenotype. Subsequently, the affected genes could be sorted according to their contribution to the mechanical properties. This would lead to a stiffness-map of genes ivolved in cell wall formation in Arabidopsis. Experiments on LRX proteins revealed an additional insight of their contributions to cell wall formation. As a next step it would be interesting to find the interaction partner of LRX to identify proteins involved in this complex cell wall developmental process. Localization of the LRX protein would be another aspect for further work. Previous protoplast experiments revealed that LRX possibly interact with the plasma membrane. Therefore, covalently bound LRX may stabilize the cell wall by physically connecting the plasma membrane with the cell wall.

8. REFERENCES

Aouar, L., Chebli, Y., and Geitmann, A. (2010). Morphogenesis complex plant cell shapes: the mechanical role of crystalline cellulose in growing pollen tubes. Sexual Plant Reproduction 23, 15-27.

Astrom, H., Sorri, O., and Raudaskoski, M., (1995). Role of microtubules in the movement of the vegetative nucleus and generative cell in tobacco pollen tubes. Sexual Plant Reproduction 8, 61-69.

Baumberger, N., Ringli, C., and Keller, B. (2001). The chimeric leucine-rich repeat/extensin cell wall protein LRX1 is required for root hair morphogenesis in *Arabidopsis thaliana*. Genes & Development 15, 1128-1139.

Baumberger, N., Steiner, M., Ryser, U., Keller, B., and Ringli, C. (2003a). Synergistic interaction of the two paralogous Arabidopsis genes LRX1 and LRX2 in cell wall formation during root hair development. Plant Journal 35, 71-81.

Baumberger, N., Doesseger, B., Guyot, R., Diet, A., Parsons, R.L., Clark, M.A., Simmons, M.P., Bedinger, P., Goff, S.A., Ringli, C., and Keller, B. (2003b). Whole-genome comparison of leucine-rich repeat extensins in Arabidopsis and rice. A conserved family of cell wall proteins form a vegetative and a reproductive clade. Plant Physiology 131, 1313-1326.

Benkert, R., Obermeyer, G., and Bentrup, F.W. (1997). The turgor pressure of growing lily pollen tubes. Protoplasma 198, 1-8.

Biochemistry and Molecular Biology of Plants. Edited by Buchanan BB, Gruissem W, Jones RL. pp. 52-108. American Society of Plant Physiologists, Rockville, Maryland.

Boavida, L.C., and McCormick, S. (2007). Temperature as a determinant factor for increased and reproducible in vitro pollen germination in *Arabidopsis thaliana*. Plant Journal 52, 570-582.

Bosch, M., and Hepler, P.K. (2005). Pectin methylesterases and pectin dynamics in pollen tubes. Plant Cell 17, 3219-3226.

Bosch, M., Cheung, A.Y., and Hepler, P.K. (2005). Pectin methylesterase, a regulator of pollen tube growth. Plant Physiology 138, 1334-1346.

Brady, J.D., Sadler, I.H., and Fry, S.C. (1998). Pulcherosine, an oxidatively coupled trimer of tyrosine in plant cell walls: its role in cross-link formation. Phytochemistry 47, 349-353.

Brewbacker, J. L., and Kwack, B. H. (1963). The essential role of calcium ion in pollen germination and pollen tube growth. American Journal of Botany 50, 859-865.

Brisson, L.F., Tenhaken, R., and Lamb, C. (1994). Function of oxidative cross-linking of cell-wall structural proteins in plant-disease resistance. Plant Cell 6, 1703-1712.

Buchanan, S.G.S., and Gay, N.J. (1996). Structural and functional diversity in the leucine rich repeat family of proteins. Progress in Biophysics & Molecular Biology 65, 1-44.

Camirand, A., Brummell, D., and Maclachlan, G. (1987). Fucosylation of xyloglucan:localization of the transferase in dictyosomes of pea stem cells. Plant Physiology 84, 753-56.

Cannon, M.C., Terneus, K., Hall, Q., Tan, L., Wang, Y., Wegenhart, B.L., Chen, L., Lamport, D.T.A., Chen, Y., and Kieliszewski, M.J. (2008). Self-assembly of the plant cell wall requires an extensin scaffold. Proceedings of the National Academy of Sciences of the United States of America 105, 2226-2231.

Cardenas, L., Lovy-Wheeler, A., Kunkel, J.G., and Hepler, P.K. (2008). Pollen tube growth oscillations and intracellular calcium levels are reversibly modulated by actin polymerization. Plant Physiology 146, 1611-1621.

Carpita, N.C., and Gibeaut, D.M. (1993). Structural models of primary cell walls in flowering plants - Consistency of molecular structure with the physical properties of the walls during growth. Plant Journal 3, 1-30.

Carpita N.C., and McCann M.C., (2000) The cell wall. In Biochemistry and Molecular Biology of Plants. Edited by Buchanan BB, Gruissem W, Jones RL. pp. 52-108. American Society of Plant Physiologists, Rockville, Maryland.

Cassab, G.I. (1998). Plant cell wall proteins. Annual Review of Plant Physiology and Plant Molecular Biology 49, 281-309.

Cavalier, D.M., Lerouxel, O., Neumetzler, L., Yamauchi, K., Reinecke, A., Freshour, G., Zabotina, O.A., Hahn, M.G., Burgert, I., Pauly, M., Raikhel, N.V., and Keegstra, K. (2008). Disrupting two *Arabidopsis thaliana* xylosyltransferase genes results in plants deficient in xyloglucan, a major primary cell wall component. Plant Cell 20, 1519-1537.

Chebli, Y., and Geitmann, A., (2007). Mechanical principles governing pollen tube growth. Functional Plant Science and Biotechnology 1, 232-245.

Cheung, A.Y., and Wu, H.-M. (2008). Structural and signaling networks for the polar cell growth machinery in pollen tubes. Annual Review of Plant Biology 59, 547-572.

Cheung, A.Y., Niroomand, S., Zou, Y., and Wu, H.-M. (2010a). A transmembrane formin nucleates subapical actin assembly and controls tip-focused growth in pollen tubes. Proceedings of the National Academy of Sciences of the United States of America 107, 16390-16395.

Cheung, A.Y., Boavida, L.C., Aggarwal, M., Wu, H.-M., and Feijo, J.A. (2010b). The pollen tube journey in the pistil and imaging the *in vivo* process by two-photon microscopy. Journal of Experimental Botany 61, 1907-1915.

Cleland, R. (1971). CELL WALL EXTENSION. Annual Review of Plant Physiology 22, 197-222.

Cosgrove, D.J. (1989). Characterization of long-term extension of isolated cell walls from growing cucumber hypocotyls. Planta 177, 121-30.

Cosgrove, D.J. (1999). Enzymes and other agents that enhance cell wall extensibility. Annual Review of Plant Physiology and Plant Molecular Biology 50, 391-417.

Cosgrove, D.J. (2005). Growth of the plant cell wall. Nature Reviews Molecular Cell Biology 6, 850-861.

Crawford, B.C.W., Ditta, G., and Yanofsky, M.F. (2007). The *NTT* gene is required for transmitting-tract development in carpels of *Arabidopsis thaliana*. Current Biology 17, 1101-1108.

Cutler, S., and Somerville, C. (1997). Cellulose synthesis: Cloning in silico. Current Biology 7, 108-111.

Dardelle, F., Lehner, A., Ramdani, Y., Bardor, M., Lerouge, P., Driouich, A., and Mollet, J.-C. (2010). Biochemical and immunocytological characterizations of Arabidopsis pollen tube cell wall. Plant Physiology 153, 1563-1576.

DeLorenzo, G., D'Ovidio, R., and Cervone, F. (2001). The role of polygalacturonase-inhibiting proteins (PGIPs) in defense against pathogenic fungi. Phytopathology 39, 313-35.

Diet, A., Link, B., Seifert, G.J., Schellenberg, B., Wagner, U., Pauly, M., Reiter, W.-D., and Ringli, C. (2006). The Arabidopsis root hair cell wall formation mutant *lrx1* is suppressed by mutations in the *RHM1* gene encoding a UDP-L-rhamnose synthase. Plant Cell 18, 1630-1641.

Duan, Q., Kita, D., Li, C., Cheung, A.Y., and Wu, H.-M. (2010). FERONIA receptor-like kinase regulates RHO GTPase signaling of root hair development. Proceedings of the National Academy of Sciences of the United States of America 107, 17821-17826.

Dumais, J., Long, S.R., and Shaw, S.L. (2004). The mechanics of surf ace expansion anisotropy in *Medicago truncatula* root hairs. Plant Physiology 136, 3266-3275.

Dumais, J., Shaw, S.L., Steele, C.R., Long, S.R., and Ray, P.M. (2006). An anisotropic-viscoplastic model of plant cell morphogenesis by tip growth. International Journal of Developmental Biology 50, 209-222.

Dutta, R., and Robinson, K.R. (2004). Identification and characterization of stretch-activated ion channels in pollen protoplasts. Plant Physiology 135, 1398-1406.

Eamus, D., and Jennings, D.H. (1986). Water turgor and osmotic potentials of fungi. Ayres, P. G. and L. Boddy (Ed.). British Mycological Society Symposium, 11. Water, Fungi and Plants; Lancaster, England, Apr. 1985. Xiv+413p. Cambridge University Press: Cambridge, England; New York, N.Y., USA. Illus, 27-48.

Edlund, A.F., Swanson, R., and Preuss, D. (2004). Pollen and stigma structure and function: The role of diversity in pollination. Plant Cell 16, 84-S97.

Epstein, L., and Lamport, D.T.A. (1984). An intramolecular linkage involving isodityrosine in extensin. Phytochemistry 23, 1241-1246.

Escobar-Restrepo, J.-M., Huck, N., Kessler, S., Gagliardini, V., Gheyselinck, J., Yang, W.-C., and Grossniklaus, U. (2007). The FERONIA receptor-like kinase mediates male-female interactions during pollen tube reception. Science 317, 656-660.

Feijo, J.A., Sainhas, J., Hackett, G.R., Kunkel, J.G., and Hepler, P.K. (1999). Growing pollen tubes possess a constitutive alkaline band in the clear zone and a growth-dependent acidic tip. Journal of Cell Biology 144, 483-496.

Felekis, D., Muntwyler, S., Vogler, H., Beyeler, F., Grossniklaus, U., and Nelson, B.J. (2011). Quantifying growth mechanics of living, growing plant cells in situ using microrobotics. Micro & Nano Letters 6, 311-316.

Ferguson, C., Teeri, T.T., Siika-aho, M., Read, S.M., and Bacic, A. (1998). Location of cellulose and callose in pollen tubes and grains of *Nicotiana tabacum*. Planta 206, 452-460.

Fong, C., Kieliszewski, M.J., de Zacks, R., Leykam, J.F., and Lamport, D.T.A., 1992. A gymnosperm extensin contains the serine-tetrahydroxyproline motif. Plant Physiology 99, 548-552.

Franklin, K.A., Praekelt, U., Stoddart, W.M., Billingham, O.E., Halliday, K.J. and Whitelam, G.C. (2003) Phytochromes B, D, and E act redundantly to control multiple physiological responses in Arabidopsis. Plant Physiology, 131, 1340-1346.

Fry, S.C. (1982). Isodityrosine, a new cross-linking amino-acid from plant cell-wall glycoprotein. Biochemical Journal 204, 449-455.

Fry, S.C., Smith, R. C., Renwick, K. F., Martin, D. J., Hodge, S. K. and Matthews, K. J. (1992). Xyloglucan endotransglycosylase, a new wall-loosening enzyme activity from plants. Biochemical Journal 282, 821-828.

Geitmann, A. (2006). Experimental approaches used to quantify physical parameters at cellular and subcellular levels. American Journal of Botany 93, 1380-1390.

Geitmann, A., and Parre, E. (2004). The local cytomechanical properties of growing pollen tubes correspond to the axial distribution of structural cellular elements. Sexual Plant Reproduction 17, 9-16.

Gleave, A.P. (1992). A versatile binary vector system with a TDNA organizational structure conducive to efficient integration of cloned DNA into the plant genome. Plant Molecular Biolology 20, 1203-1207.

Hayashi, T. (1989). Xyloglucans in the primary cell wall. Annual Review of Plant Physiology and Plant Molecular Biology 40, 139-168.

Held, M.A., Tan, L., Kamyab, A., Hare, M., Shpak, E., and Kieliszewski, M.J. (2004). Di-isodityrosine is the intermolecular cross-link of isodityrosine-rich extensin analogs cross-linked *in vitro*. Journal of Biological Chemistry 279, 55474-55482.

Hematy, K., and Höfte, H. (2006) Verbelen, J.-P., and Vissenberg, K.: The expanding cell. Springer-Verlag Berlin Heidelberg 2006, 34-56.
Hepler, P.K., Vidali, L., and Cheung, A.Y. (2001). Polarized cell growth in higher plants. Annual Review of Cell and Developmental Biology 17, 159-187.

Horiguchi, G., Fujikura, U., Ferjani, A., Ishikawa, N., and Tsukaya, H. (2006). Large-scale histological analysis of leaf mutants using two simple leaf observation methods: identification of novel genetic pathways governing the size and shape of leaves. Plant Journal 48, 638-644.

Hwang, J.U., Gu, Y., Lee, Y.J., and Yang, Z., (2005). Oscillatory ROP GTPase activation leads the oscillatory polarized growth of pollen tubes. Molecular Biology of the Cell 16, 5385-5399.

Jones, L., Milne, J.L., Ashford, D., and McQueen-Mason S.J. (2003). Cell wall arabinan is essential for guard cell function. Proceedings of the National Academy of Sciences of the United States of America 100, 11783-11788.

Jones, L., Seymour, G.B., and Knox, J.P. (1997). Localization of pectic galactan in tomato cell walls using a monoclonal antibody specific to (1→4)-beta-D-galactan. Plant Physiology 113, 1405-1412.

Keegstra, K., Talmadge, K.W., Bauer, W.D., and Albershe. P. (1973). Structure of plant-cell walls - Model of walls of suspension-cultured sycamore cells based on interconnections of macromolecular components. Plant Physiology 51, 188-196.

Kimura, S., Laosinchai, W., Itoh, T., Cui, X.J., Linder, C.R., and Brown, R.M. (1999). Immunogold labeling of rosette terminal cellulose-synthesizing complexes in the vascular plant *Vigna angularis*. Plant Cell 11, 2075-2085.

Kitano, H. (2005). Scientific and technical challenges systems biology. Systems Biology, Topics in Current Genetics 13, 373-385.

Knox, J.P. (1995). The extracellular-matrix in higher plants - Developmentally regulated proteoglycans and glycoproteins of the plant-cell surface. Faseb Journal 9, 1004-1012.

Knox, J.P., Linstead, P.J., Peart, J., Cooper, C., and Roberts, K. (1991). Developmentally regulated epitopes of cell-surface arabinogalactan proteins and their relation to root-tissue pattern-formation. Plant Journal 1, 317-326.

Lamport, D.T.A., Kieliszewski, M.J., Chen, Y., and Cannon, M.C. (2011). Role of the extensin superfamily in primary cell wall architecture. Plant Physiology 156, 11-19.

Lausser, A., Kliwer, I., Srilunchang, K.,and Dresselhaus, T. (2010). Sporophytic control of pollen tube growth and guidance in maize. Journal of Experimental Botany, 61, 673-682.

Lennon, K.A., Roy, S., Hepler, P.K., and Lord, E.M. (1998). The structure of the transmitting tissue of *Arabidopsis thaliana* and the path of pollen tube growth. Sexual Plant Reproduction 11, 49-59.

Lind, J.L., Bacic, A., Clarke, A.E., and Anderson, M.A. (1994). A style-specific hydroxyproline-rich glycoprotein with properties of both extensins and arabinogalactan proteins. Plant Journal 6, 491-502.

Malho, R., Read, N.D., Trewavas, A.J., and Pais, M.S. (1995). Calcium-channel activity during pollen-tube growth and reorientation. Plant Cell 7, 1173-1184.
McCartney, L., Marcus, S.E., and Knox, J.P. (2005). Monoclonal antibodies to plant cell wall xylans and arabinoxylans. Journal of Histochemistry & Cytochemistry 53, 543-546.

McCue, A.D., Cresti, M., Feijo, J.A., and Slotkin, R.K. (2011). Cytoplasmic connection of sperm cells to the pollen vegetative cell nucleus: potential roles of the male germ unit revisited. Journal of Experimental Botany 62, 1621-1631.

McKenna, S.T., Kunkel, J.G., Bosch, M., Rounds, C.M., Vidali, L., Winship, L.J., and Hepler, P.K. (2009). Exocytosis precedes and predicts the increase in growth in oscillating pollen tubes. Plant Cell 21, 3026-3040.

McQueen-Mason, S., and Cosgrove, D.J. (1994). Disruption of hydrogen-bonding between plant-cell wall polymers by proteins that induce wall extension. Proceedings of the National Academy of Sciences of the United States of America 91, 6574-6578.

Miller, D.D., Callaham, D.A., Gross, D.J., and Hepler, P.K. (1992). Free Ca^{2+} gradient in growing pollen tubes of lilium. Journal of Cell Science 101, 7-12.

Mohnen, D. (2008). Pectin structure and biosynthesis. Current Opinion in Plant Biology 11, 266-277.

Moller, I., Marcus, S.E., Haeger, A., Verhertbruggen, Y., Verhoef, R., Schols, H., Ulvskov, P., Mikkelsen, J.D., Knox, J.P., and Willats, W. (2008). High-throughput screening of monoclonal antibodies against plant cell wall glycans by hierarchical clustering of their carbohydrate microarray binding profiles. Glycoconjugate Journal 25, 37-48.

Moller, I., Sorensen, I., Bernal, A.J., Blaukopf, C., Lee, K., Obro, J., Pettolino, F., Roberts, A., Mikkelsen, J.D., Knox, J.P., Bacic, A., and Willats, W.G.T. (2007). High-throughput mapping of cell-wall polymers within and between plants using novel microarrays. Plant Journal 50, 1118-1128.

Mort, A.J., and Lamport, D.T.A. (1977). Anhydrous hydrogen-fluoride deglycosylates glycoproteins. Analytical Biochemistry 82, 289-309.

Mucha, E., Fricke, I., Schaefer, A., Wittinghofer, A., and Berken, A. (2011). Rho proteins of plants - Functional cycle and regulation of cytoskeletal dynamics. European Journal of Cell Biology 90, 934-943.

Obel, N., Erben, V., Schwarz, T., Kühnel, S., Fodor, A., and Pauly, M. (2009). Microanalysis of plant cell wall polysaccharides. Molecular Plant 2, 922-932.

Okuda, S., Tsutsui, H., Shiina, K., Sprunck, S., Takeuchi, H., Yui, R., Kasahara, R.D., Hamamura, Y., Mizukami, A., Susaki, D., Kawano, N., Sakakibara, T., Namiki, S., Itoh, K., Otsuka, K., Matsuzaki, M., Nozaki, H., Kuroiwa, T., Nakano, A., Kanaoka, M.M., Dresselhaus, T., Sasaki, N., and Higashiyama, T. (2009). Defensin-like polypeptide LUREs are pollen tube attractants secreted from synergid cells. Nature 458, 357-U122.

Pauly, M., Andersen, L.N., Kauppinen, S., Kofod, L.V., York, W.S., Albersheim, P., and Darvill, A. (1999). A xyloglucan-specific endo-beta-1,4-glucanase from *Aspergillus aculeatus*: expression cloning in yeast, purification and characterization of the recombinant enzyme. Glycobiology 9, 93-100.

Peaucelle, A., Braybrook, S.A., Le Guillou, L., Bron, E., Kuhlemeier, C., and Hoefte, H. (2011). Pectin-induced changes in cell wall mechanics underlie organ initiation in Arabidopsis. Current Biology 21, 1720-1726.

Pierson, E.S., Miller, D.D., Callaham, D.A., Shipley, A.M., Rivers, B.A., Cresti, M., and Hepler, P.K. (1994). Pollen tube growth is coupled to the extracellular calcium ion flux and the intracellular calcium gradient: effect of BAPTA-type buffers and hypertonic media. Plant Cell 6, 1815-1828.

Pierson, E.S., Miller, D.D., Callaham, D.A., van Aken, J., Hackett, G., and Hepler, P.K. (1996). Tip-localized calcium entry fluctuates during pollen tube growth. Developmental Biology 174, 160-173.

Protsenko, M.A., Buza, N.L., Krinitsyna, A.A., Bulantseva, E.A., and Korableva, N.P. (2008). Polygalacturonase-inhibiting protein is a structural component of plant cell wall. Biochemistry-Moscow 73, 1053-1062.

Puhlmann, J., Bucheli, E., Swain, M.J., Dunning, N., Albersheim, P., Darvill, A.G., and Hahn, M.G. (1994). Generation of monoclonal antibodies against plant cell wall polysaccharides. Plant Physiology 104, 699-710.

Qi, X.Y., Behrens, B.X., West, P.R., and Mort, A.J. (1995). Solubilization and partial characterization of extensin fragements from cell-walls of cotton suspension-cultures - Evidence for a covalent cross-link between extensin and pectin. Plant Physiology 108, 1691-1701.

Ringli, C. (2005). The role of extracellular LRR-extensin (LRX) proteins in cell wall formation. Plant Biosystems 139, 32-35.

Ringli, C. (2010). The hydroxyproline-rich glycoprotein domain of the Arabidopsis LRX1 requires Tyr for function but not for insolubilization in the cell wall. Plant Journal 63, 662-669.

Ringli, C., Bigler, L., Kuhn, B.M., Leiber, R.-M., Diet, A., Santelia, D., Frey, B., Pollmann, S., and Klein, M. (2008). The modified flavonol glycosylation profile in the Arabidopsis *rol1* mutants results in alterations in plant growth and cell shape formation. Plant Cell 20, 1470-1481.

Ringli, C., Hauf, G., and Keller, B. (2001). Hydrophobic interactions of the structural protein GRP1.8 in the cell wall of protoxylem elements. Plant Physiology 125, 673-682.

Romagnoli, S., Cai, G., and Cresti, M. (2003). *In vitro* assays demonstrate that pollen tube organelles use kinesin-related motor proteins to move along microtubules. Plant Cell 15, 251-269.

Rose, J.K.C., Braam, J., Fry, S.C., and Nishitani, K. (2002). The XTH family of enzymes involved in xyloglucan endotransglucosylation and endohydrolysis: Current perspectives and a new unifying nomenclature. Plant and Cell Physiology 43, 1421-1435.

Routier-Kierzkowska, A.-L., Weber, A., Kochova, P., Felekis, D., Nelson, B.J., Kuhlemeier, C., and Smith, R.S. (2012). Cellular force microscopy for *in vivo* measurements of plant tissue mechanics. Plant Physiology 158, 1514-1522.

Roy, S.J., Holdaway-Clarke, T.L., Hackett, G.R., Kunkel, J.G., Lord, E.M., and Hepler, P.K. (1999). Uncoupling secretion and tip growth in lily pollen tubes: Evidence for the role of calcium in exocytosis. Plant Journal 19, 379-386.

Rubinstein, A.L., Broadwater, A.H., Lowrey, K.B., and Bedinger, P.A. (1995a). *PEX1*, a pollen-specific gene with an extensin-like domain. Proceedings of the National Academy of Sciences of the United States of America 92, 3086-3090.

Rubinstein, A.L., Marquez, J., SuarezCervera, M., and Bedinger, P.A. (1995b). Extensin-like glycoproteins in the maize pollen tube wall. Plant Cell 7, 2211-2225.

Schiott, M., Romanowsky, S.M., Baekgaard, L., Jakobsen, M.K., Palmgren, M.G., and Harper, J.F. (2004). A plant plasma membrane Ca^{2+} pump is required for normal pollen tube growth and fertilization. Proceedings of the National Academy of Sciences of the United States of America 101, 9502-9507.

Showalter, A.M. (1993). Structure and function of plant-cell wall proteins. Plant Cell 5, 9-23.

Smallwood, M., Beven, A., Donovan, N., Neill, S.J., Peart, J., Roberts, K., and Knox, J.P. (1994). Localization of cell-wall proteins in relation to the developmental anatomy of the carrot root apex. Plant Journal 5, 237-246.

Smallwood, M., Yates, E.A., Willats, W.G.T., Martin, H., and Knox, J.P. (1996). Immunochemical comparison of membrane-associated and secreted arabinogalactan-proteins in rice and carrot. Planta 198, 452-459.

Somerville, C., Bauer, S., Brininstool, G., Facette, M., Hamann, T., Milne, J., Osborne, E., Paredez, A., Persson, S., Raab, T., Vorwerk, S., and Youngs, H. (2004). Toward a systems approach to understanding plant-cell walls. Science 306, 2206-2211.

Staehelin, L.A., and Moore, I. (1995). The palnt golgi-apparatus - Structure, fuctional-organization and trafficking mechanisms. Annual Review of Plant Physiology and Plant Molecular Biology 46, 261-288.

Strominger, J. L., and Mapson, L. W. (1957). Uridine diphosphoglucose dehydrogenase of pea seedlings. Biochemical Journal 66, 567-72.

Takeda, T., Fry, S.C. (2004). Control of xyloglucan endotransglucosylase activity by salts and anionic polymers. Planta 219, 722-732.

Velasquez, S.M., Ricardi, M.M., Dorosz, J.G., Fernandez, P.V., Nadra, A.D., Pol-Fachin, L., Egelund, J., Gille, S., Harholt, J., Ciancia, M., Verli, H., Pauly, M., Bacic, A., Olsen, C.E., Ulvskov, P., Petersen, B.L., Somerville, C., Iusem, N.D., and Estevez, J.M. (2011). O-glycosylated cell wall proteins are essential in root hair growth. Science 332, 1401-1403.

Verhertbruggen, Y., Marcus, S.E., Haeger, A., Ordaz-Ortiz, J.J., and Knox, J.P. (2009a). An extended set of monoclonal antibodies to pectic homogalacturonan. Carbohydrate Research 344, 1858-1862.

Verhertbruggen, Y., Marcus, S.E., Haeger, A., Verhoef, R., Schols, H.A., McCleary, B.V., McKee, L., Gilbert, H.J., and Knox, J.P. (2009b). Developmental complexity of arabinan polysaccharides and their processing in plant cell walls. Plant Journal 59, 413-425.

Vidali, L., McKenna, S.T., and Hepler, P.K. (2001). Actin polymerization is essential for pollen tube growth. Molecular Biology of the Cell 12, 2534-2545.

Vorwerk, S., Somerville, S., and Somerville, C. (2004). The role of plant cell wall polysaccharide composition in disease resistance. Trends in Plant Science 9, 203-209.

Wang, H.-J., Huang, J.-C., and Jauh, G.-Y. (2010). Pollen germination and tube growth. Advances in Botanical Research, Vol 54 54, 1-52.

Willats, W.G.T., Marcus, S.E., and Knox, J.P. (1998). Generation of a monoclonal antibody specific to (1→5)-alpha-L-arabinan. Carbohydrate Research 308, 149-152.

Willats, W.G.T., McCartney, L., Mackie, W., and Knox, J.P. (2001). Pectin: cell biology and prospects for functional analysis. Plant Molecular Biology 47, 9-27.

Williamson, R.E., Burn, J.E., Birch, R., Baskin, T.I., Arioli, T., Betzner, A.S., and Cork, A. (2001). Morphology of *rsw1*, a cellulose-deficient mutant of *Arabidopsis thaliana*. Protoplasma 215, 116-127.

Yates, E.A., Valdor, J.F., Haslam, S.M., Morris, H.R., Dell, A., Mackie, W., and Knox, J.P. (1996). Characterization of carbohydrate structural features recognized by anti-a198rabinogalactan-protein monoclonal antibodies. Glycobiology 6, 131-139.

Zamir, E.A., and Taber, L.A. (2004). On the effects of residual stress in microindentation tests of soft tissue structures. Journal of Biomechanical Engineering 126, 276-283.

Zerzour, R., Kroeger, J., and Geitmann, A. (2009). Polar growth in pollen tubes is associated with spatially confined dynamic changes in cell mechanical properties. Developmental Biology 334, 437-446.

Zhao, L.M., Schaefer, D., Xu, H.X., Modi, S.J., LaCourse, W.R., and Marten, M.R. (2005). Elastic properties of the cell wall of *Aspergillus nidulans* studied with atomic force microscopy. Biotechnology Progress 21, 292-299.

Zhou, J., Rumeau, D., and Showalter, A.M. (1992). Isolation and characterization of two wound-regulated tomato extensin genes. Plant Molecular Biolology 20, 5-17.

Zykwinska, A., Ralet, M.C., Garnier C.D., and Thibault J.F. (2005). Evidence for *in vitro* binding of pectin side chains to cellulose. Plant Physiology 139, 397-407.

9. ABBREVIATIONS

AFM	Atomic Force Microscopy
AGP	Arabinogalactan Protein
AIR	Alcohol Insoluble Residues
ATP	Adenosine-di-Phosphate
ATPEX	Arabidopsis LRX Pollen Expressed
CDTA	Diamino-Cyclo-Hexane-Tetra-Acetic Acid
CESA	Cellulose Synthase
CFM	Cellular Force Microscope
Col-0	Ecotype Columbia
CoMPP	Comprehensive Microarray Polymer Profiling
CLSM	Confocal Laser Scanning Microscopy
CRP	Cysteine-Rich Polypeptides
EtOH	Ethanol
EXGT	Endoxyloglucan-Transferase
EXLA	α-Expansins
EXLB	β-Expansins
EXPLA/B	Expansin-like A/B
EXT	Extensin
FER	Feronia
Fuc	Fucose
Gal	Galactose
GDP	Guadinidine di-Phosphate
GTP	Guadinidine tri-Phosphate
HG	Homogalacturonan
HRGP	Hydroxyprolin (Hyp)-Rich Glycoproteins
Hz	Hertz
LIM	F-actin binding protein
LRR	Leuchin Repeat Rich
LRX	LRR-Extensin
mAb	Monoclonal Antibody
MEMS	Microelectromechanical Systems
NaOH	Natrium Hydroxide
PCD	Programmed Cell Death
PI	Propidium Iodide
PME	Pectin Methy Esterases
PT	Pollen Tube
RGI	Rhamnogalacturonan I
RGII	Rhamnogalacturonan II
RNA	Ribonuclein acid
ROP	Rho of Plants
RSW	Root Swollen
SEM	Scanning Electron Microscope
TEM	Transmission Electron Microscopy
TT	Tramitting Tract
UDP	Uridin-di-Phosphate
WT	Wild-type
XEG	Xyloglucan-endoglucanase
XET	Endoxyloglucan-transferase
XGA	Xylogalacturonan
XTH	Endotransglucosylase/hydrolase
XyG	Xyloglucan
XXT	Xylosyltransferase

10. ACKNOWLEDGEMENTS

Thanks to Dr. Christoph Ringli for great supervision during my work on a very interesting project.

Thanks to Prof. Dr. Beat Keller, Prof. Dr. Ueli Grossniklaus and Prof. Dr. Brad Nelson giving me the opportunity to make my PhD in their labs.

Thanks to Dr. Hannes Vogler, Dr. Christof Eichenberger, Alain Weber, Dimitris Felekis, Dr. Aurel Biosson-Dernier, Prof. Dr. Richard Smith, Prof. Dr. Cris Kuhlemeier for the interdisciplinary environment. Scientific communication and help, and they provided technical support.

Thanks to SystemsX.ch (Swiss initative for sytems Biology) for financing the project.

Thanks to the P3 group members for permanent technical support during my time as a PhD student.

Thanks to Lisa Haldemann for critical reading of my manuscript and mental support during my PhD thesis.

Thanks to my Family and Friends supporting me the long way to my PhD.

Curriculum Vitae

Christian Draeger

Personal Data

Profession:	PhD Student, Graduate Biologist
Place of Birth:	Soltau, Germany
Date of Birth:	02 October 1980
Nationality:	German

Education

11/2008-*Current* | **PhD Student**, University of Zurich, Institute of Plant Biology
Assessing structural changes in plant cell walls
Investigation of genes, proteins and complex components related to cell wall assembly and dynamics in *Arabidopsis* pollen tubes. Quantification of the stiffness of mutant pollen tubes by Cellular Force Microscopy. Interdisciplinary work and communication of datasets during the developmental process of the Cellular Force Microscope.

03/2007-03/2008 | **Diploma thesis**, University of Freiburg, Plant Biochemistry
Quantifiation of complex membrane proteins
Establishment of a new method to synthesize peptides, to quanitify subunits of PSI and the NDH complex of tylakoid membranes in *Zea mays*. Improvement of the isolation method of bundle sheath chloroplasts.

10/2001-01/2007 | **Undergraduate Studies in Biology**, University of Freiburg
Major Subject:*Plant Biochemistry*
Minor Subjects:*Genetics, Microbiology, Clinical Chemistry*

Work Experience

04/2008-10/2008 | **Research Scientist**, University of Freiburg, Plant Biochemistry
Identification of new protein subunits of the NDH complex in maize
Improvement and optimization of methods and work processes.

01/2006-10/2008 | **Service Staff**, Cinemaxx Freiburg
Ticket-counter and hall organization

Languages

German:	Native
English:	Fluent (C2-Level, CEFR)
French:	Basic Knowledge (A1-Level,CEFR)

Skills

MS-Office, LaTeX, basic R statistics

Supervision Experience

2004-2010	Advisory: Exercises for Biologists "Introduction to Biochemistry"
	Course Instruction: Practical course "Methods in Biochemistry"
	Tutorial: Guide to lecture "Anorganic Chemistry"
	Course Instruction: Practical course "Plant environment Interactions"

Attended Courses

2008-2010	Project Management for Research
	Scientific Writing Practice I: General principles
	Scientific Writing Practice II: Writing up Research
	Science Communication Practice
	Self-marketing Skills: Indispensable to Boost your Career

Lower Education

2000-2001	Civilian service: Deutsches Rotes Kreuz (Paramedic)
1998-2000	Technical Gymnasium